Supplementary Information

Supramolecular CRISPR-OFF switches with host-guest chemistry

Wei Xiong, Xingyu Liu, Qianqian Qi, Huimin Ji, Fengbo Liu, Cheng Zhong, Simin Liu, Tian Tian*, Xiang Zhou

Email: ttian@whu.edu.cn

Table of contents

General methods and materials

Materials

The sequences of all used oligonucleotides are demonstrated in Table S1. These oligonucleotides were ordered from TaKaRa company (Dalian, China). The DFHBI (product# SML1627) and Thiazolyl Blue Tetrazolium Bromide (MTT, CAS# 298-93-1) were purchased from Sigma-Aldrich (Shanghai, China). Unless otherwise specified, glycoluril (CAS# 496-46-8), formaldehyde solution (36.5-38% in H_2O, CAS# 50-00-0) and all other chemicals were purchased from Shanghai Aladdin Bio-Chem Technology Co.,LTD. The HIV-1 RT, Recombinant, *E. coli* (product number: 382129) was purchased from EMD Millipore Corporation (Merck KGaA, Germany). The M-MuLV RT (product number: M0253), the Cas9 Nuclease, Streptococcus pyogenes (product# M0646), the ribonucleotide solution mix (NTPs) and deoxy-ribonucleoside triphosphates (dNTPs) were purchased from New England Biolabs, Inc. (USA). The Pyrobest™ DNA Polymerase were purchased from TaKaRa Shuzo Co. Ltd. (Tokyo, Japan). Transcript Aid T7 High Yield Transcription kit (product# K0441) and Glycogen (product# R0561) were purchased from Thermo Fisher Scientific Inc. The nucleic acid stains Super GelRed (NO.: S-2001) was purchased from US Everbright Inc. (Suzhou, China). The DNA Clean & Concentrator™-5 kit (product# D4014) was purchased from Zymo Research Corp. The pH was measured with Mettler Toledo, FE20-Five Easy™ pH (Mettler Toledo, Switzerland). The concentration of nucleic acids was quantified by NanoDrop 2000c (Thermo Scientific, USA).

Chemical synthesis

All reactions in anhydrous solvents were performed in flame-dried glassware under a nitrogen (N_2) atmosphere. Unless otherwise indicated, commercially available reagents were used without further purification. Chromatographic purification was performed on silica gel (100-200 mesh). Analytical thin layer chromatography (TLC) was performed on silica gel 60-F_{254} (Yantai, China) using UV-detection at 230 nm. ^{1}H NMR and ^{13}C NMR were recorded on 400 MHz ^{1}H (101 MHz. ^{13}C) spectrometer in deuterochloroform ($CDCl_3$). The peaks around δ 7.26 (^{1}H NMR) and 77.16 (^{13}C NMR) correspond to $CDCl_3$. Multiplicities are indicated as follows: s (singlet), d (doublet), t (triplet), m (multiplet), dd (doublet of doublets), etc. Coupling constants (J) are given in hertz. Chemical shifts (δ) are reported in parts per million relative to TMS as an internal standard. The ESI-HRMS was carried out on a Bruker Bio TOF IIIQ (quadrupole time of flight) mass spectrometer.

The synthesis of ADI-1

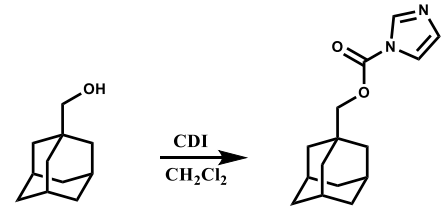

Compound 1 ADI-1

The **ADI-1** was synthesized according to a previous protocol[1].

1-Adamantanemethanol (compound **1**, 166 mg, 1.0 mmol) was dissolved in anhydrous CH_2Cl_2 (5 mL) in a flame-dried flask. Carbonyldiimidazole (CDI, 194 mg, 1.2 mmol) was added and the solution was stirred at room temperature for 2 hr. The mixture was diluted into CH_2Cl_2 (20 mL) and washed with water (2 × 25 mL). The organic phase was washed with brine (1 × 25 mL), dried over anhydrous $MgSO_4$, filtered, and concentrated in vacuum to obtain the crude product. The crude product was purified by column chromatography (ethyl acetate: petroleum ether = 1:5). After removal of solvents under reduced pressure to give compound **ADI-1** (198 mg, 76%) as a white solid.

^{1}H NMR (400 MHz, $CDCl_3$) δ 8.15 (s, 1H), 7.44 (t, *J* = 1.4 Hz, 1H), 7.08 (dd, *J* = 1.5, 0.8 Hz, 1H), 4.01 (s, 2H), 2.00-2.07 (m, 3H), 1.65-1.80(m, 6H), 1.61 (d, *J* = 2.5 Hz, 6H).

^{13}C NMR (101 MHz, $CDCl_3$) δ 148.91, 137.05, 130.64, 117.08, 77.54, 39.13, 36.77, 33.57, 27.85.

HRMS *m*/*z* calculated for $C_{16}H_{20}NaO_4Si$ ($[M + Na]^+$): 327.1023 found: 327.1013.

The synthesis of ADI-2

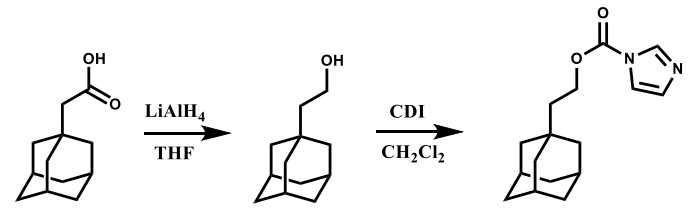

Compound 2 Compound 3 ADI-2

2-(Adamant-1yl)ethan-1-ol (Compound **3**)[2]

To a solution of 2-(adamant-1-yl)acetic acid (compound **2**, 1.94 g, 10 mmol) in THF (20 mL) at 0 °C was slowly added $LiAlH_4$ (0.569 g, 15 mmol). After 12 hr at room temperature, water (100 mL) was added at 0 °C and the reaction mixture was extracted with EtOAc (3 × 80 mL). The organic phases were combined, washed with 3 N NaOH, and brine, dried over anhydrous Na_2SO_4, filtered and concentrated in vacuum. The desired product (Compound **3**, 1.78 g, 9.78 mmol, 96%) was isolated as a white solid which was used without further purification.

^{1}H NMR (400 MHz, $CDCl_3$) δ 3.71 (t, *J* = 7.5 Hz, 2H), 1.91-1.97 (m, 3H), 1.73-1.60 (m, 6H), 1.53 (d, *J* = 2.5 Hz, 6H), 1.41-1.35 (m, 2H).

^{13}C NMR (101 MHz, $CDCl_3$) δ 58.84, 47.26, 42.78, 37.09, 31.88, 28.64.

HRMS (ESI^+) m/z calcd for $C_{12}H_{21}O$ $[M + H]^+$: 181.1587. Found: 181.1582.

ADI-2

2-(Adamant-1yl)ethan-1-ol (compound **3**, 180 mg, 1.0 mmol) was dissolved in anhydrous CH_2Cl_2 (5 mL) in a flame-dried flask. Carbonyldiimidazole (CDI, 194 mg, 1.2 mmol) was added and the solution was stirred at room temperature for 2 hr. The mixture was diluted into CH_2Cl_2 (20 mL) and washed with water (2 × 25 mL). The organic phase was washed with brine (1 × 25 mL), dried over anhydrous $MgSO_4$, filtered, and concentrated in vacuum to obtain the crude product. The crude product was purified by column chromatography (ethyl acetate: petroleum ether = 1:5). After removal of solvents under reduced pressure to give compound **ADI-2** (192 mg, 70%) as a white solid.

^{1}H NMR (400 MHz, $CDCl_3$) δ 8.13 (s, 1H), 7.42 (t, *J* = 1.3 Hz, 1H), 7.05-7.07 (m, 1H), 4.48 (t, *J* = 7.2 Hz, 2H), 1.96-2.01 (m, 3H), 1.61-1.76 (m, 6H), 1.62-1.53 (m, 8H).

^{13}C NMR (101 MHz, $CDCl_3$) δ 148.75, 137.09, 130.58, 117.10, 65.05, 42.49, 42.22, 36.88, 31.82, 28.49.

HRMS (ESI^+) m/z calcd for $C_{16}H_{23}N_2O_2$ $[M + H]^+$: 275.1754. Found: 275.1758.

Molecular optimization study using Gaussian09

All optimizations were done at M062X/def2-SVP level with Grimme's D3 empirical dispersion correction[3]. The volume of the optimized geometries are computed, defined as the volume inside a contour of 0.001 electrons/Bohr^3 density. All the calculations are performed using Gaussian09 program[4].

General methods of biological assay

Denaturing polyacrylamide gel electrophoresis

The denaturing polyacrylamide gel electrophoresis was run in a temperature-controlled vertical electrophoretic apparatus (DYCZ-22A, Liuyi Instrument Factory, Beijing, China). The acrylamide concentration of the separating gel was 20 % (19 : 1 monomer to bis ratio). About one hundred nanograms of DNA were loaded on the gel. Electrophoresis was run at 10 °C for 12 hr at 400 V. The Super GelRed was used for post-electrophoresis gel staining. The target nucleic acids in the gel were visualized using a Pharos FX Molecular imager (Bio-Rad, USA) in the fluorescence mode (λex = 590 nm).

Supramolecular control of reverse transcription

For the M-MuLV RT, this reaction was performed in 1 × M-MuLV buffer, which contained 50 mM Tris-HCl, 75 mM KCl, 3 mM $MgCl_2$, 10 mM DTT, pH 8.3 @ 25 °C. For this assay, the 5'-FAM-labeled DNA primer (primer1) was mixed with RNA templates (R-32nt) with or without adamantoylation. The extension scaffold was then preincubated with M-MuLV RT and different concentrations of CB7 in 1 × M-MuLV buffer to make the enzyme:scaffold complex. The extension reaction was started by rapid

mixing of equal volumes of the enzyme:scaffold complex with an solution containing twofold concentrations of dNTPs in 1 × reaction buffer. The final concentration of each component for a typical 10 μL reaction are as follow: 2.0 U M-MuLV, 100 nM primer1, 500 nM R-32nt and 200 μM dNTPs. Incubation was performed at 37 °C for 2 hr. The reactions were quenched by adding 4 ×v:v of stop buffer (95% formamide, 25 mM EDTA at pH 8.0), followed by immediate heating at 90 °C for 5 min. After cooling down to 4 °C, products were analyzed by denaturing electrophoresis (20% polyacrylamide, 19:1). Finally, the products were imaged with a Pharos FX Molecular imager (Bio-Rad, USA) operated in the fluorescence mode (λex = 488 nm). The unmodified Rtemplate1 was used in the control reactions.

For the HIV-1 RT, this reaction was performed in 1 × HIV-1 buffer, which contained 50 mM Tris-HCl (pH 8.3), 6 mM $MgCl_2$ and 40 mM KCl. For this assay, the 5'-FAM-labeled DNA primer (primer1) was mixed with RNA templates (R-32nt) with or without 2'-O-adamantoylation. The extension scaffold was then preincubated with HIV-1 RT and different concentrations of CB7 in 1 × reaction buffer to make the enzyme:scaffold complex. The extension reaction was started by rapid mixing of equal volumes of the enzyme:scaffold complex with an solution containing twofold concentrations of dNTPs in 1 × reaction buffer. The final concentration of each component for a typical 10 μL reaction are as follow: 2.0 U HIV-1 RT, 100 nM primer1, 500 nM R-32nt and 200 μM dNTPs. Incubation was performed at 37 °C for 2 hr. The following quenching and electrophoresis steps are similar to the progression steps of the procedure described above (the M-MuLV RT).

RNase degrading assay

Adamantoyl RNAs (R-21nt-FAM) were prepared using the general protocol for RNA adamantoylation. Adamantoyl RNAs (100 ng) were treated with CB7 at varied concentrations for 20 min, and were subjected to RNase degradation.

For RNase I assay, this assay was performed in 1 × buffer in PCR grade water, which contained 20 mM Tris-HCl (pH 8.0), 100 mM NaCl, 0.1 mM EDTA and 0.01% Triton X-100. The fluorescently labeled RNA (100 ng) with or without adamantoylation was incubated in the presence of 1.5 U RNase I in a reaction volume of 10 μL at 37 °C for 10 min. Reaction was quenched by adding a 4.0-fold excess of quenching solution (0.1% SDS in formamide). RNA products were immediately separated on a denaturing 20% polyacrylamide gel (350 V, 1.0 hr).

For RNase T1 assay, this assay was performed in 1 × buffer in PCR grade water, which contained 50 mM Tris-HCl and 2 mM EDTA at pH 7.5 @ 25 °C. The fluorescently labeled RNA (100 ng) with or without adamantoylation was incubated in the presence of 1.5 U RNase T1 in a reaction volume of 10 μL at 37 °C for 30 min. The following quenching and electrophoresis steps are similar to the progression steps of the procedure described above (RNase I).

LwCas13a expression

The wild type and mutated LbuCas13a genes were purchased from Addgene (Plasmid #83482 and #91861). The fusion proteins contained an N-terminal His6-MBP-TEV protease cleavage site. Target plasmids were transformed in E. coli Rosetta (DE3) (Novagen) cells. A 16 mL starter culture was grown overnight, which was used to inoculate 4 L expression culture for growth at 37 °C and 300 RPM until an OD600 of 0.6. At this time, protein expression was induced by supplementation with IPTG (isopropyl-β-D-thiogalactoside, Sigma) to a final concentration of 500 μM, and cells were cooled to 16 °C for 16 hr for protein expression. Cells were collected by centrifugation and were lysed by sonication in a buffer (20 mM Tris-HCl, 500 mM NaCl, pH 7.5). All subsequent steps of the protein purification were performed at 4 °C. After centrifugation, the supernatant was incubated with Ni Sepharose (GE Healthcare). The bound protein was eluted with buffer containing 100 mM imidazole. The His6-MBP tag of eluted proteins were removed by TEV protease digestion. Target proteins were purified on an SP column (GE Healthcare), eluting with a buffer (20 mM Tris-HCl, 1M NaCl, pH 7.5). Target proteins were further purified by size-exclusion chromatography (Superdex 200 Increase 10/300, GE Healthcare) in a buffer (20 mM Tris-HCl, 100 mM NaCl, pH 7.5), and then concentrated to a concentration of 20 mg/ml.

dCas9 expression and purification[5]

The pET302-6His-dCas9-Halo gene (Plasmid #72269) was bought from Addgene. dCas9 protein was overexpressed in *E. coli* BL21 (DE3) (Novagen) cells that were induced with 0.5 mM isopropyl-1-thio-b-D-galactopyranoside (IPTG) at OD_{600} = 0.6 for 15 hr at 18 °C. Cells were collected and lysed by sonication in a lysis buffer containing 50 mM Na_3PO_4, pH 7.0, 300 mM NaCl. Upon centrifugation, the supernatant was incubated with Ni Sepharose (GE Healthcare), and the bound protein was eluted with an elution buffer containing 50 mM Na_3PO_4, pH 7.0, 300 mM NaCl and 150 mM imidazole. The eluted protein was exchanged into buffer [50 mM HEPES (pH 7.5), 100 mM KCl, 1 mM DTT] by a 50-K molecular weight cut off (MWCO) centrifugal filter (Millipore Amicon). The protein was further purified on the ÄKTA FPLC system by ion exchange chromatography using a prepacked HiTrap SP HP column (GE Healthcare), eluting with a linear gradient of buffers containing 0-1.0 M KCl. The protein was further purified by size-exclusion chromatography (Superdex 200 Increase 10/300, GE Healthcare) in a buffer containing 50 mM HEPES, pH 7.5, 150 mM KCl, and then concentrated to a concentration of 10 mg/mL. This study was performed by using fluorescently labeled nuclease-deficient Cas9 (dCas9), which was expressed and purified according to a previous literature.

Cell survival assay

Human HeLa-OC cells were grown in Gibco™ DMEM (Dulbecco's modification of Eagle medium), High Glucose medium (Thermo Fisher Scientific) containing 10% (v/v) Gibco™ fetal bovine serum (FBS, Thermo Fisher Scientific) and 1% penicillin/streptomycin (Invitrogen) at 37 °C, 5% CO_2 humidified atmosphere. HeLa-OC cells (5×10^4) were seeded into wells of a 96-well plate and incubated for 16 hr. Then cells were treated with different amounts of freshly dissolved DPBM or DMSO control for 24 hr. After centrifugation at 2000 rpm for 10 min, the medium was discarded and fresh medium was added. Subsequently, MTT (20 μL, 5 mg/mL in DMSO) was added to each well and the mixture was incubated for an additional 4 hr. After centrifugation at 2000 rpm for 10 min, the medium was removed. Subsequently, DMSO (150 μL) was added to each well and the OD values at 570 nm were detected by a microplate reader (SpectraMax M5, Molecular Devices) to evaluate cell viability.

Table S1. DNA and RNA sequences used in the current study

Oligomer	Sequence(from 5'to 3')	Construct
R-32nt	5'-AAGUCGAUCUCAGUGCAGUACAAGUAAUCCAU-3'	RNA
R-44nt	5'-GGGAUGCCGUUCUUCUGCUUGUGUUUUAGAGCU AUGCUGUUUUG-3'	RNA
R-64nt (Cas13a gRNA)	5'-GAUUUAGACUACCCCAAAAACGAAGGGGACUAAA ACUAGAUUGCUGUUCUACCAAGUAAUCCAU-3'	RNA
R-21nt	5'-AAGCUGAUCUCGAUGACGUAC-3'	RNA
R-22nt	5'-AAGCUGAUCUCGAUGACGUACU-3'	RNA
R-23nt	5'-AAGCUGAUCUCGAUGACGUACUA-3'	RNA
R-24nt	5'-AAGCUGAUCUCGAUGACGUACUAC-3'	RNA
R-25nt	5'-AAGCUGAUCUCGAUGACGUACUACG-3'	RNA
R-21nt-c	5'-GUACGUCAUCGAGAUCAGCUU-3'	RNA
R-65nt	5'-GAUUUAGACUACCCCAAAAACGAAGGGGACUAAA ACUAGAUUGCUGUUCUACCAAGUAAUCCAUU-3'	RNA
R-66nt	5'-GAUUUAGACUACCCCAAAAACGAAGGGGACUAAA ACUAGAUUGCUGUUCUACCAAGUAAUCCAUUA-3'	RNA
R-67nt	5'-GAUUUAGACUACCCCAAAAACGAAGGGGACUAAA ACUAGAUUGCUGUUCUACCAAGUAAUCCAUUAC-3'	RNA
R-68nt	5'-GAUUUAGACUACCCCAAAAACGAAGGGGACUAAA ACUAGAUUGCUGUUCUACCAAGUAAUCCAUUACG-3'	RNA
R-102nt (sg-GFP)	5'-GGGAUGCCGUUCUUCUGCUUGUGUUUUAGAGCU AGAAAUAGCAAGUUAAAAUAAGGCUAGUCCGUUAU CAACUUGAAAAAGUGGCACCGAGUCGGUGCUUUU-3'	transcribed RNA
R-106nt	5'-GGGAUGCAUGCCGUUCUUCUGCUUGUGUUUUAG AGCUAGAAAUAGCAAGUUAAAAUAAGGCUAGUCCG UUAUCAACUUGAAAAAGUGGCACCGAGUCGGUGCU UUU-3'	transcribed RNA
R-110nt	5'-GGGAUGCAUGCAUGCCGUUCUUCUGCUUGUGUUU UAGAGCUAGAAAUAGCAAGUUAAAAUAAGGCUAGU CCGUUAUCAACUUGAAAAAGUGGCACCGAGUCGGU GCUUUU-3'	transcribed RNA
R-102nt-F	5'-TCTAATACGACTCACTATAGGGATGCCGTTCTTCTG CTTGTGTTTTAGAGCTAGAAATAGCA-3'	The forward primer for R-102nt construct
R-106nt-F	5'-TCTAATACGACTCACTATAGGGATGCATGCCGTTC TTCTGCTTGTGTTTTAGAGCTAGAAATAGCA-3'	The forward primer for R-106nt construct
R-110nt-F	5'-TCTAATACGACTCACTATAGGGATGCATGCATGCC GTTCTTCTGCTTGTGTTTTAGAGCTAGAAATAGCA-3'	The forward primer for R-110nt construct
long-R	5'-AAAAGCACCGACTCGGTGCCACTTTTTCAAGTTGA TAACGGACTAGCCTTATTTTAACTTGCTATTTCTAGCT CTAAAAC-3'	The reverse primer for R-102nt, R-106nt, R-110nt construct
R-21nt-FAM	5'-FAM-AAGCUGAUCUCGAUGACGUAC-3'	RNA
R-64nt-Cy3 (gRNA-Cy3)	5'-Cy3-GAUUUAGACUACCCCAAAAACGAAGGGGACU AAAACUAGAUUGCUGUUCUACCAAGUAAUCCAU-3'	RNA
MB	5'-FAM-CGCGCTTGGTAGAACAGCAATCCGCG-Dabcyl-3'	DNA
Spinach-F	5'-TAATACGACTCACTATAGGGAGACGCAACTGAATG AAATGGTGAAGGACGGGTCCAGGTGTGGCTGCTTC-3'	For Spinach RNA construct
Spinach-R	5'-GACGCGACTAGTTACGGAGCTCACACTCTACTCAA CAAGCTGCACTGCC GAAGCAGCCACACCTGGACCC-3'	
Spinach RNA	5'-GGGAGACGCAACUGAAUGAAAUGGUGAAGGACG GGUCCAGGUGUGGCUGCUUCGGCAGUGCAGCUUGU UGAGUAGAGUGUGAGCUCCGUAACUAGUCGCGUC-3'	transcribed RNA
primer1	5'-FAM-ATGGATTACTT-3'	DNA primer

sg-SLX4IP	5’-GGGCCACAGCCAGGAUUUAAGA GUUUUAGAGCUAGAAAUAGCAAGUUAAAAUAAGGCUA GUCCGUUAUCAACUUGAAAAAGUGGCACCGAGUCGGU GCUUUU-3’	transcribed RNA
sg-HPRT1	5’-GGGCCCAAGGAAAGACUAUGAAA GUUUUAGAGCUAGAAAUAGCAAGUUAAAAUAAGGCUA GUCCGUUAUCAACUUGAAAAAGUGGCACCGAGUCGGU GCUUUU-3’	transcribed RNA
sg-HBEGF	5’-GGGUUCUCUCGGCACUGGUGACGUUUUAGAGCUAG AAAUAGCAAGUUAAAAUAAGGCUAGUCCGUUAUCAAC UUGAAAAAGUGGCACCGAGUCGGUGCUUUU-3’	transcribed RNA
sg-SLX4IP-F	5’-TCTAATACGACTCACTATAGGGCCACAGCCAGGAT TTAAGAGTTTTAGAGCTAGAAATAGCAAGTTAAAAT A-3’	The forward primer for sg-SLX4IP construct
sg-HPRT1-F	5’-TCTAATACGACTCACTATAGGGCCCAAGGAAAGAC TATGAAAGTTTTAGAGCTAGAAATAGCAAGTTAAAA TA-3’	The forward primer for sg-HPRT1 construct
sg-HBEGF-F	5’-TCTAATACGACTCACTATAGGGTTCTCTCGGCACT GGTGACGTTTTAGAGCTAGAAATAGCAAGTTAAAAT A-3’	The forward primer for sg-HBEGF construct
sg-R	5’-AAAAGCACCGACTCGGTGCCACTTTTTCAAGTTGA TAACGGACTAGCCTTATTTTAACTTGCTATTTCTA-3’	The reverse primer for sgRNA construct
cr-SLX4IP	5’-GGGCCACAGCCAGGAUUUAAGAGUUUUAGAGCUAU GCUGUUUUG-3’	RNA
cr-HPRT1	5’-GGGCCCAAGGAAAGACUAUGAAAGUUUUAGAGCUA UGCUGUUUUG-3’	RNA
cr-HBEGF	5’-GGGUUCUCUCGGCACUGGUGACGUUUUAGAGCUAU GCUGUUUUG-3’	RNA
tracrRNA-F	5’-TCTAATACGACTCACTATAGGGTTGGAACCATTCAAA ACAGCAT**A**GCAAGTTAAAATAAGGCTAG-3’	For tracrRNA construct
tracrRNA-R	5’-AAAAAAAGCACCGACTCGGTGCCACTTTTTCAAGTTGAT AACGGA**C**TAGCCTTATTTTAACTTGCT-3’	
tracrRNA	5’-GGGUUGGAACCAUUCAAAACAGCAUAGCAAGUUAA AAUAAGGCUAGUCCGUUAUCAACUUGAAAAAGUGG CACCGAGUCGGUGCUUUUUUU-3’	transcribed RNA
t-SLX4IP-F	5’-TTATCC GGCACT GTG AAAGCT-3’	For PCR of t-SLX4IP
t-SLX4IP-R	5’-CCTGAT GTTTAG CAAC TTTTTGG-3’	
t-HPRT1-F	5’-GTTGTGATAAAAGGTGATGCTC-3’	For PCR of t-HPRT1
t- HPRT1-R	5’-TCATAAACACATCCATGGGAC-3’	
t-HBEGF-F	5’-GCCGCTTCGAAAGTGACTGG-3’	For PCR of t-HBEGF
t-HBEGF-R	5’-GATCCCCCAGTGCCCATCAG-3’	
target-FAM	5’-FAM-UUACUUGGUAGAACAGCAAUCUA-3’	RNA
Cas13a target1	5’-AUGGAUUACUUGGUAGAACAGCAAUCUA-3’	RNA
Cas13a target2	5’-UUACUUGGUAGAACAGCAAUCUA-3’	RNA
Cas13a reporter	5’-FAM-UUUUU-BHQ1-3’	RNA

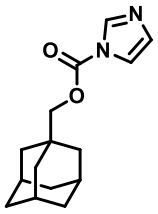

ADI-1

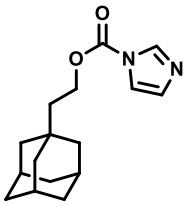

ADI-2

Figure S1: Structures of ADIs

ADI-1 and ADI-2 are designed and synthesized for the preparation of adamantoyl RNAs. All of these molecules were well characterized by spectroscopic techniques such as ^{1}H NMR, ^{13}C NMR and mass spectrometry.

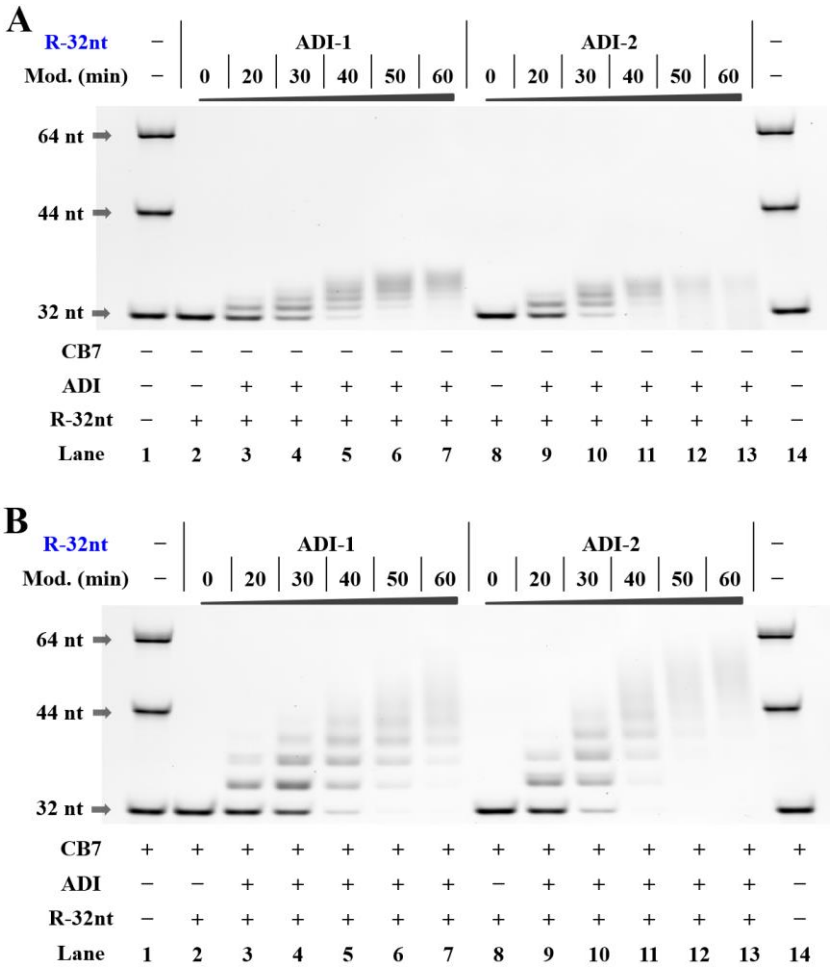

Figure S2. Native PAGE analysis of adamantoyl R-32nt in the absence or presence of CB7

Reactions were carried out as described in the Experimental Section. R-32nt was used in this study. All samples were tested in three biological replicates. Image of representative data is shown here. In gel RNAs were seen with GelRed staining. The CB7-bound RNA molecule experiences greater resistance and moves more slowly during electrophoresis. (**A**) Native PAGE analysis of RNA strands in the absence of CB7. The electrophoretic mobility of the adamantoyl RNA differs from that of unmodified control. (**B**) Native PAGE analysis of RNA strands in the presence of 33 μM CB7. Supramolecular complexation significantly impedes the movement of adamantoyl RNAs on the gel. For (**A**) and (**B**), lanes 1, 14: RNA marker (R-32nt, R-44nt, R-64 nt in Table S1); lanes 2, 8: unmodified RNAs; lanes 3-7, 9-13: adamantoyl RNA with different modification levels.

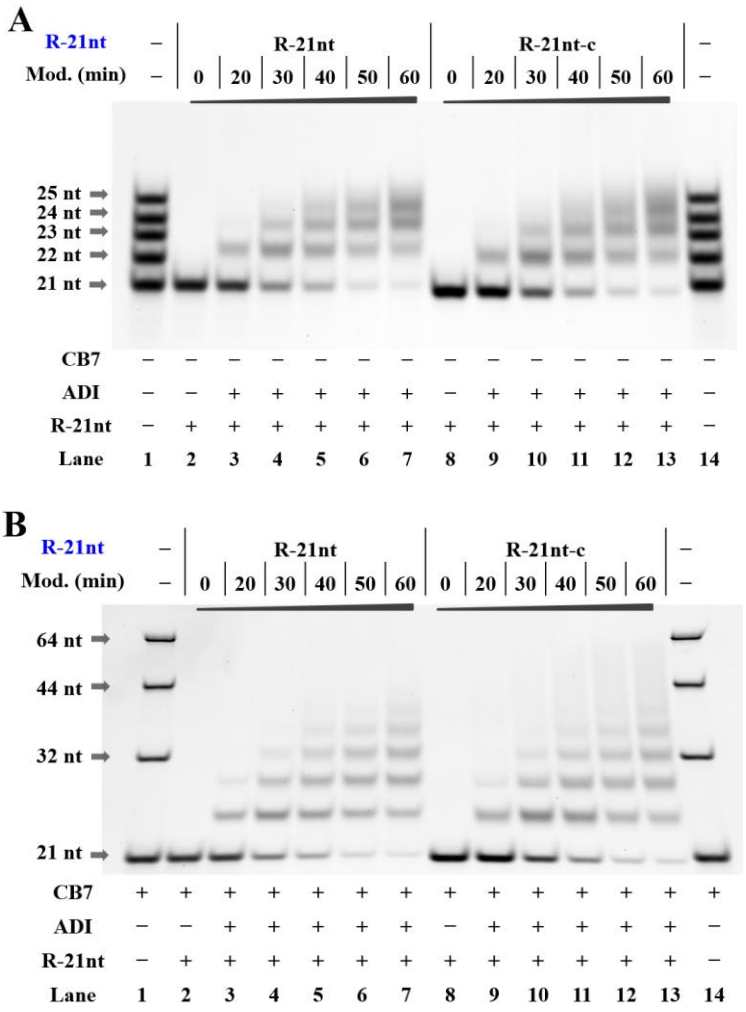

Figure S3. Supramolecular complexation in unstructured RNA contexts (R-21nt and R-21nt-c)

Reactions were carried out as described in the Experimental Section. R-21nt and R-21nt-c were used in this study. All samples were tested in three biological replicates. Image of representative data is shown here. In gel RNAs were seen with GelRed staining. The CB7-bound RNA molecule experiences greater resistance and moves more slowly during electrophoresis. (**A**) Denaturing PAGE analysis of RNA strands in the absence of CB7. Lanes 1, 14: RNA marker (R-21 nt, R-22nt, R-23nt, R-24nt, R-25nt in Table S1); lanes 2, 8: unmodified RNAs; lanes 3-7, 9-13: adamantoyl RNAs with different modification levels. (**B**) Denaturing PAGE analysis of RNA strands in the presence of 33 μM CB7. The CB7 complexation significantly impedes the movement of adamantoyl RNAs on the gel. Lanes 1, 14: RNA marker (R-21nt, R-32nt, R-44nt, R-64nt in Table S1); lanes 2, 8: unmodified RNAs; lanes 3-7, 9-13: adamantoyl RNAs with different modification levels.

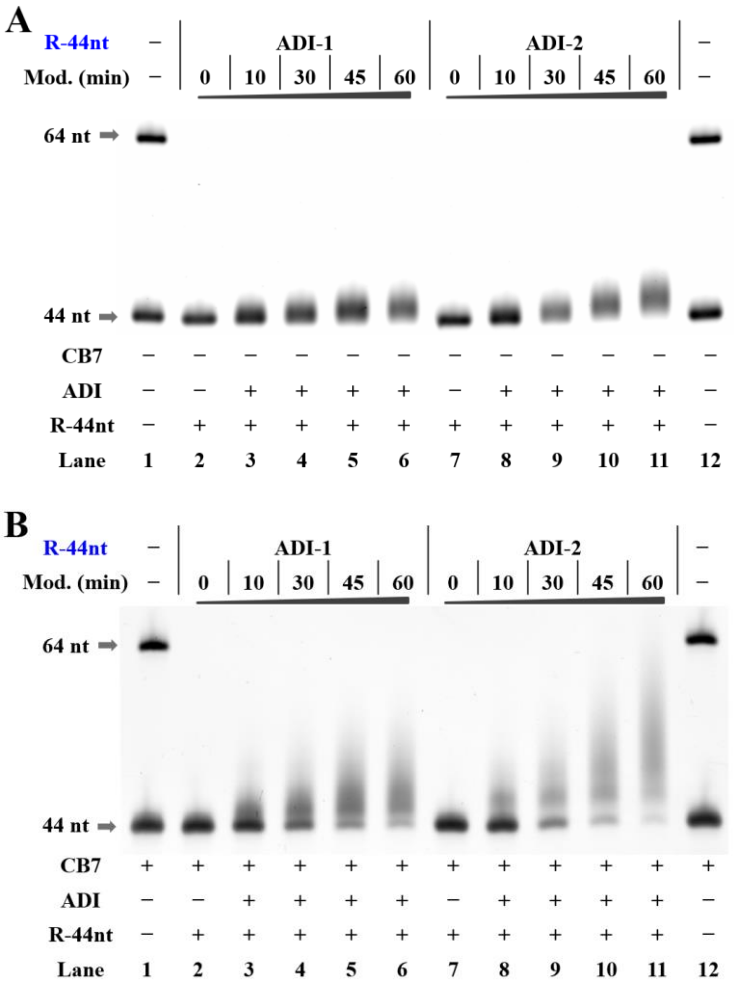

Figure S4. Supramolecular complexation in unstructured RNA contexts (R-44nt)

Reactions were carried out as described in the Experimental Section. R-44nt was used in this study. All samples were tested in three biological replicates. Image of representative data is shown here. In gel RNAs were seen with GelRed staining. The CB7-bound RNA molecule experiences greater resistance and moves more slowly during electrophoresis. (**A**) Denaturing PAGE analysis of RNA strands in the absence of CB7. The electrophoretic mobility of the adamantoyl RNA differs from that of unmodified control. (**B**) Denaturing PAGE analysis of RNA strands in the presence of 33 μM CB7. Supramolecular complexation significantly impedes the movement of adamantoyl RNA on the gel. For (**A**) and (**B**), lanes 1, 14: RNA marker (R-44nt, R-64 nt in Table S1); lanes 2, 8: unmodified RNAs; lanes 3-7, 9-13: adamantoyl RNAs with different modification levels.

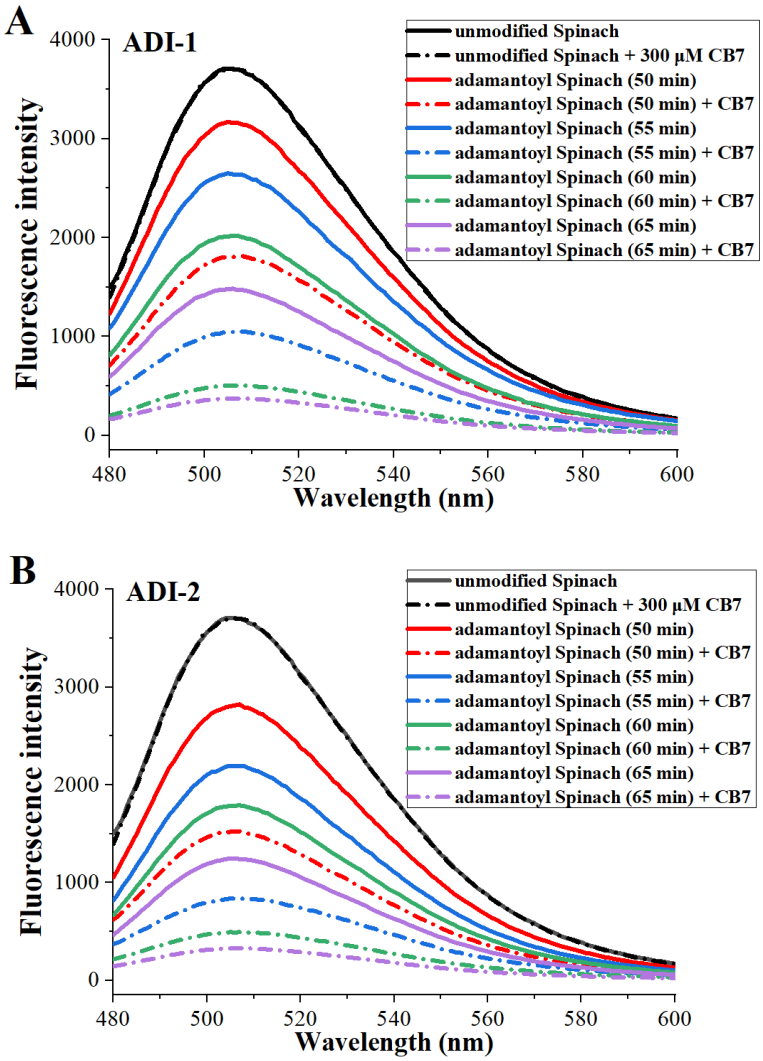

Figure S5. Supramolecular complexation in structured RNA contexts (Spinach RNAs)

Reactions were carried out as described in the Experimental Section. All samples were tested in three biological replicates. Image of representative data is shown here. The Spinach RNAs were used in this study. Complexes of DFHBI with adamantoylated Spinach exhibit evident fluorescence *in vitro*, but they exhibit much lower fluorescence in the presence of CB7 molecules. (**A**) The adamantoylation was performed by treating Spinach RNA with ADI-1 at room temperature for different periods. (**B**) The adamantoylation was performed by treating Spinach RNA with ADI-2 at room temperature for different periods. For (**A**) and (**B**), supramolecular complexation was performed by incubating RNAs with 300 μM CB7 at room temperature.

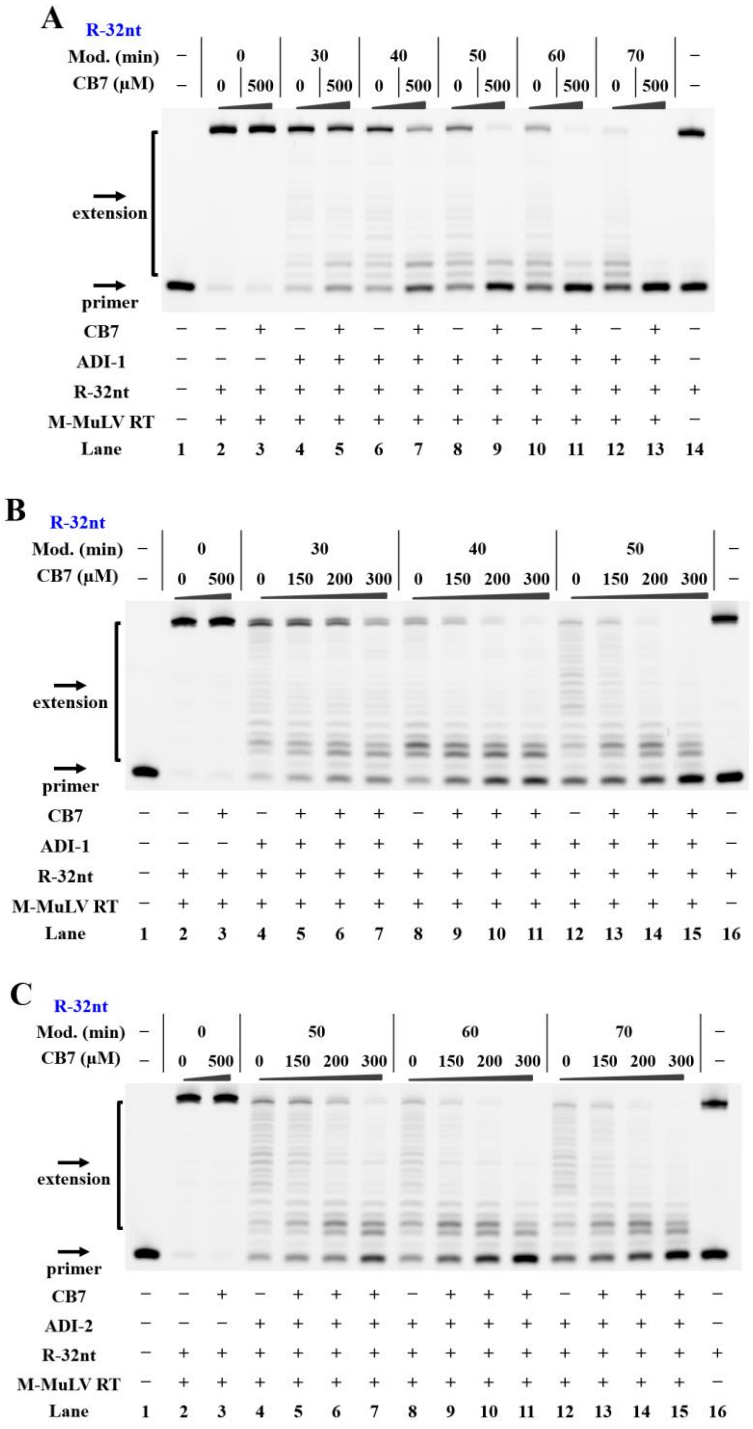

Figure S6. Supramolecular control of reverse transcription with M-MuLV RT

Reactions were carried out as described in the Experimental Section. All samples were tested in three biological replicates. Image of representative data is shown here. (**A**) The influence of supramolecular complexation on reverse transcription of adamantoyl RNAs with ADI-1. Lane 1: no enzyme control; lanes 2-3 contain unmodified R-32nt; lanes 4-5, 6-7, 8-9, 10-11, 12-13 contain adamantoyl R-32nt with increasing modification levels. (**B**) Dependence of inhibition of reverse transcription on CB7 concentration. (**C**) Dependence of inhibition of reverse transcription on CB7 concentration. For (**B**) and (**C**), lane 1: no enzyme control; lanes 2-3 contain unmodified R-32nt; lanes 4-7, 8-11, 12-15 contain adamantoyl R-32nt with increasing modification levels; lane 16: RNA marker.

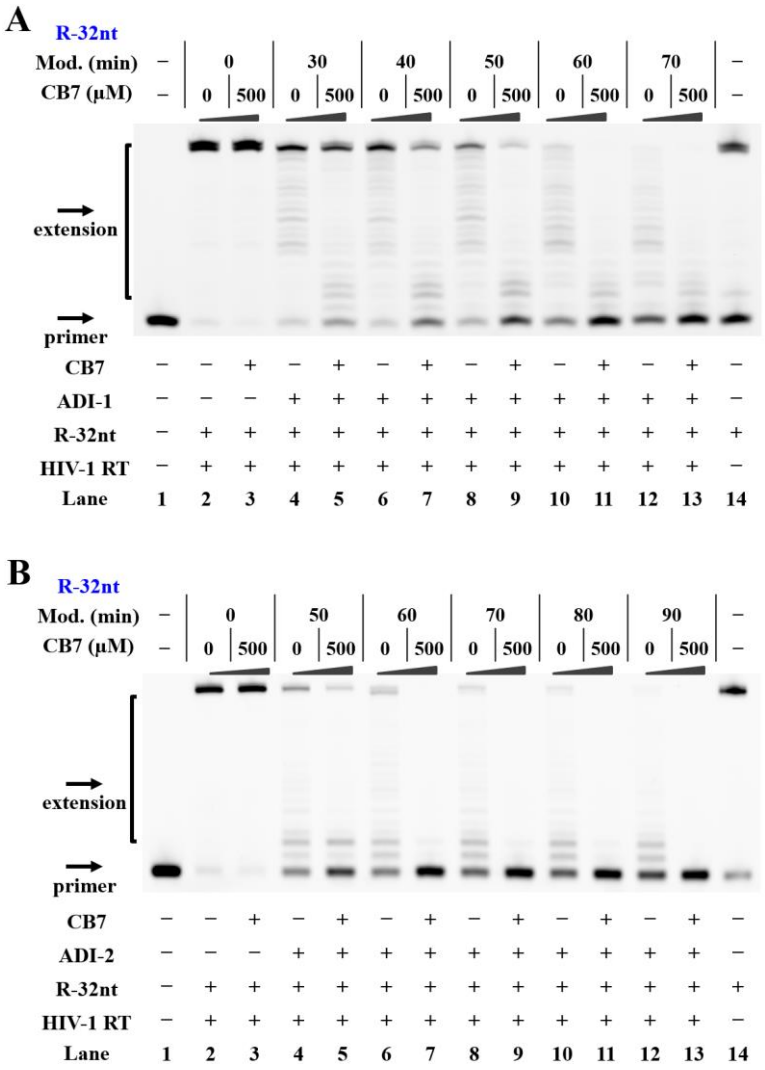

Figure S7. Supramolecular control of reverse transcription with HIV-1 RT

Reactions were carried out as described in the Experimental Section. All samples were tested in three biological replicates. Image of representative data is shown here. (**A**) The influence of supramolecular complexation on reverse transcription of adamantoyl RNAs with ADI-1. (**B**) The influence of supramolecular complexation on reverse transcription of adamantoyl RNAs with ADI-2. For (**A**) and (**B**), lane 1: no enzyme control; lanes 2, 4, 6, 8, 10, 12: no CB7 control; lanes 3, 5, 7, 9, 11, 13: the 500-μM CB7 treatments; lane 14: RNA marker. Lanes 2-3 contain unmodified R-32nt; lanes 4-5, 6-7, 8-9, 10-11, 12-13 contain adamantoyl R-32nt with increasing modification levels.

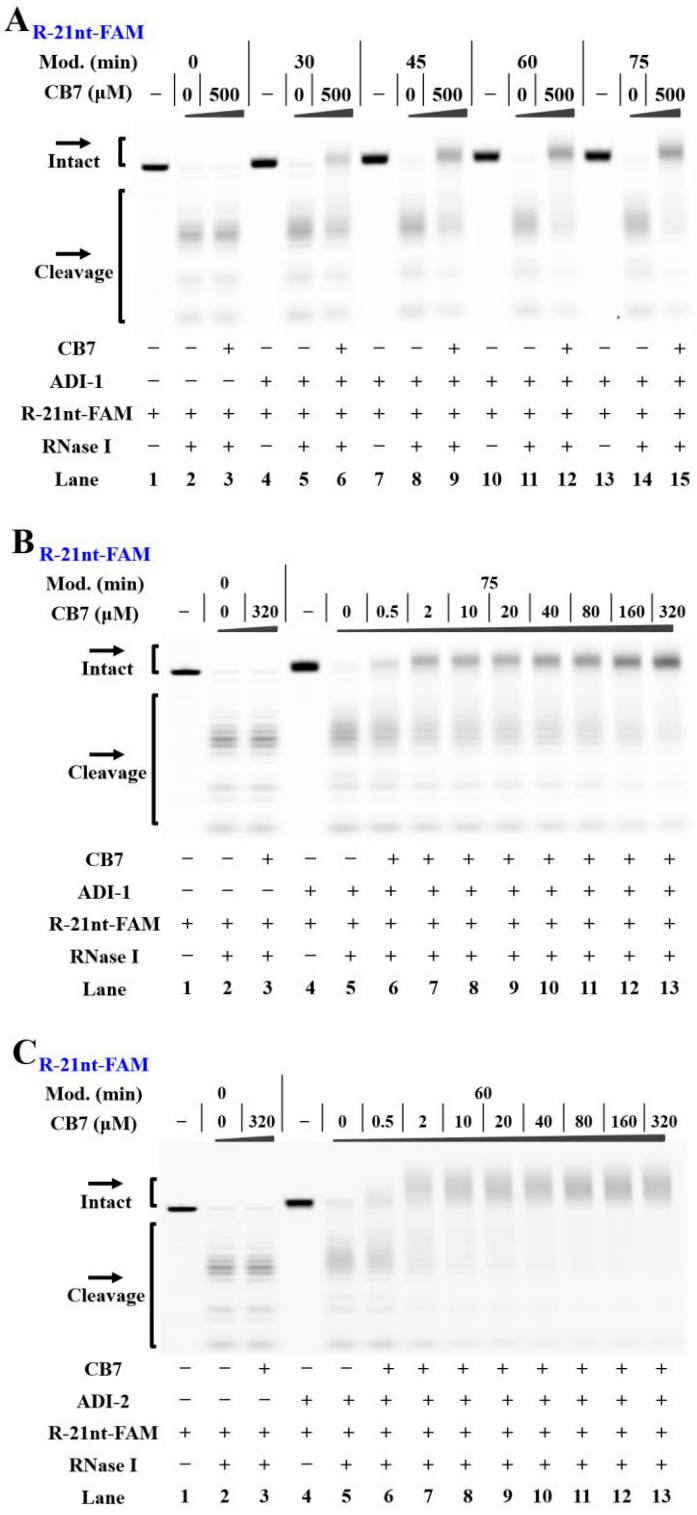

Figure S8. The influence of supramolecular complexation on RNase I degradation

Reactions were carried out as described in the Experimental Section. All samples were tested in three biological replicates. Image of representative data is shown here. (**A**) Influence of supramolecular complexation on degradation of adamantoyl RNAs with ADI-1. Lanes 1, 4, 7, 10, 13: no enzyme control; lanes 2, 5, 8, 11, 14: no CB7 control; lanes 3, 6, 9, 12, 15: the 500-μM CB7 treatments. (**B**) Dependence of inhibition of RNA degradation on CB7 concentration. (**C**) Dependence of inhibition of RNA degradation on CB7 concentration. For (**B**) and (**C**), lane 1: no enzyme control; lanes 2-3 contain unmodified R-21nt-FAM; lanes 4-13 contain adamantoyl R-21nt-FAM (a 75-min modification with 100 mM ADI-1 or a 60-min modification with 100 mM ADI-2).

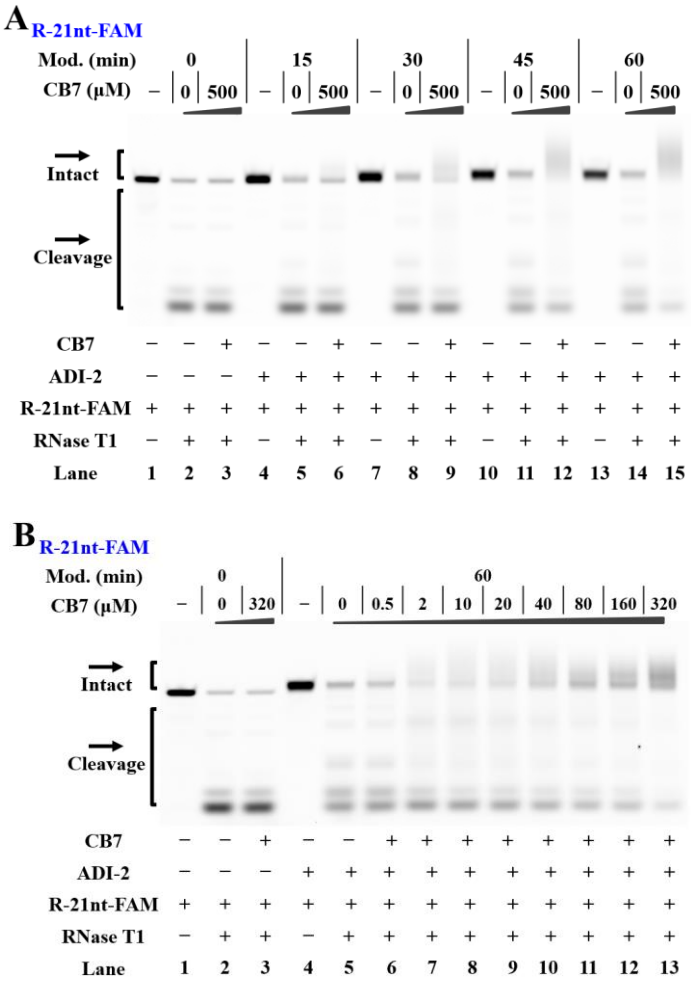

Figure S9. The influence of supramolecular complexation on RNase T1 degradation

Reactions were carried out as described in the Experimental Section. All samples were tested in three biological replicates. Image of representative data is shown here. (**A**) Influence of supramolecular complexation on degradation of adamantoyl RNAs with ADI-2. Lanes 1, 4, 7, 10, 13: no enzyme control; lanes 2, 5, 8, 11, 14: no CB7 control; lanes 3, 6, 9, 12, 15: the 500-μM CB7 treatments. Lanes 1-3 contain unmodified R-21nt-FAM; lanes 4-6, 7-9, 10-12, 13-15 contain adamantoyl R-21nt-FAM with increasing modification levels. (**B**) Dependence of inhibition of RNA degradation on CB7 concentration. Lane 1: no enzyme control; lanes 2-3 contain unmodified R-21nt-FAM; lanes 4-13 contain adamantoyl R-21nt-FAM with a specified level of modification (a 60-min modification with 100 mM ADI-2).

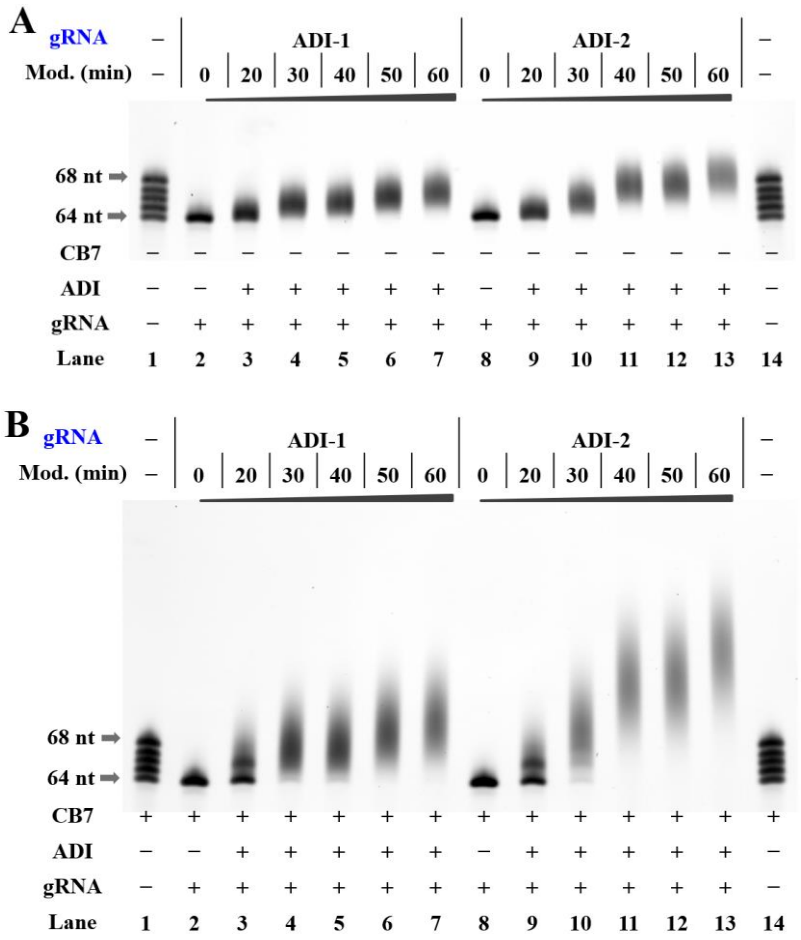

Figure S10. Supramolecular complexation on Cas13a gRNAs

Reactions were carried out as described in the Experimental Section. The gRNA for Cas13a was used in this study. All samples were tested in three biological replicates. Image of representative data is shown here. In gel RNAs were seen with GelRed staining. The CB7-bound gRNA experiences greater resistance and moves more slowly during electrophoresis. (**A**) Denaturing PAGE analysis of RNA strands in the absence of CB7. The electrophoretic mobility of the adamantoyl gRNA differs from that of unmodified control. (**B**) Denaturing PAGE analysis of gRNA strands in the presence of 33 μM CB7. Supramolecular complexation significantly impedes the movement of adamantoyl gRNAs on gel. For (**A**) and (**B**), lanes 1, 14: RNA marker (R-64nt, R-65nt, R-66nt, R-67nt, R-68nt in Table S1); lanes 2, 8: unmodified gRNAs; lanes 3-7, 9-13: adamantoyl gRNAs with different modification levels.

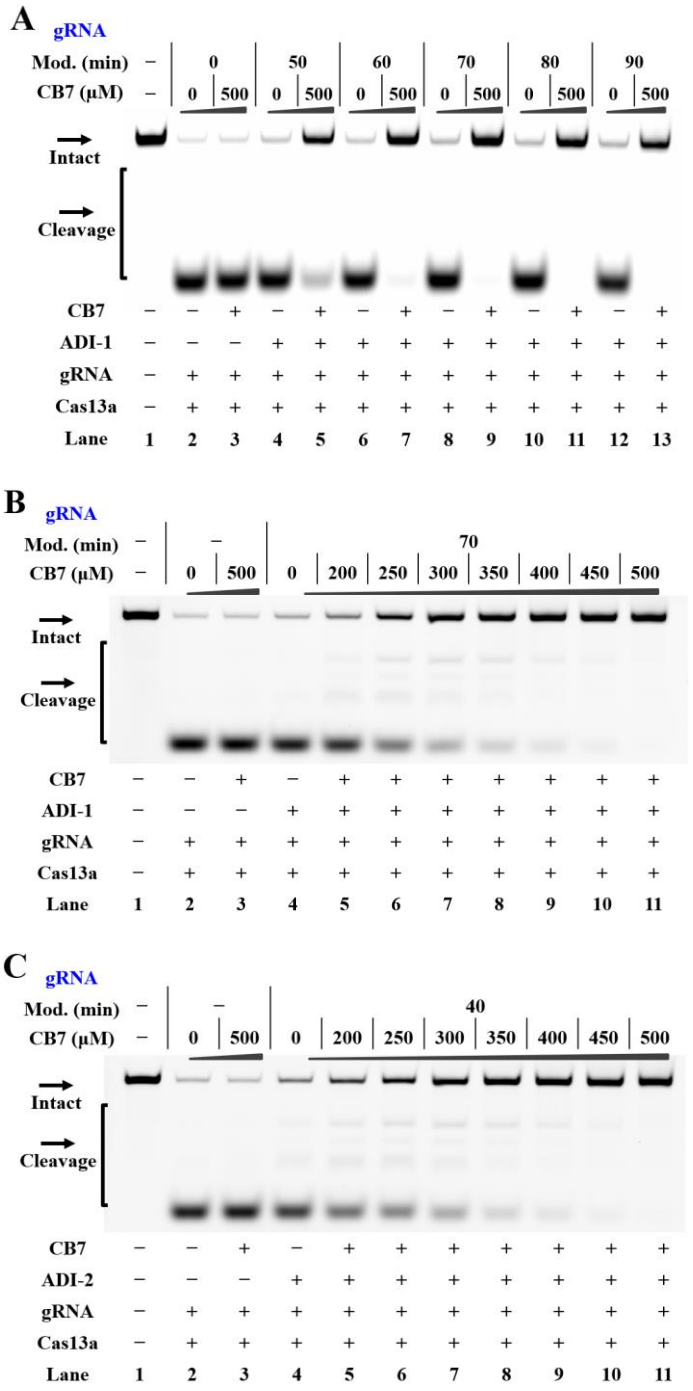

Figure S11. The influence of supramolecular complexation on Cas13a-mediated RNA cleavage (target1)

Reactions were performed as described in the Experimental Section. All samples were tested in three biological replicates. Image of representative data was shown here. (**A**) Modification-dependent inhibition of adamantoyl gRNA with ADI-1. In this study, adamantoyl gRNAs were employed to support Cas13a-mediated RNA cleavage in the absence or presence of 500 μM CB7. Lane 1: no enzyme control; lanes 2, 4, 6, 8, 10, 12: no CB7 control; lanes 3, 5, 7, 9, 11, 13: the 500-μM CB7 treatments. Lanes 2-3 contain unmodified gRNAs; lanes 4-5, 6-7, 8-9, 10-11, 12-13 contain adamantoyl gRNAs with increasing modification levels. (**B**) Dependence of inhibition of CRISPR/Cas13a on CB7 concentration. (**C**) Dependence of inhibition of CRISPR/Cas13a on CB7 concentration. For (**B**) and (**C**), lane 1: no enzyme control; lanes 2-3 contain unmodified gRNAs; lanes 4-11 contain adamantoyl gRNAs (a 70-min modification with 100 mM ADI-1 or a 40-min modification with 100 mM ADI-2).

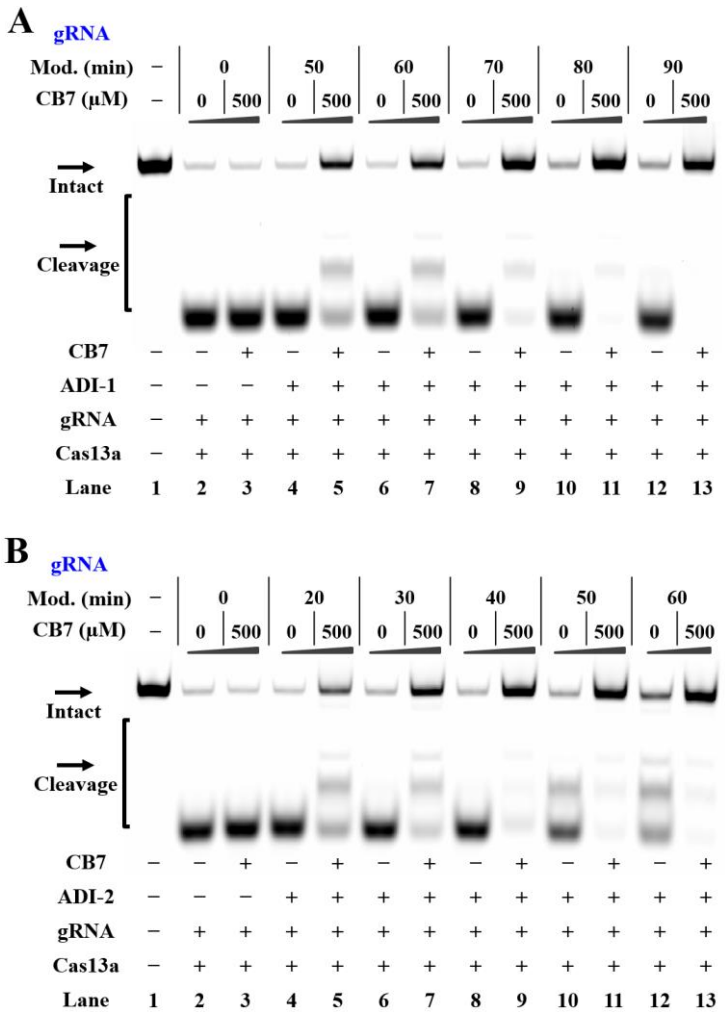

Figure S12. The influence of supramolecular complexation on Cas13a-mediated RNA cleavage (target2)

Reactions were performed as described in the Experimental Section. All samples were tested in three biological replicates. Image of representative data was shown here. (**A**) Modification-dependent inhibition of adamantoyl gRNA with ADI-1. (**B**) Modification-dependent inhibition of adamantoyl gRNA with ADI-2. For (**A**) and (**B**), adamantoyl gRNAs in varying levels of modification were employed to support Cas13a-mediated RNA cleavage in the absence or presence of 500 μM CB7. Lane 1: no enzyme control; lanes 2, 4, 6, 8, 10, 12: no CB7 control; lanes 3, 5, 7, 9, 11, 13: the 500-μM CB7 treatments. Lanes 2-3 contain unmodified gRNA; lanes 4-5, 6-7, 8-9, 10-11, 12-13 contain adamantoyl gRNA with increasing modification levels.

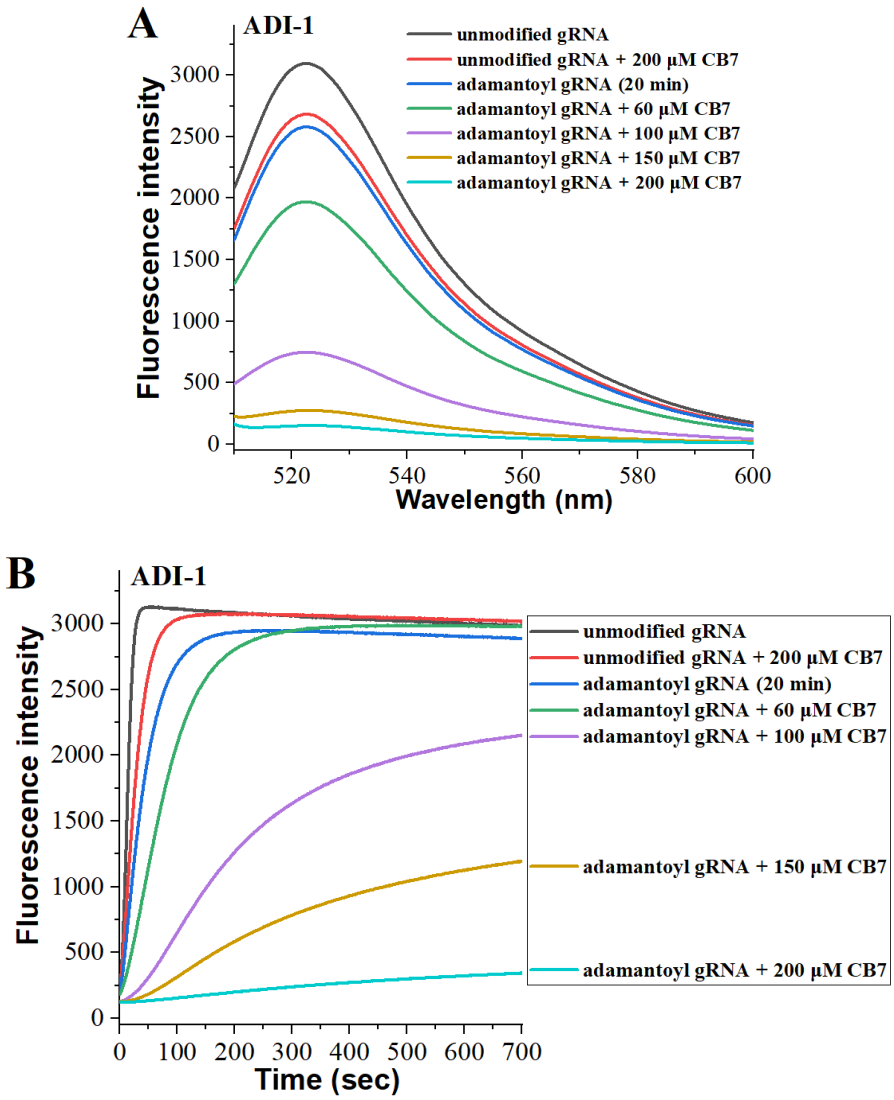

Figure S13. The influence of supramolecular complexation on the Cas13a collateral cleavage

Reactions were performed as described in the Experimental Section. All samples were tested in three biological replicates. Image of representative data was shown here. (**A**) The influence of supramolecular complexation on the Cas13a collateral cleavage. The fluorescence spectra were measured at room temperature after 100 sec incubation at 37 °C. (**B**) Dose-dependent effect of CB7 on inhibition of CRISPR/Cas13a with adamantoyl gRNAs. The fluorescence of the sample versus time is shown. For (**A**) and (**B**), adamantoyl gRNAs with a specified level of modification (a 20-min modification with 100 mM ADI-1) were treated with increasing concentrations of CB7.

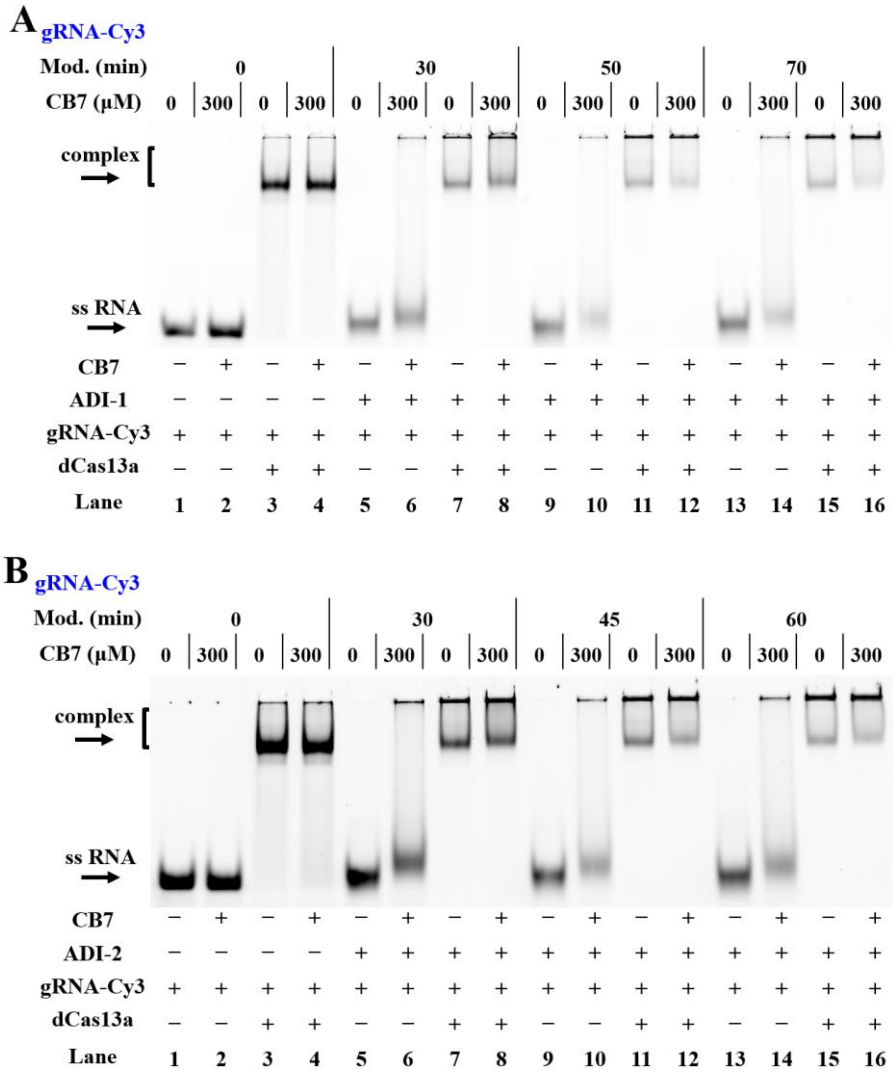

Figure S14. Effect of supramolecular complexation on the formation of binary dCas13a-gRNA complexes

Reactions were performed as described in the Experimental Section. The treatment for each sample is indicated by the signs at the bottom of each lane. All samples were tested in three biological replicates. Image of representative data is shown here. (**A**) Modification-dependent inhibition of complex formation between dCas13a and adamantoyl gRNA with ADI-1. (**B**) Modification-dependent inhibition of complex formation between dCas13a and adamantoyl gRNA with ADI-2. The control lane (gRNA-Cy3 without dCas13a present) contains a single band corresponding to the unbound gRNA fragment, while the lane with dCas13a contains another band that represents the less mobile RNP complex. For (**A**) and (**B**), lanes 1-4 contain unmodified gRNA-Cy3; lanes 5-8, 9-12, 13-16 contain adamantoyl gRNA-Cy3 with increasing modification levels.

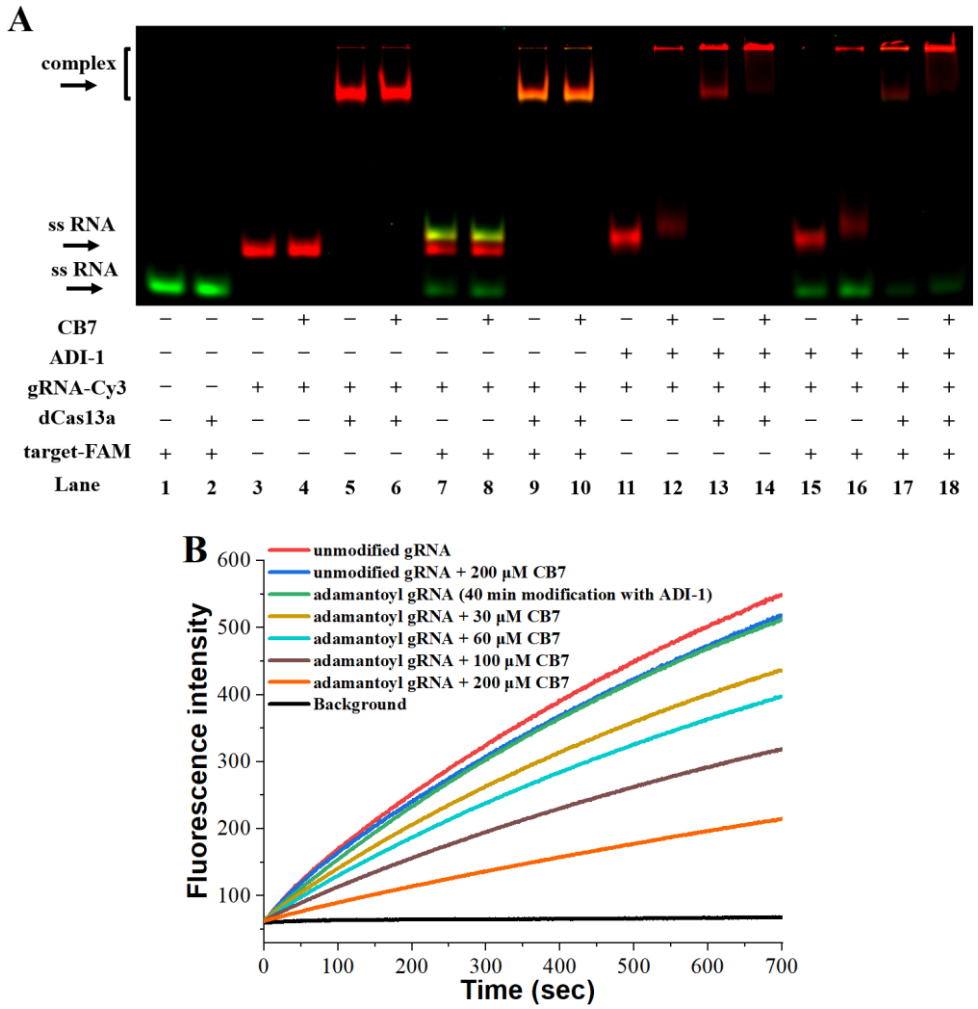

Figure S15. Effect of supramolecular complexation on the formation of ternary dCas13a-gRNA-target complexes

Reactions were performed as described in the Experimental Section. All samples were tested in three biological replicates. Image of representative data is shown here. (**A**) Effect of supramolecular complexation on the formation of ternary dCas13a-gRNA-target complexes. The treatment for each sample is indicated by the signs at the bottom of each lane. The dCas13a was incubated with the Cy3-labeled gRNA (gRNA-Cy3) with different treatments and FAM-labeled target RNA (target-FAM). The samples were resolved by native PAGE and imaged using a gel scanner at FAM and Cy3 wavelengths. Lanes 1-2: target-FAM control; lanes 3-10 contain unmodified gRNA-Cy3; lanes 11-18 contain adamantoyl gRNA-Cy3 with a specified level of modification (a 60-min modification with 100 mM ADI-1). (**B**) Effect of supramolecular complexation on RNA hybridization. Supramolecular complexation blocks the interactions between gRNA and MB. In this study, adamantoyl gRNA with a specified level of modification (a 40-min modification with 100 mM ADI-1) was treated with increasing concentrations of CB7.

A

>20 dna:chromosome chromosome:GRCh38:20:10435305:10636829:1

TTATCCGGCACTGTGAAAGCTACCTTTCCTTTCTCACAATCTTTCGCACCGAATATATGTTCCATTCTT
GAGCTAGTCATTTTCCAATGTTAAGAAAACACACCACAGAAAAGCGTTTTTTTTTCTCTCGGTCAGTT
CAACTGCCTAGCACCGTGAGTTACCATGATACGTTATTTGCTAATGAGAGTCATTGGGGTCCCAGCCT
TTAAAAATAGCCTGCGTCCGGCGCCATTTTTGTTTTGGGCCCACTTTGAAAGCCGCGATATTCTGAAC
AGAGGCCATTTTTCTTTTGGGCAGATTCCACGGGCCATCGAAGTGTTTCGCTGCCA**TCT^TAAATCCT**
GGCTGTGGCCTCAATCCTGCAGCGAAGCTGCCCAGATCATTTTGTGTTTGGGCGGCGGCTGAGTTCC
CAAACGCGCGCGGAGACCCTGGGAAGGAGGAAGTAAGCGCGAAAGTGCTTCCCTTAAGCTTCTGAA
GGTTGGCTGCAGTTCCGGCTACCTGTGTAGTCCGAGTTTCCACAGCCAGGTACTACTCCGCCAGTGAC
CCTGGACAGTAACAAAACATATAAAGCCCGAGCCCAAACCCCGCCACCATCATAGGTAAGCACATGG
ACCTCTGACAACCTCAGATGTTCCTTCAAGTGAACTGAACTGTTTGCCCATCTCCTCCCTCCTGGTTTT
TGGCTTTGATTTTTTGAGACTTTTCCGAATCCTTCTCCCTGTACTTCCACCTTTCTTCATTGTTTTCAAA
AAGCCAAAAAGTTGCTAAACATCAGG

B

>X dna:chromosome chromosome:GRCh38:X:134460165:134520513:1

GTTGTGATAAAAGGTGATGCTCACCTCTCCCACACCCTTTTATAGTTTAGGGATTGTATTTCCAAGGTT
TCTAGACTGAGAGCCCTTTTCATCTTTGCTCATTGACACTCTGTACCCATTAATCCTCCTTATTAGCTC
CCCTTCAATGGACACATGGGTAGTCAGGGTGCAGGTCTCAGAACTGTCCTTCAGGTTCCAGGTGATCA
ACCAAGTGCCTTGTCTGTAGTGTCAACTCATTGCTGCCCCTTCCTAGTAATCCCCATAATTTAGCTCTC
CA**TTT^CATAGTCTTTCCTTGGG**TGTGTTAAAAGTGACCATGGTACACTCAGCACGGATGAAATGA
AACAGTGTTTAGAAACGTCAGTCTTCTCTTTTGTAATGCCCTGTAGTCTCTCTGTATGTTATATGTCAC
ATTTTGTAATTAACAGCTTGCTGGTGAAAAGGACCCCACGAAGTGTTGGATATAAGCCAGACTGTAA
GTGAATTACTTTTTTTGTCAATCATTTAACCATCTTTAACCTAAAAGAGTTTTATGTGAAATGGCTTAT
AATTGCTTAGAGAATATTTGTAGAGAGGCACATTTGCCAGTATTAGATTTAAAAGTGATGTTTTCTTT
ATCTAAATGATGAATTATGATTCTTTTTAGTTGTTGGATTTGAAATTCCAGACAAGTTTGTTGTAGGAT
ATGCCCTTGACTATAATGAATACTTCAGGGATTTGAATGTAAGTAATTGCTTCTTTTTCTCACTCATTT
TTCAAAACACGCATAAAAATTTAGGAAAGAGAATTGTTTTCTCCTTCCAGCACCTCATAATTTGAACA
GACTGATGGTTCCCATTAGTCACATAAAGCTGTAGTCTAGTACAGACGTCCTTAGAACTGGAACCTGG
CCAGGCTAGGGTGACACTTCTTGTTGGCTGAAATAGTTGAACAGCTTTAATATACAATAATTGTTGCA
TTATTATTTCAGATGATAAATGTGGTCATAAGTAAGAAATAAATGATCGAGTTTAGTCTTTTAATTCA
CTGTCCTTTGAATACCTGCCTCTTACTCTGGAGGCAGAAGTCCCATGGATGTGTTTATGA

C

>gi|74230048|gb|CH471062.2|:13429990-13430610 Homo sapiens 211000035832302 genomic scaffold, whole genome shotgun sequence

GCCGCTTCGAAAGTGACTGGTGCCTCGCCGCCTCCTCTCGGTGCGGGACCATGAAGCTGCTGCCGTCG
GTGGTGCTGAAGCTCTTTCTGGCTGCAGGTAAGAGGGCTGCCGACGCCCCCGGAGATCGGGGGGATG
GGGGCGTTGTGCTGGGGGCATGGGGGAAGGTCGCCGCAGCGCACCCGGCACGGGCCACTTGGTGGG
GCCCTTGCGCTCTGGCGGACGGGCGTCGGCATCGGTGCGTGTTGGTCAGGGGTCTGGGCGGGTGTCT
GATGCGGCCTGGCCTCTCGCCCGCA**GTTCTCTCGGCACTGGT^GAC**TGGCGAGAGCCTGGAGCGGC
TTCGGAGAGGGCTAGCTGCTGGAACCAGCAACCCGGACCCTCCCACTGTATCCACGGACCAGCTGCT
ACCCCTAGGAGGCGGCCGGGACCGGAAAGTCCGTGACTTGCAAGAGGCAGATCTGGACCTTTTGAGA
GGTGGGTGTGGAGGCCCCCCATCCTTGGACCTTGGTGGGCTGTTGAAGAATAAGCAGATCCAAGATT
CTTGCTGTTTGGGCAATACTGTGGGTTGAGGGTATTCATGGAGAACCTCGGGGAAAAGCTGATCGGC
CTGATGGGCACTGGGGGATC

Figure S16. The location of sequences recognised by gRNAs and PCR primers

The target loci and PCR primer loci were indicated by blue color and underlining, respectively. Red caret showed the cleavage sites by Cas9 nuclease. PCR primers flanking the target regions were designed by BLAST search

and procedures. (**A**) Schematic illustration of the sequence of *SLX4IP* gene around target loci. The SLX4IP gene is located on the short arm (p) of chromosome 20 at position 12.2 (20p12.2). We generated target SLX4IP DNA (t-SLX4IP) carrying the target loci from HeLa-OC genomic DNA. The 20-nt sequence was the exact same sequence as the target sequence. (**B**) Schematic illustration of the sequence of *HPRT1* gene around target loci. We generated target HPRT1 DNA (t-HPRT1) carrying the target loci from HeLa-OC genomic DNA. The 20-nt sequence was the exact same sequence as the target sequence. (**C**) Schematic illustration of the 5'-UTR sequence of *HBEGF* gene around target loci. We generated target HBEGF DNA (t-HBEGF) carrying the target loci from HeLa-OC genomic DNA. The 20-nt sequence was the exact same sequence as the target sequence.

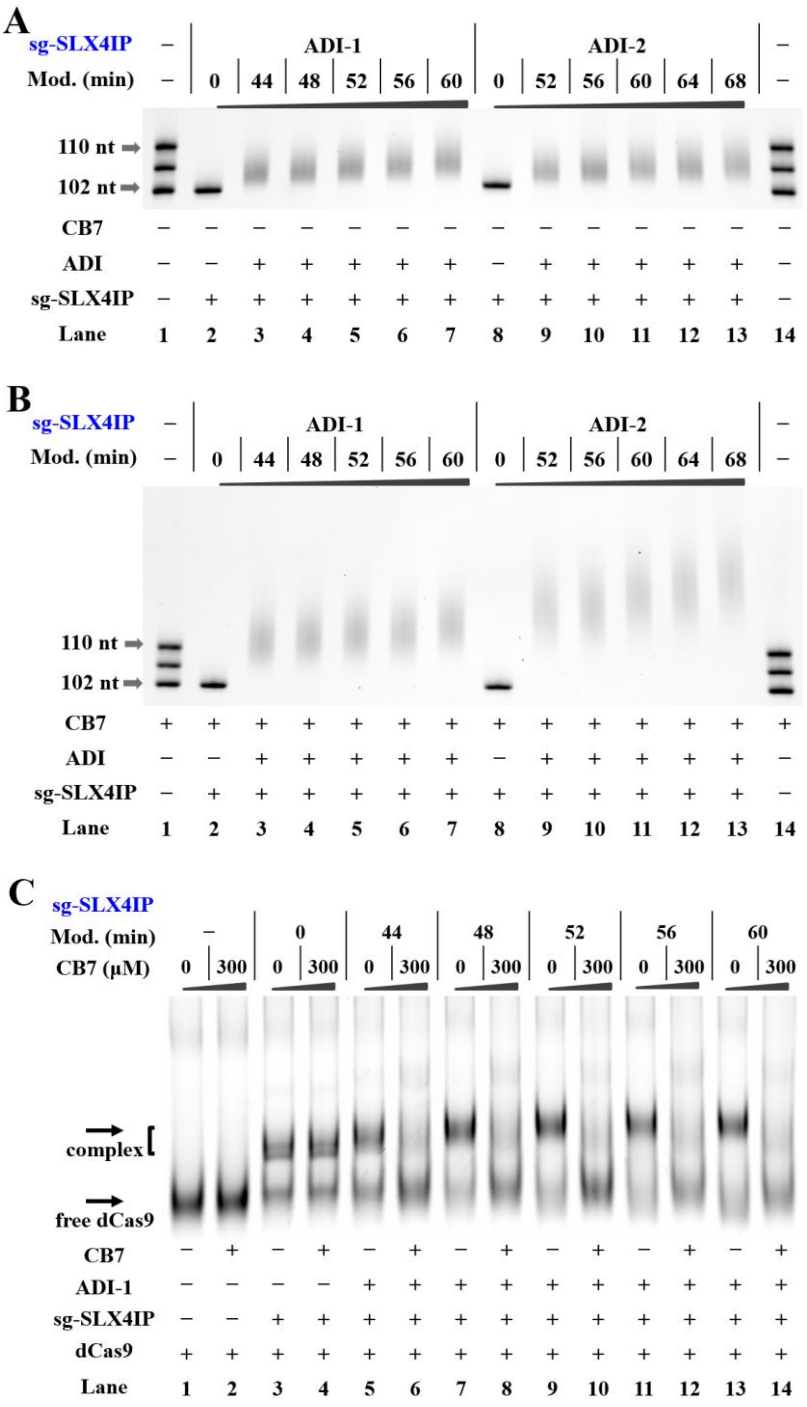

Figure S17. Supramolecular complexation on sg-SLX4IP

Reactions were carried out as described in the Experimental Section. All samples were tested in three biological replicates. Image of representative data is shown here. (**A**) Denaturing PAGE analysis of adamantoyl sg-SLX4IP in the absence of CB7. (**B**) Denaturing PAGE analysis of adamantoyl sg-SLX4IP in the presence of 33 μM CB7. Supramolecular complexation significantly impedes the movement of adamantoyl sg-SLX4IP on the gel. (**C**) Supramolecular control of the complex formation of Cas9/sgRNA. EMSA analysis of fluorescently labeled dCas9 is demonstrated. The CB7 blocks the access of the Cas9 to adamantoyl sg-SLX4IP. Lanes 1-2: no sgRNA control; lanes 3-4 contain unmodified sg-SLX4IP; lanes 5-6, 7-8, 9-10, 11-12, 13-14 contain adamantoyl sg-SLX4IP with increasing modification level. For (**A**) and (**B**), lanes 1, 14: RNA marker (sg-SLX4IP, R-106nt, R-110nt in Table S1); lanes 2, 8: unmodified sg-SLX4IP; lanes 3-7, 9-13: adamantoyl sg-SLX4IP with different modification levels.

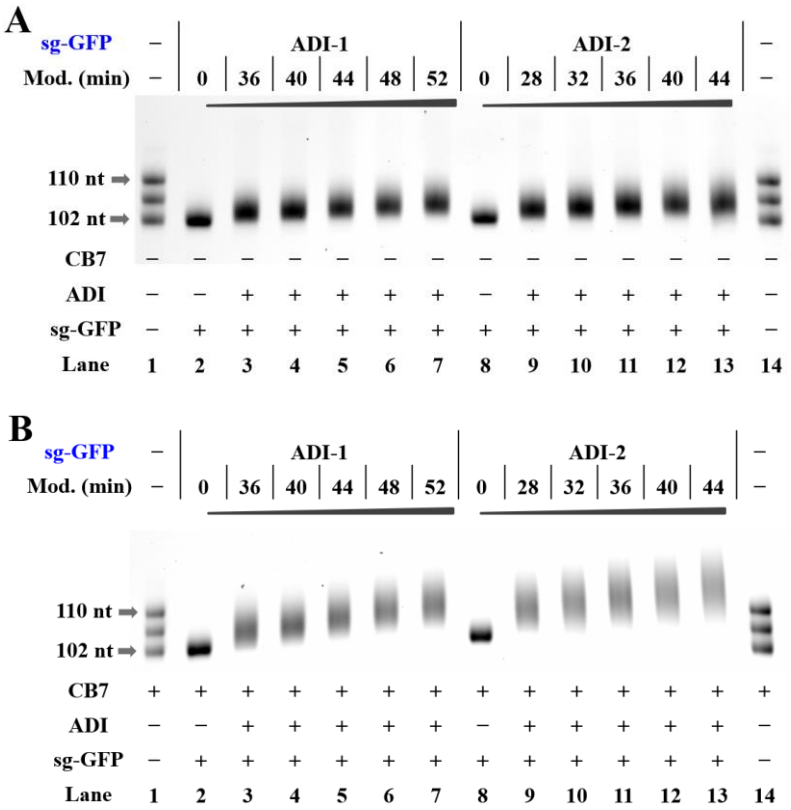

Figure S18. Supramolecular complexation on sg-GFP

Reactions were carried out as described in the Experimental Section. All samples were tested in three biological replicates. Image of representative data is shown here. (**A**) Denaturing PAGE analysis of adamantoyl sg-GFP in the absence of CB7. (**B**) Denaturing PAGE analysis of adamantoyl sg-GFP in the presence of 33 μM CB7. Supramolecular complexation significantly impedes the movement of adamantoyl sg-GFP on the gel. For (**A**) and (**B**), lanes 1, 14: RNA marker (sg-GFP, R-106nt, R-110nt in Table S1); lanes 2, 8: unmodified sg-GFP; lanes 3-7, 9-13: adamantoyl sg-GFP with different modification levels.

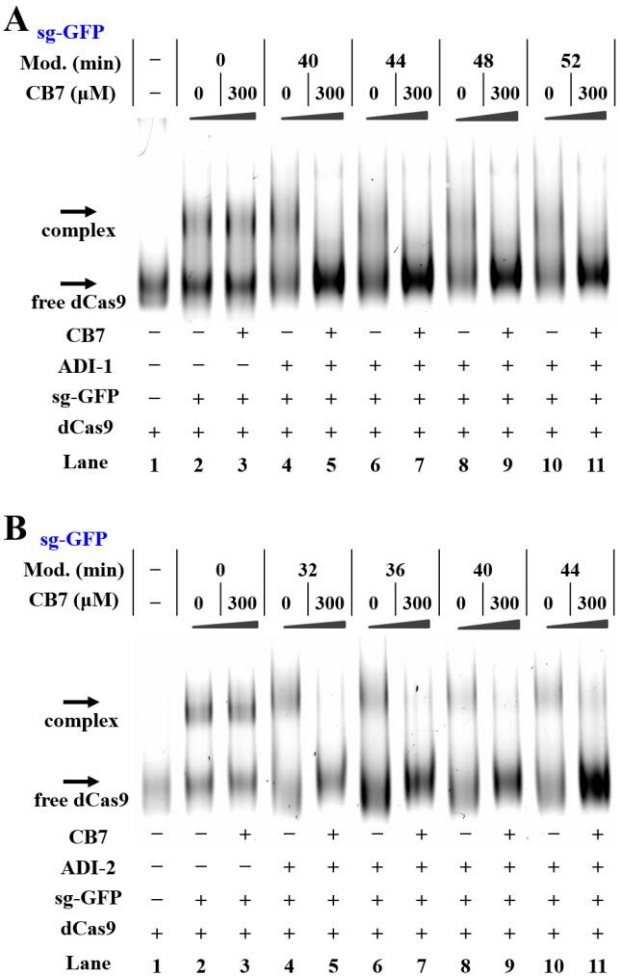

Figure S19. Supramolecular control of the complex formation of Cas9/sg-GFP

Reactions were performed as described in the Experimental Section. EMSA analysis of fluorescently labeled dCas9 is demonstrated. The samples were separated on native 6% PAGE gels. The CB7 treatment blocks the access of the Cas9 to adamantoyl sg-GFP. All samples were tested in three biological replicates. Image of representative data was shown here. (**A**) Modification-dependent inhibition of complex formation between dCas9 and adamantoyl sg-GFP with ADI-1. (**B**) Modification-dependent inhibition of complex formation between dCas9 and adamantoyl sg-GFP with ADI-2. For (**A**) and (**B**), lane 1: no sgRNA control; lanes 2-3 contain unmodified sg-GFP; lanes 4-5, 6-7, 8-9, 10-11 contain adamantoyl sg-GFP with increasing modification levels.

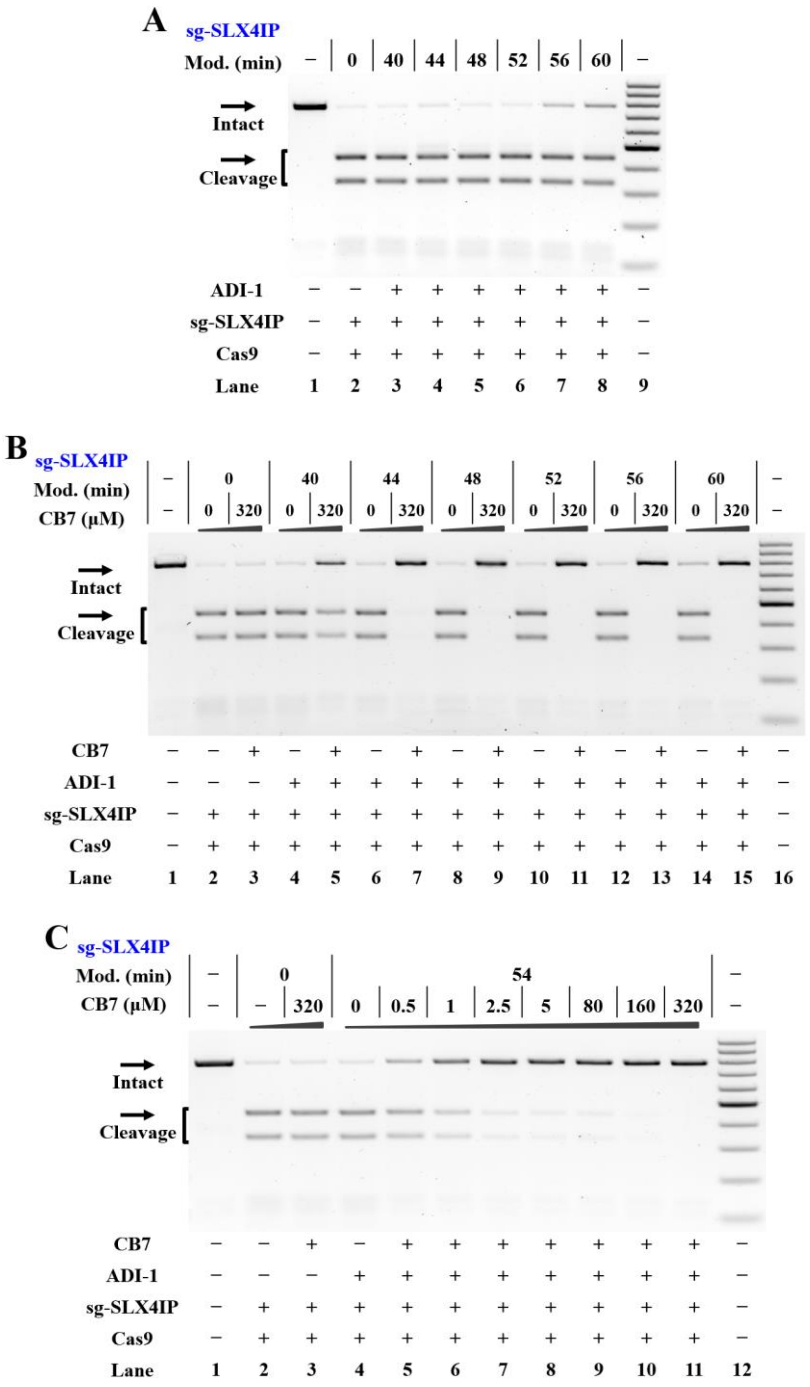

Figure S20. Supramolecular control of Cas9-mediated DNA cleavage (adamantoyl sg-SLX4IP with ADI-1)

Reactions were performed as described in the Experimental Section. All samples were tested in three biological replicates. Image of representative data was shown here. (**A**) The tolerance of Cas9 to adamantoyl sgRNAs (sg-SLX4IP). Lane 1: no Cas9 control; lane 2 contains unmodified sg-SLX4IP; lanes 3-8 contain adamantoyl sg-SLX4IP with increasing modification level; lane 9: DNA marker (GeneRuler 100-bp DNA Ladder). (**B**) Modification-dependent inhibition of CRISPR/Cas9 with adamantoyl sg-SLX4IP with ADI-1. Lane 1: target control; lanes 2-3 contain unmodified sg-SLX4IP; lanes 4-5, 6-7, 8-9, 10-11, 12-13, 14-15 contain adamantoyl sg-SLX4IP with increasing modification level; lane 16: DNA marker. (**C**) Dose-dependent effect of CB7 on inhibition of CRISPR/Cas9. Lane 1: no Cas9 control; lanes 2-3 contain unmodified sg-SLX4IP; lanes 4-11 contain adamantoyl sg-SLX4IP (a 54-min modification with 100 mM ADI-1); lane 12: DNA marker.

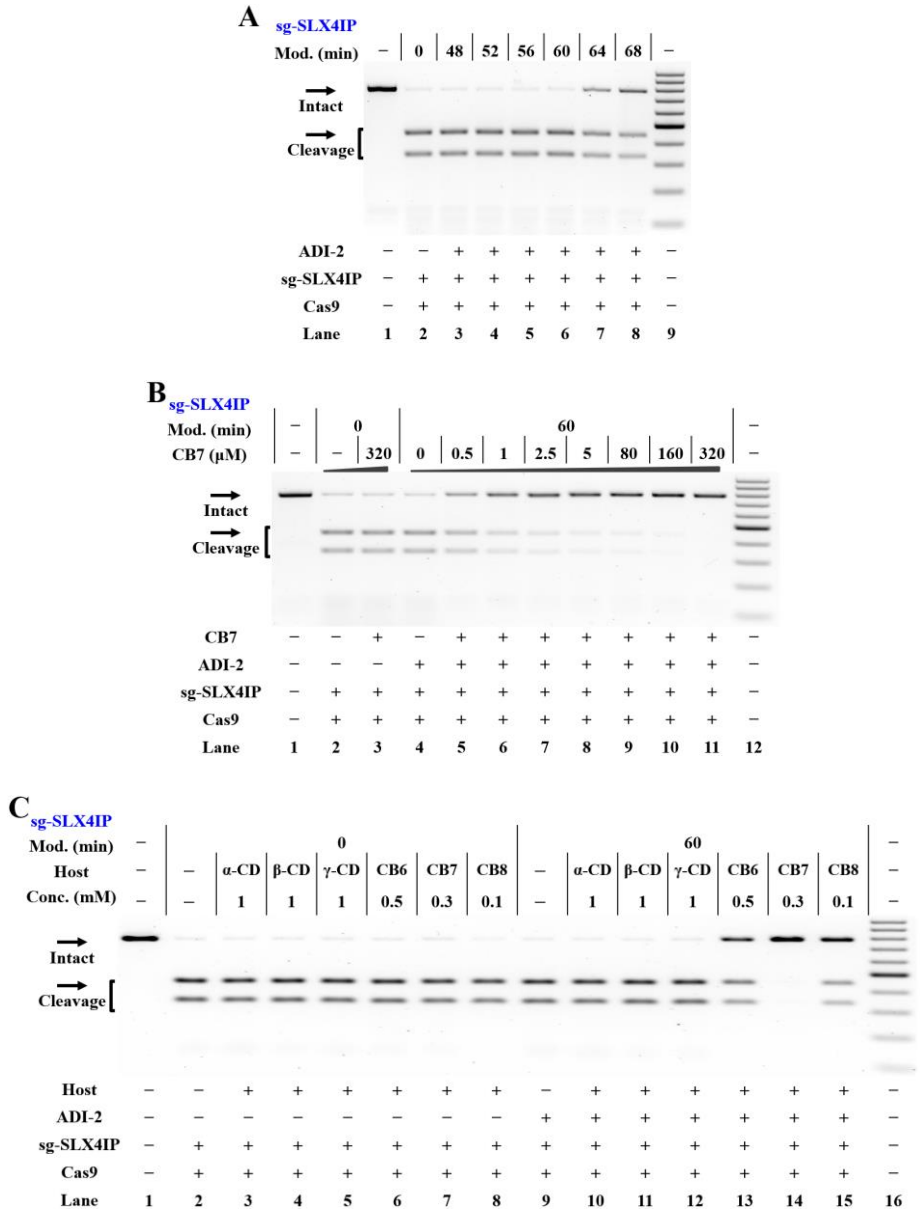

Figure S21. Supramolecular control of Cas9-mediated DNA cleavage (adamantoyl sg-SLX4IP with ADI-2)

Reactions were performed as described in the Experimental Section. All samples were tested in three biological replicates. Image of representative data was shown here. (**A**) The tolerance of Cas9 to adamantoyl sgRNAs (sg-SLX4IP). Lane 1: no Cas9 control; lane 2 contains unmodified sg-SLX4IP; lanes 3-8 contain adamantoyl sg-SLX4IP with increasing modification level; lane 9: DNA marker (GeneRuler 100-bp DNA Ladder). (**B**) Dose-dependent effect of CB7 on inhibition of CRISPR/Cas9. Lane 1: no Cas9 control; lanes 2-3 contain unmodified sg-SLX4IP; lanes 4-11 contain adamantoyl sg-SLX4IP (a 60-min modification with 100 mM ADI-2); lane 12: DNA marker. (**C**) The specificity demonstration for supramolecular regulation. A variety of other host molecules, such as CB6, CB8, α-cyclodextrin (α-CD), β-CD and γ-CD, were included in this study. For poorly soluble CB derivatives (CB6 and CB8), the tests were conducted up to the maximum dissolved concentration under the test conditions. Lane 1: target control; lanes 2-8 contain unmodified sg-SLX4IP; lanes 9-15 contain adamantoyl sg-SLX4IP with a specified modification level (a 60-min modification with 100 mM ADI-2); lane 16: DNA marker.

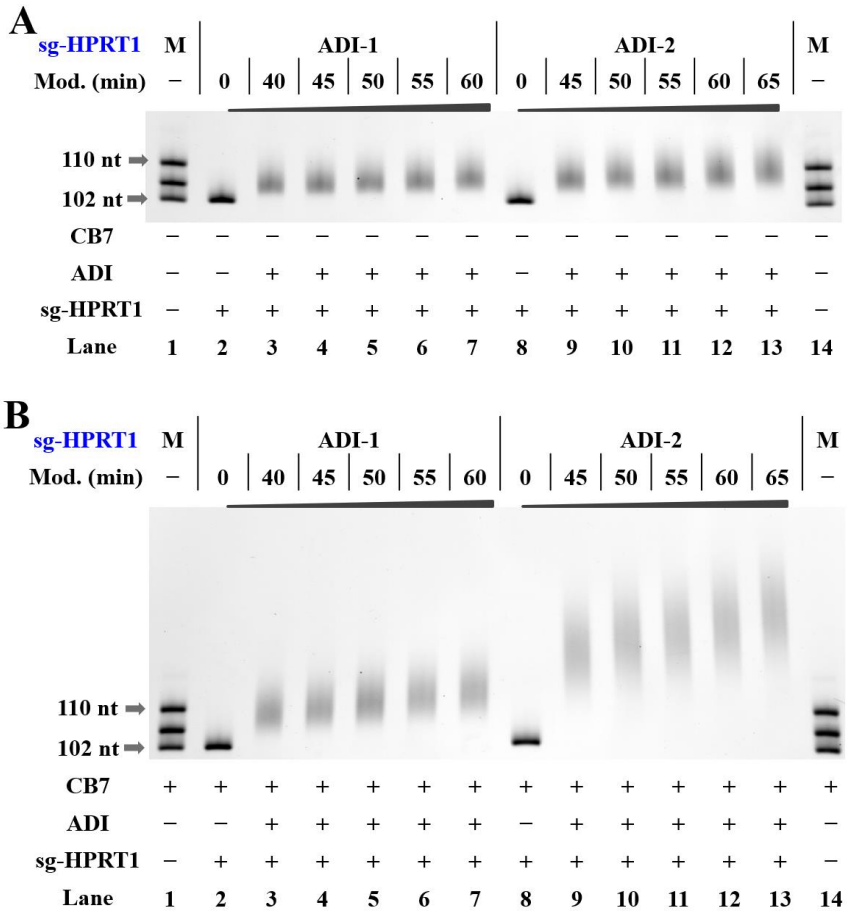

Figure S22. Supramolecular complexation on sg-HPRT1

Reactions were carried out as described in the Experimental Section. All samples were tested in three biological replicates. Image of representative data is shown here. (**A**) Denaturing PAGE analysis of adamantoyl sg-HPRT1 in the absence of CB7. (**B**) Denaturing PAGE analysis of adamantoyl sg-HPRT1 in the presence of 33 μM CB7. Supramolecular complexation significantly impedes the movement of adamantoyl sg-HPRT1 on the gel. For (**A**) and (**B**), lanes 1, 14: RNA marker (sg-HPRT1, R-106nt, R-110nt in Table S1); lanes 2, 8: unmodified sg-HPRT1; lanes 3-7, 9-13: adamantoyl sg-HPRT1 with different modification levels.

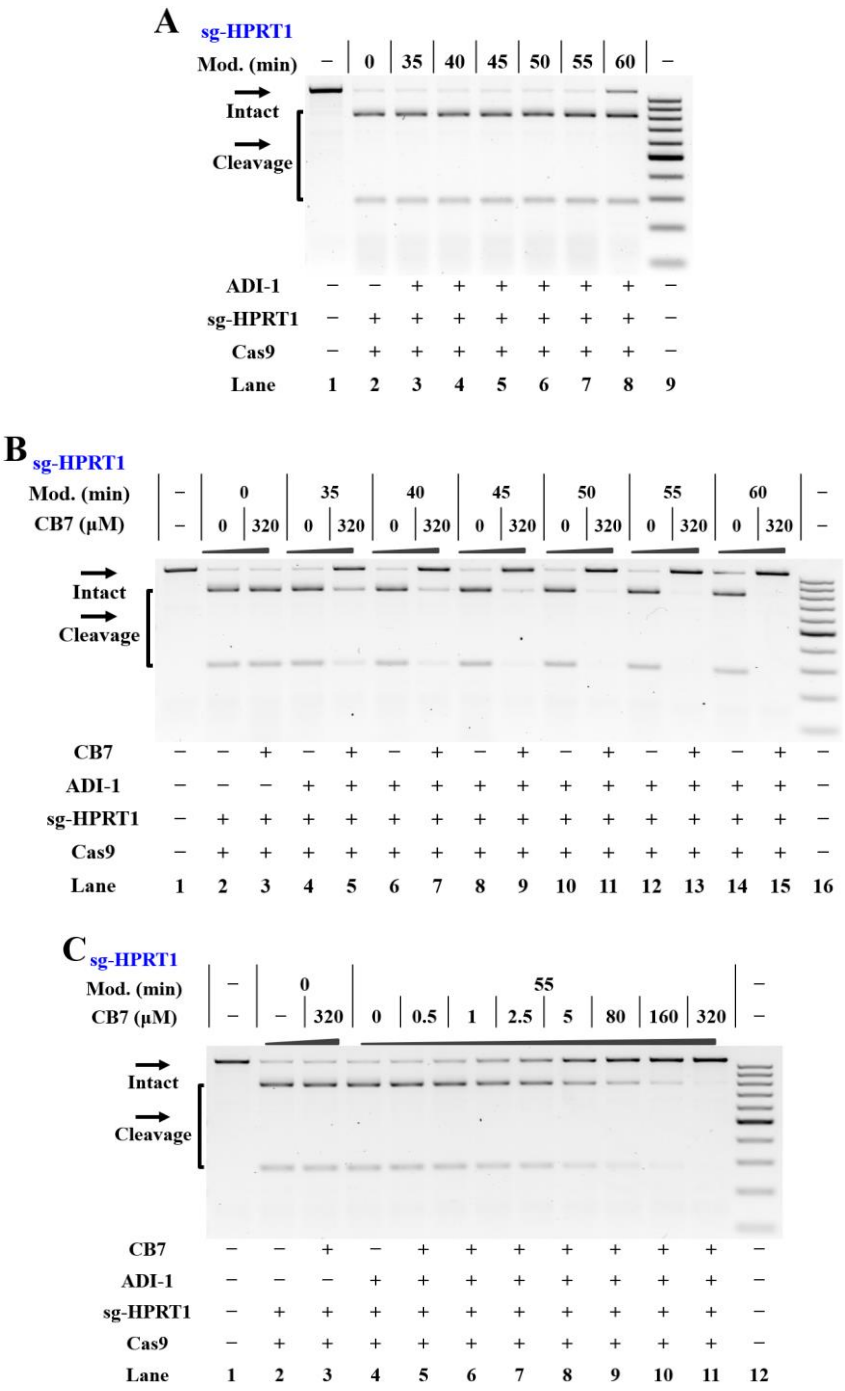

Figure S23. Supramolecular control of Cas9-mediated DNA cleavage (adamantoyl sg-HPRT1 with ADI-1)

Reactions were performed as described in the Experimental Section. All samples were tested in three biological replicates. Image of representative data was shown here. (**A**) The tolerance of Cas9 to adamantoyl sgRNAs (sg-HPRT1). Lane 1: no Cas9 control; lane 2 contains unmodified sg-HPRT1; lanes 3-8 contain adamantoyl sg-HPRT1 with increasing modification level; lane 9: DNA marker (GeneRuler 100-bp DNA Ladder). (**B**) Modification-dependent inhibition of CRISPR/Cas9 with adamantoyl sg-HPRT1 with ADI-1. Lane 1: target control; lanes 2-3 contain unmodified sg-HPRT1; lanes 4-5, 6-7, 8-9, 10-11, 12-13, 14-15 contain adamantoyl sg-HPRT1 with increasing modification levels; lane 16: DNA marker. (**C**) Dose-dependent effect of CB7 on inhibition of CRISPR/Cas9. Lane 1: no Cas9 control; lanes 2-3 contain unmodified sg-HPRT1; lanes 4-11 contain adamantoyl sg-HPRT1 (a 55-min modification with 100 mM ADI-1); lane 12: DNA marker.

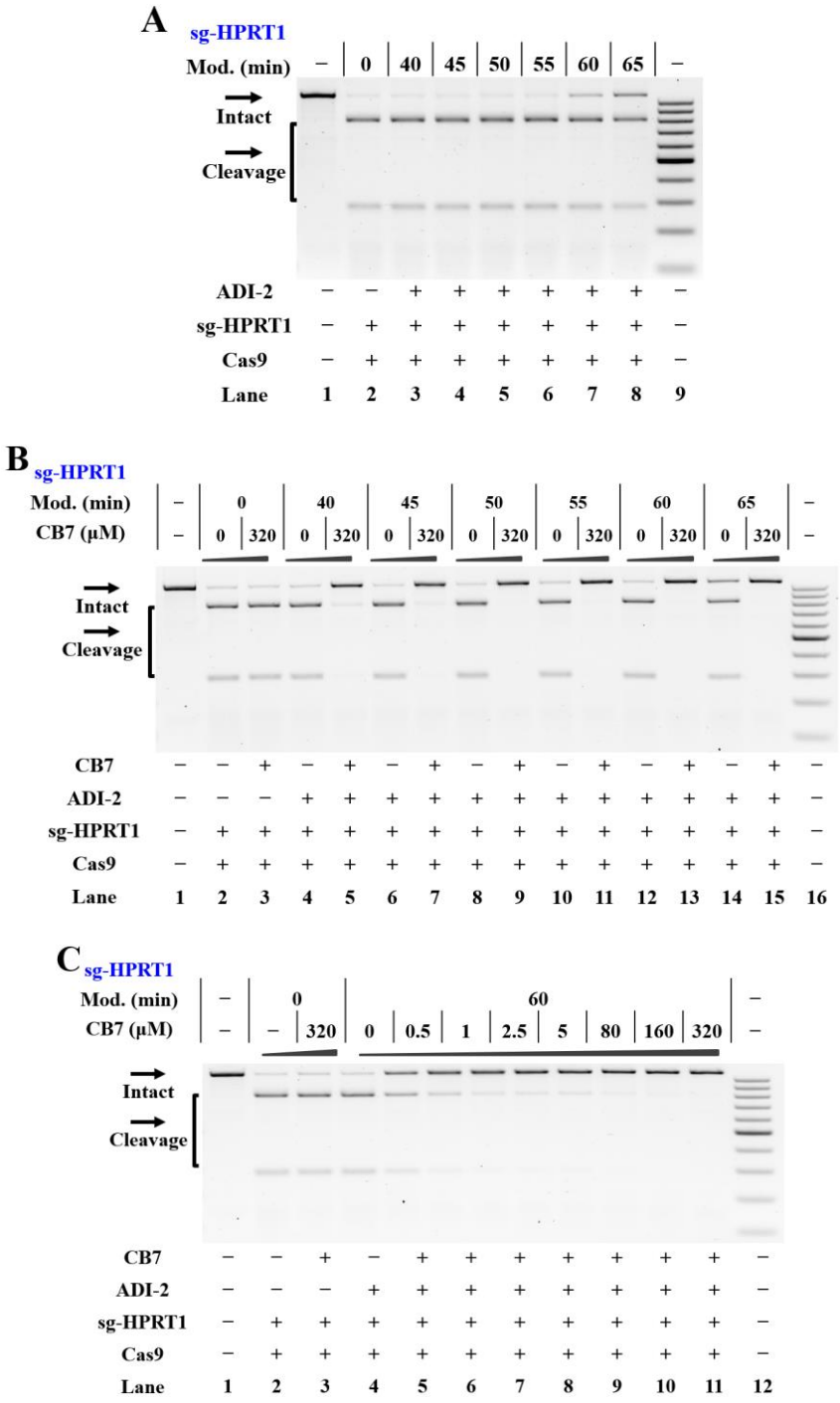

Figure S24. Supramolecular control of Cas9-mediated DNA cleavage (adamantoyl sg-HPRT1 with ADI-2)

Reactions were performed as described in the Experimental Section. All samples were tested in three biological replicates. Image of representative data was shown here. (**A**) The tolerance of Cas9 to adamantoyl sgRNAs (sg-HPRT1). Lane 1: no Cas9 control; lane 2 contains unmodified sg-HPRT1; lanes 3-8 contain adamantoyl sg-HPRT1 with increasing modification level; lane 9: DNA marker (GeneRuler 100-bp DNA Ladder). (**B**) Modification-dependent inhibition of CRISPR/Cas9 with adamantoyl sg-HPRT1 with ADI-2. Lane 1: target control; lanes 2-3 contain unmodified sg-HPRT1; lanes 4-5, 6-7, 8-9, 10-11, 12-13, 14-15 contain adamantoyl sg-HPRT1 with increasing modification levels; lane 16: DNA marker. (**C**) Dose-dependent effect of CB7 on inhibition of CRISPR/Cas9. Lane 1: no Cas9 control; lanes 2-3 contain unmodified sg-HPRT1; lanes 4-11 contain adamantoyl sg-HPRT1 (a 60-min modification with 100 mM ADI-2); lane 12: DNA marker.

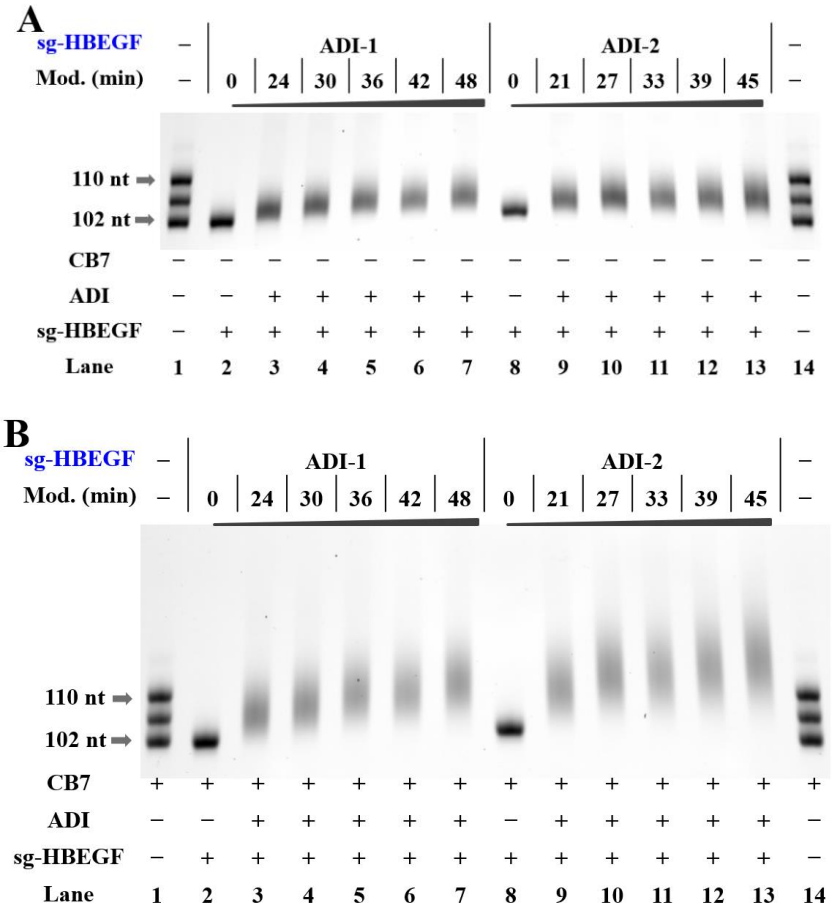

Figure S25. Supramolecular complexation on sg-HBEGF

Reactions were carried out as described in the Experimental Section. All samples were tested in three biological replicates. Image of representative data is shown here. (**A**) Denaturing PAGE analysis of adamantoyl sg-HBEGF in the absence of CB7. (**B**) Denaturing PAGE analysis of adamantoyl sg-HBEGF in the presence of 33 μM CB7. Supramolecular complexation significantly impedes the movement of adamantoyl sg-HBEGF on the gel. For (**A**) and (**B**), lanes 1, 14: RNA marker (sg-HBEGF, R-106nt, R-110nt in Table S1); lanes 2, 8: unmodified sg-HBEGF; lanes 3-7, 9-13: adamantoyl sg-HBEGF with different modification levels.

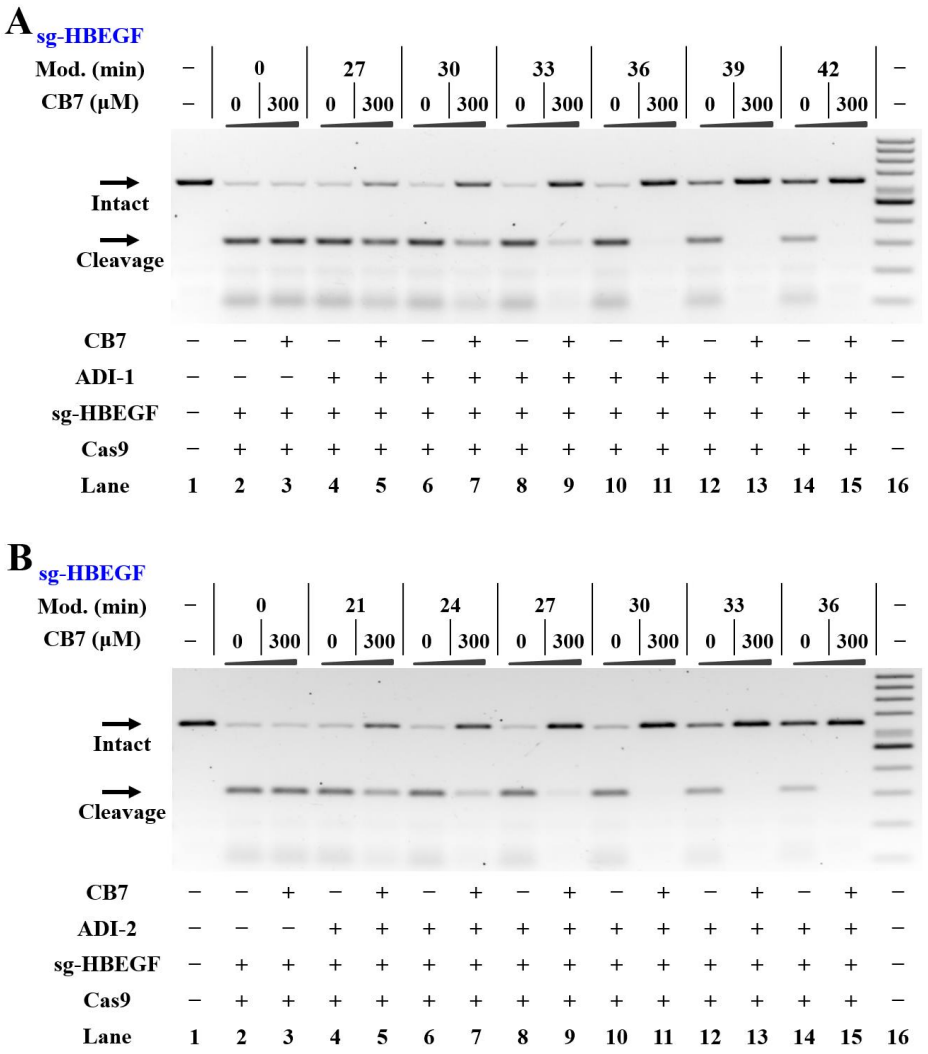

Figure S26. Supramolecular control of Cas9-mediated DNA cleavage (adamantoyl sg-HBEGF)

Reactions were performed as described in the Experimental Section. All samples were tested in three biological replicates. Image of representative data was shown here. (**A**) Modification-dependent inhibition of CRISPR/Cas9 with adamantoyl sg-HBEGF with ADI-1. (**B**) Modification-dependent inhibition of CRISPR/Cas9 with adamantoyl sg-HBEGF with ADI-2. For (**A**) and (**B**), lane 1: target control; lanes 2-3 contain unmodified sg-HBEGF; lanes 4-5, 6-7, 8-9, 10-11, 12-13, 14-15 contain adamantoyl sg-HBEGF with increasing modification levels; lane 16: DNA marker (GeneRuler 100-bp DNA Ladder).

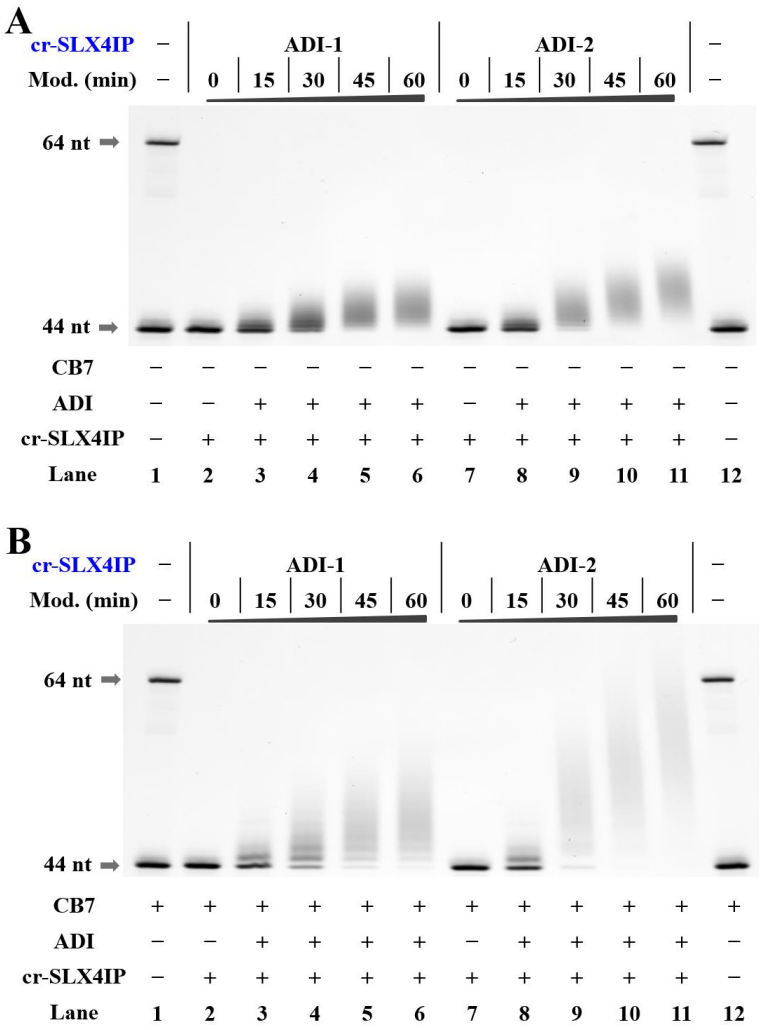

Figure S27. Supramolecular complexation on cr-SLX4IP

Reactions were carried out as described in the Experimental Section. All samples were tested in three biological replicates. Image of representative data is shown here. (**A**) Denaturing PAGE analysis of adamantoyl cr-SLX4IP in the absence of CB7. (**B**) Denaturing PAGE analysis of adamantoyl cr-SLX4IP in the presence of 33 μM CB7. Supramolecular complexation significantly impedes the movement of adamantoyl cr-SLX4IP on the gel. For (**A**) and (**B**), lanes 1, 12: RNA marker (cr-SLX4IP, R-64nt in Table S1); lanes 2, 7: unmodified cr-SLX4IP; lanes 3-6, 8-11: adamantoyl cr-SLX4IP with different modification levels.

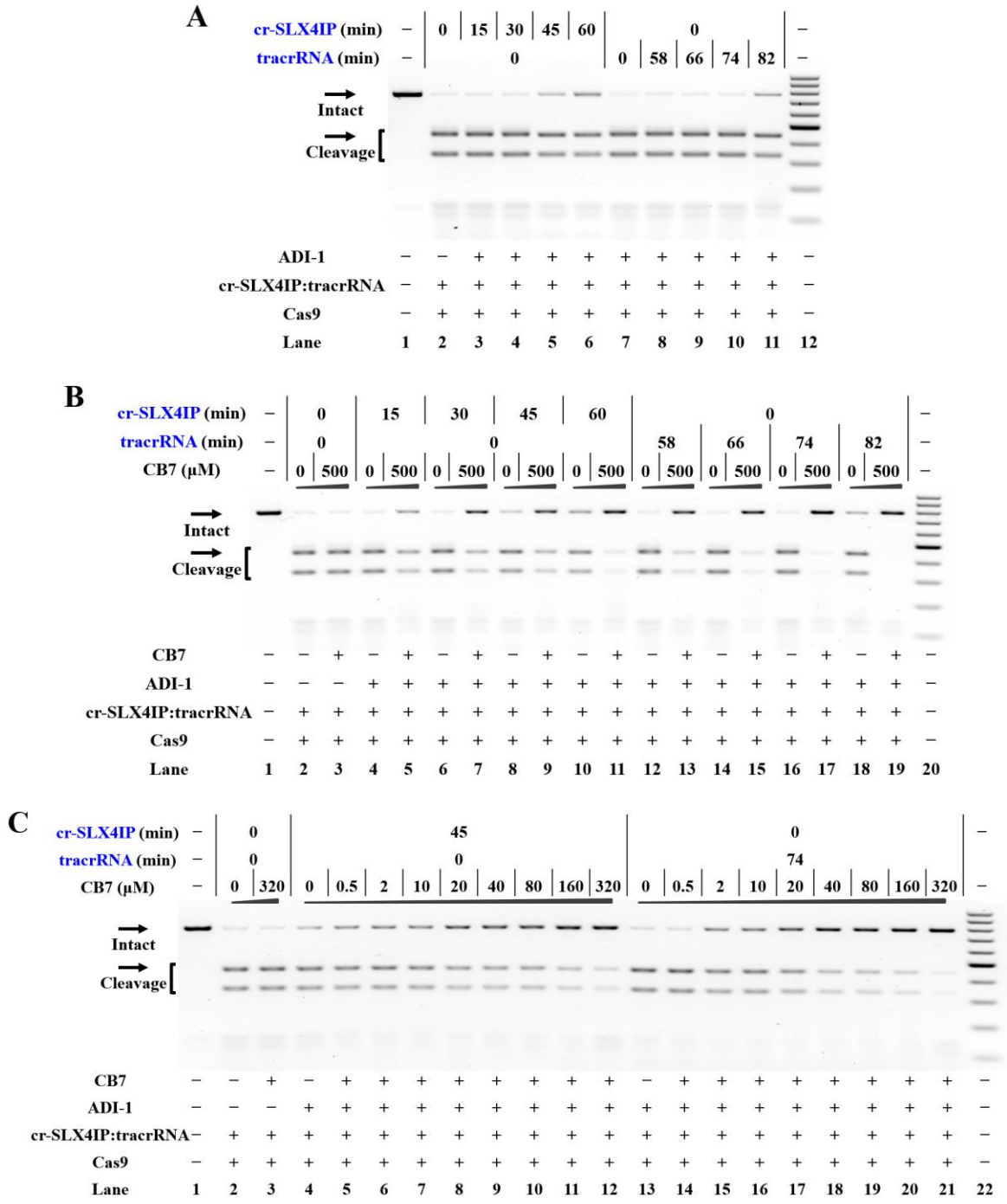

Figure S28. Supramolecular control of Cas9-medated DNA cleavage (either cr-SLX4IP or tracrRNA is modified with ADI-1)

Reactions were performed as described in the Experimental Section. All samples were tested in three biological replicates. Image of representative data was shown here. (**A**) The tolerance of Cas9 to adamantoyl cr-SLX4IP or adamantoyl tracrRNA. Lane 1: no Cas9 control; lanes 2, 7 contain unmodified cr-SLX4IP and unmodified tracrRNA; lanes 3-6 contain unmodified tracrRNA and adamantoyl cr-SLX4IP with increasing modification level; lanes 8-11 contain unmodified cr-SLX4IP and adamantoyl tracrRNA with increasing modification level; lane 12: DNA marker (GeneRuler 100-bp DNA Ladder). (**B**) Modification-dependent inhibition of CRISPR/Cas9 with adamantoyl cr-SLX4IP or adamantoyl tracrRNA. Lane 1: no Cas9 control; lanes 2-3 contain unmodified cr-SLX4IP and unmodified tracrRNA; lanes 4-11 contain unmodified tracrRNA and adamantoyl cr-SLX4IP with

increasing modification level; lanes 12-19 contain unmodified cr-SLX4IP and adamantoyl tracrRNA with increasing modification level; lane 20: DNA marker. (**C**) Dose-dependent effect of CB7 complexation on inhibition of CRISPR/Cas9 with a separate crRNA and tracrRNA. In this study, either cr-SLX4IP or tracrRNA was adamantoylated with ADI-1. Lane 1: no Cas9 control; lanes 2-3 contain unmodified cr-SLX4IP and tracrRNA; lanes 4-12 contain unmodified tracrRNA and adamantoyl cr-SLX4IP (a 45-min modification with 100 mM ADI-1); lanes 13-21 contain unmodified cr-SLX4IP and adamantoyl tracrRNA (a 74-min modification with 100 mM ADI-1); lane 22: DNA marker.

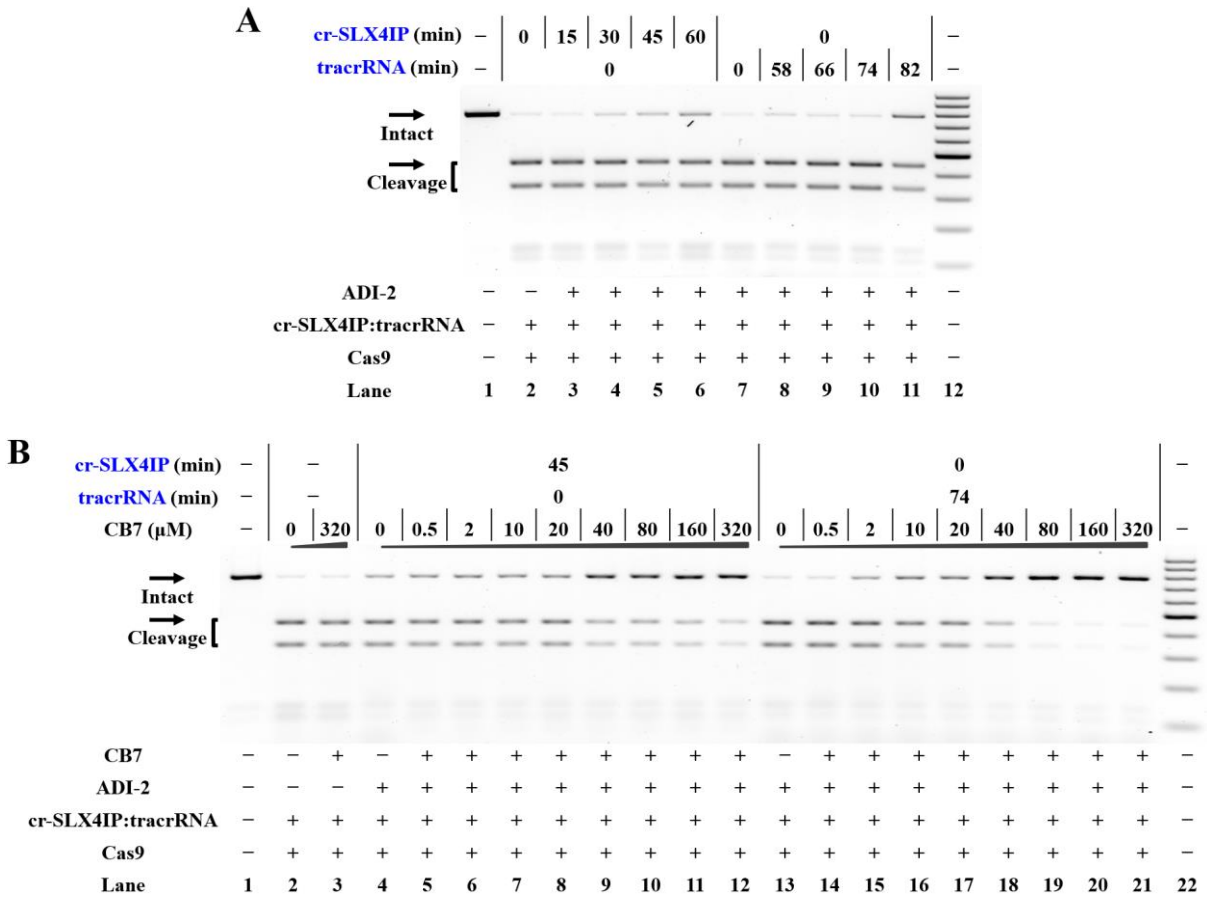

Figure S29. Supramolecular control of Cas9-medated DNA cleavage (either cr-SLX4IP or tracrRNA is modified with ADI-2)

Reactions were performed as described in the Experimental Section. All samples were tested in three biological replicates. Image of representative data was shown here. (**A**) The tolerance of Cas9 to adamantoyl cr-SLX4IP or adamantoyl tracrRNA. Lane 1: no Cas9 control; lanes 2, 7 contain unmodified cr-SLX4IP and unmodified tracrRNA; lanes 3-6 contain unmodified tracrRNA and adamantoyl cr-SLX4IP with increasing modification level; lanes 8-11 contain unmodified cr-SLX4IP and adamantoyl tracrRNA with increasing modification level; lane 12: DNA marker (GeneRuler 100-bp DNA Ladder). (**B**) Dose-dependent effect of CB7 complexation on inhibition of CRISPR/Cas9 with a separate crRNA and tracrRNA. In this study, either cr-SLX4IP or tracrRNA was adamantoylated with ADI-2. Lane 1: no Cas9 control; lanes 2-3 contain unmodified cr-SLX4IP and tracrRNA; lanes 4-12 contain unmodified tracrRNA and adamantoyl cr-SLX4IP (a 45-min modification with 100 mM ADI-2); lanes 13-21 contain unmodified cr-SLX4IP and adamantoyl tracrRNA (a 74-min modification with 100 mM ADI-2); lane 22: DNA marker.

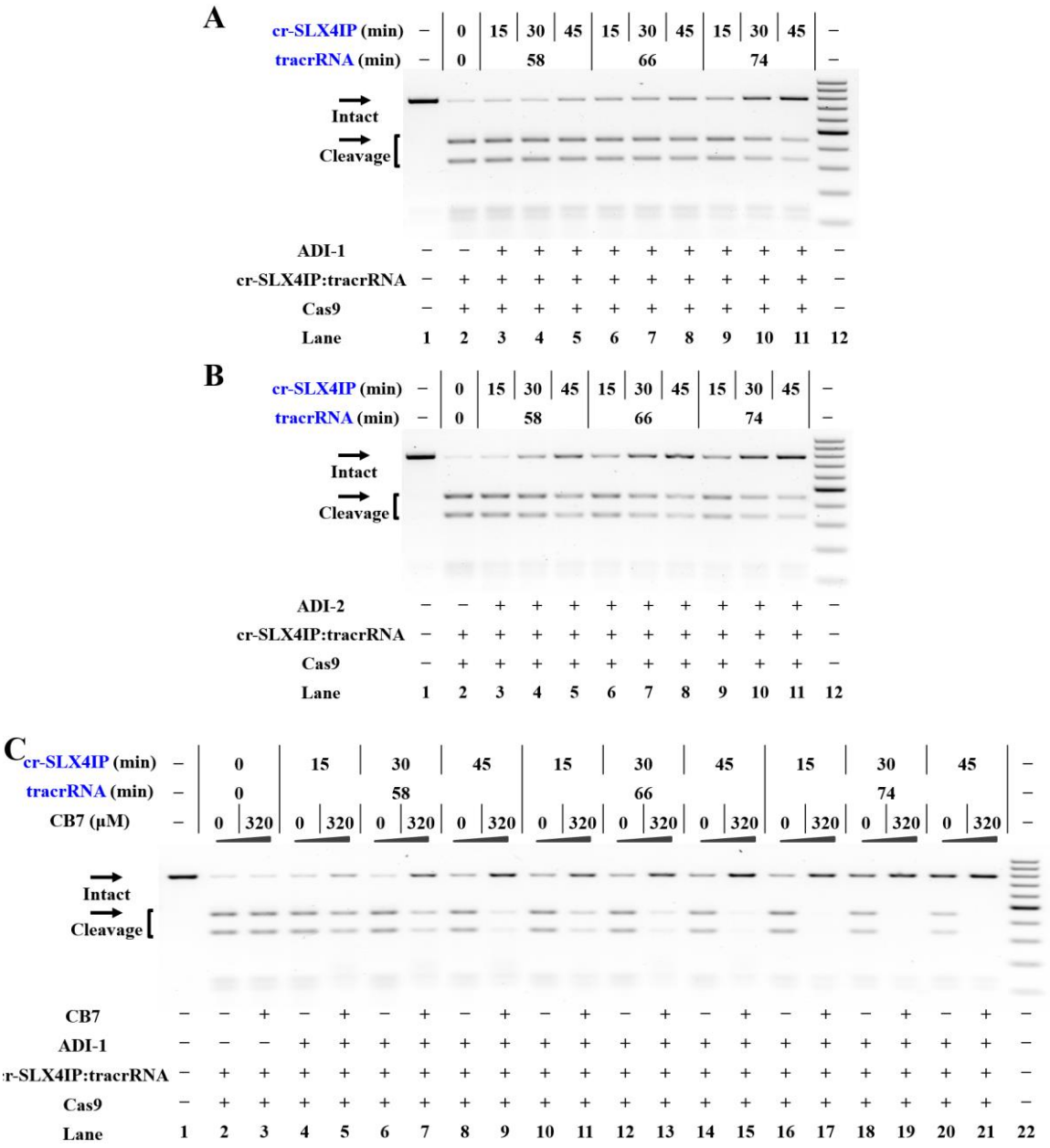

Figure S30. Supramolecular control of Cas9-medated DNA cleavage (both cr-SLX4IP and tracrRNA are adamantoylated)

Reactions were performed as described in the Experimental Section. In this study, adamantoyl cr-SLX4IP and adamantoyl tracrRNA were used. The treatment for each sample is indicated by the signs at the bottom of each lane. All samples were tested in three biological replicates. Image of representative data is shown here. (**A**) The tolerance of Cas9 to adamantoyl cr-SLX4IP and adamantoyl tracrRNA. Both cr-SLX4IP and tracrRNA are modified with ADI-1. (**B**) The tolerance of Cas9 to adamantoyl cr-SLX4IP and adamantoyl tracrRNA. Both cr-SLX4IP and tracrRNA are modified with ADI-2. (**C**) Modification-dependent inhibition of CRISPR/Cas9 with adamantoyl cr-SLX4IP and adamantoyl tracrRNA. Lane 1: no Cas9 control; lanes 2-3 contain unmodified cr-SLX4IP and unmodified tracrRNA; lanes 4-9, 10-15, 16-21 contain adamantoyl cr-SLX4IP and adamantoyl tracrRNA with increasing modification level; lane 22: DNA marker (GeneRuler 100-bp DNA Ladder). For (**A**) and (**B**), lane 1: no Cas9 control; lane 2 contains unmodified cr-SLX4IP and unmodified tracrRNA; lanes 3-11 contain adamantoyl cr-SLX4IP and adamantoyl tracrRNA with increasing modification levels; lane 12: DNA marker.

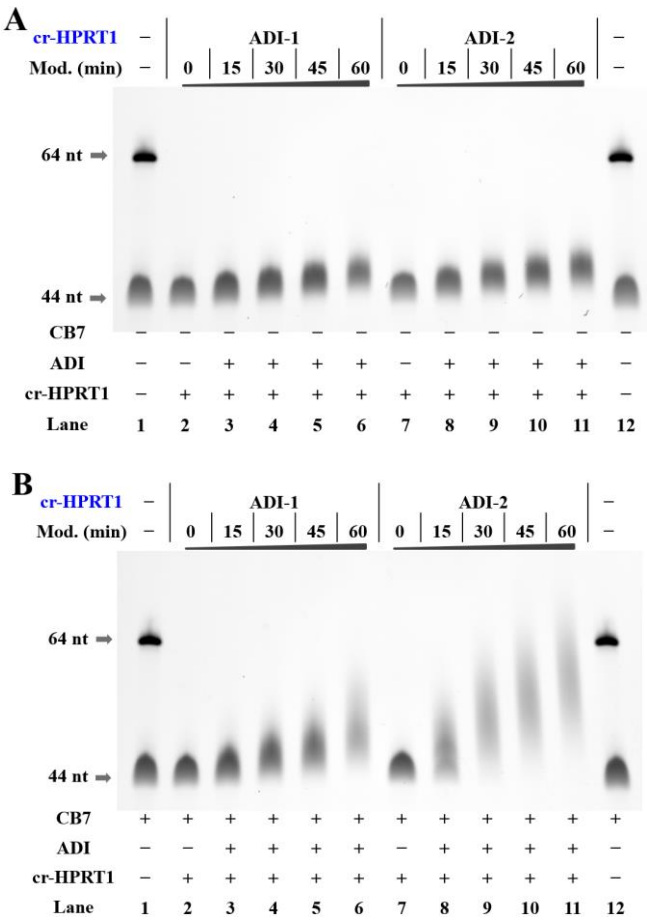

Figure S31. Supramolecular complexation on cr-HPRT1

Reactions were carried out as described in the Experimental Section. All samples were tested in three biological replicates. Image of representative data is shown here. (**A**) Denaturing PAGE analysis of adamantoyl cr-HPRT1 in the absence of CB7. (**B**) Denaturing PAGE analysis of adamantoyl cr-HPRT1 in the presence of 33 μM CB7. Supramolecular complexation significantly impedes the movement of adamantoyl cr-HPRT1 on the gel. For (**A**) and (**B**), lanes 1, 12: RNA marker (cr-HPRT1, R-64nt in Table S1); lanes 2, 7: unmodified cr-HPRT1; lanes 3-6, 8-11: adamantoyl cr-HPRT1 with different modification levels.

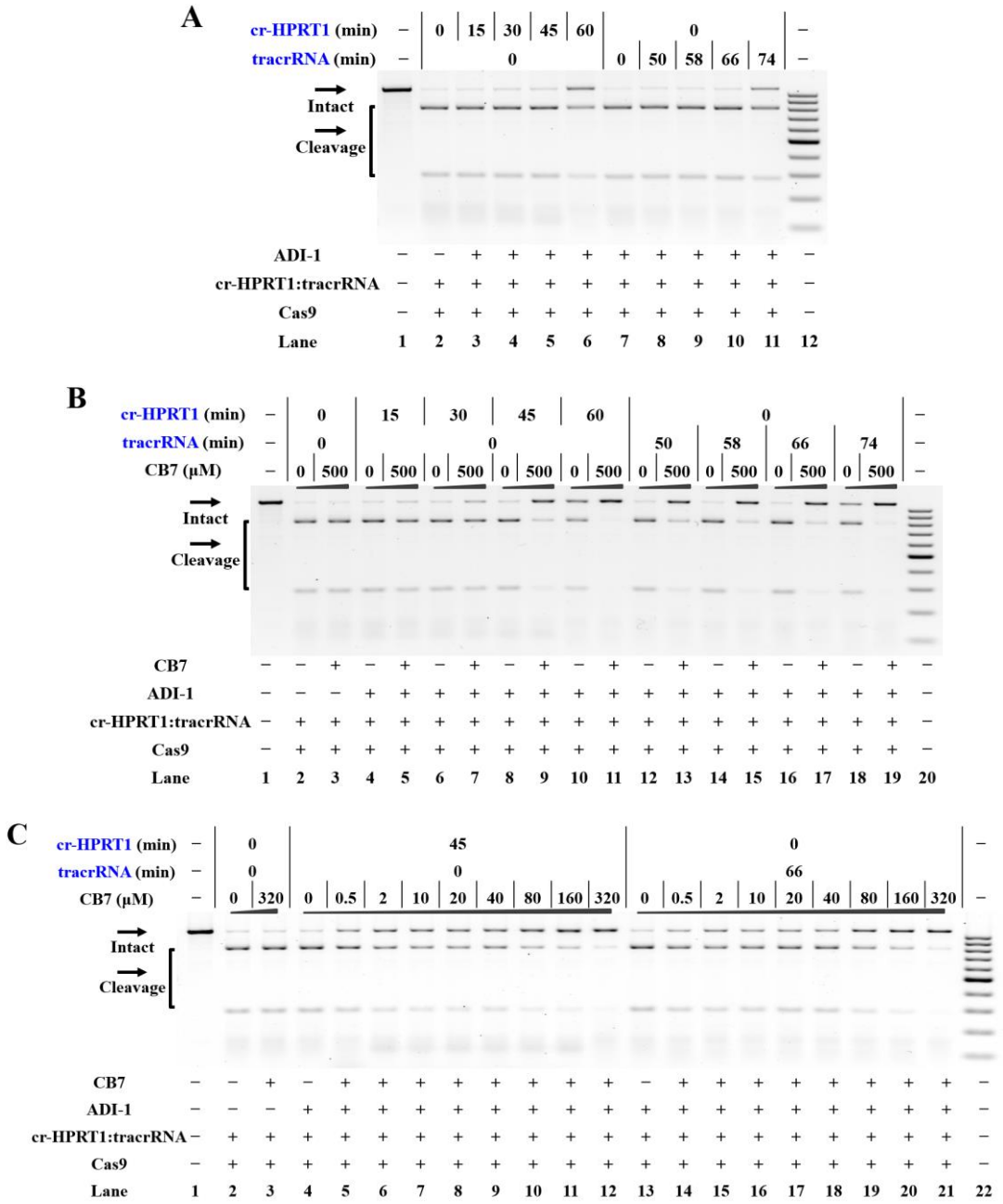

Figure S32. Supramolecular control of Cas9-medated DNA cleavage (either cr-HPRT1 or tracrRNA is modified with ADI-1)

Reactions were performed as described in the Experimental Section. All samples were tested in three biological replicates. Image of representative data was shown here. (**A**) The tolerance of Cas9 to adamantoyl cr-HPRT1 or adamantoyl tracrRNA. Lane 1: no Cas9 control; lanes 2, 7 contain unmodified cr-HPRT1 and unmodified tracrRNA; lanes 3-6 contain unmodified tracrRNA and adamantoyl cr-HPRT1 with increasing modification level; lanes 8-11 contain unmodified cr-HPRT1 and adamantoyl tracrRNA with increasing modification level; lane 12: DNA marker (GeneRuler 100-bp DNA Ladder). (**B**) Modification-dependent inhibition of CRISPR/Cas9 with adamantoyl cr-HPRT1 or adamantoyl tracrRNA. Lane 1: no Cas9 control; lanes 2-3 contain unmodified cr-HPRT1 and unmodified tracrRNA; lanes 4-11 contain unmodified tracrRNA and adamantoyl cr-HPRT1 with increasing modification level; lanes 12-19 contain unmodified cr-HPRT1 and adamantoyl tracrRNA with increasing modification level; lane 20: DNA marker. (**C**) Dose-dependent effect of CB7 complexation on inhibition of

CRISPR/Cas9 with a separate crRNA and tracrRNA. In this study, either cr-HPRT1 or tracrRNA was adamantoylated. Lane 1: no Cas9 control; lanes 2-3 contain unmodified cr-HPRT1 and tracrRNA; lanes 4-12 contain unmodified tracrRNA and adamantoyl cr-HPRT1 (a 45-min modification with 100 mM ADI-1); lanes 13-21 contain unmodified cr-HPRT1 and adamantoyl tracrRNA (a 66-min modification with 100 mM ADI-1); lane 22: DNA marker.

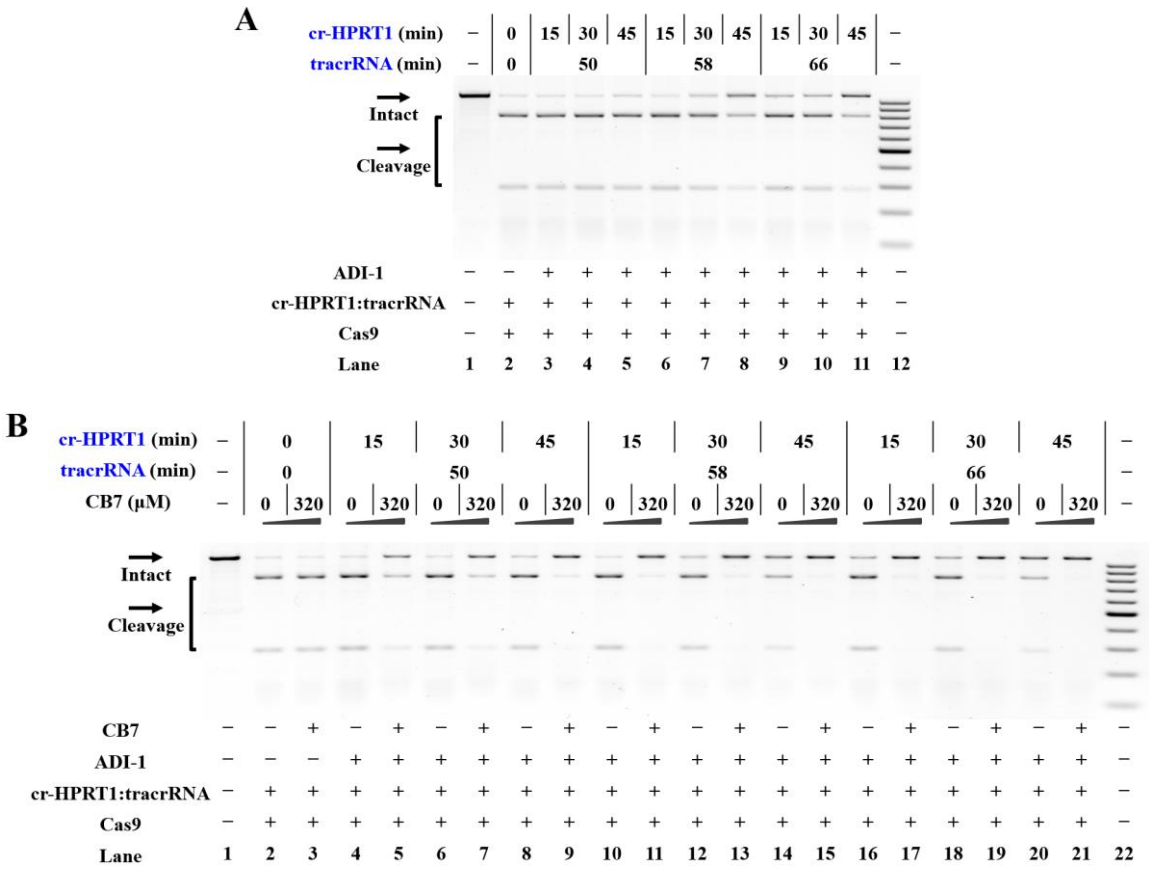

Figure S33. Supramolecular control of Cas9-medated DNA cleavage (both cr-HPRT1 and tracrRNA are modified with ADI-1)

Reactions were performed as described in the Experimental Section. In this study, adamantoyl cr-HPRT1 and adamantoyl tracrRNA were used. The treatment for each sample is indicated by the signs at the bottom of each lane. All samples were tested in three biological replicates. Image of representative data is shown here. (**A**) The tolerance of Cas9 to adamantoyl cr-HPRT1 and adamantoyl tracrRNA. Lane 1: no Cas9 control; lane 2 contains unmodified cr-HPRT1 and unmodified tracrRNA; lanes 3-11 contain adamantoyl cr-HPRT1 and adamantoyl tracrRNA with increasing modification levels; lane 12: DNA marker (GeneRuler 100-bp DNA Ladder). (**B**) Modification-dependent inhibition of CRISPR/Cas9 with adamantoyl cr-HPRT1 and adamantoyl tracrRNA. Lane 1: no Cas9 control; lanes 2-3 contain unmodified cr-HPRT1 and unmodified tracrRNA; lanes 4-9, 10-15, 16-21 contain adamantoyl cr-HPRT1 and adamantoyl tracrRNA with increasing modification levels; lane 22: DNA marker.

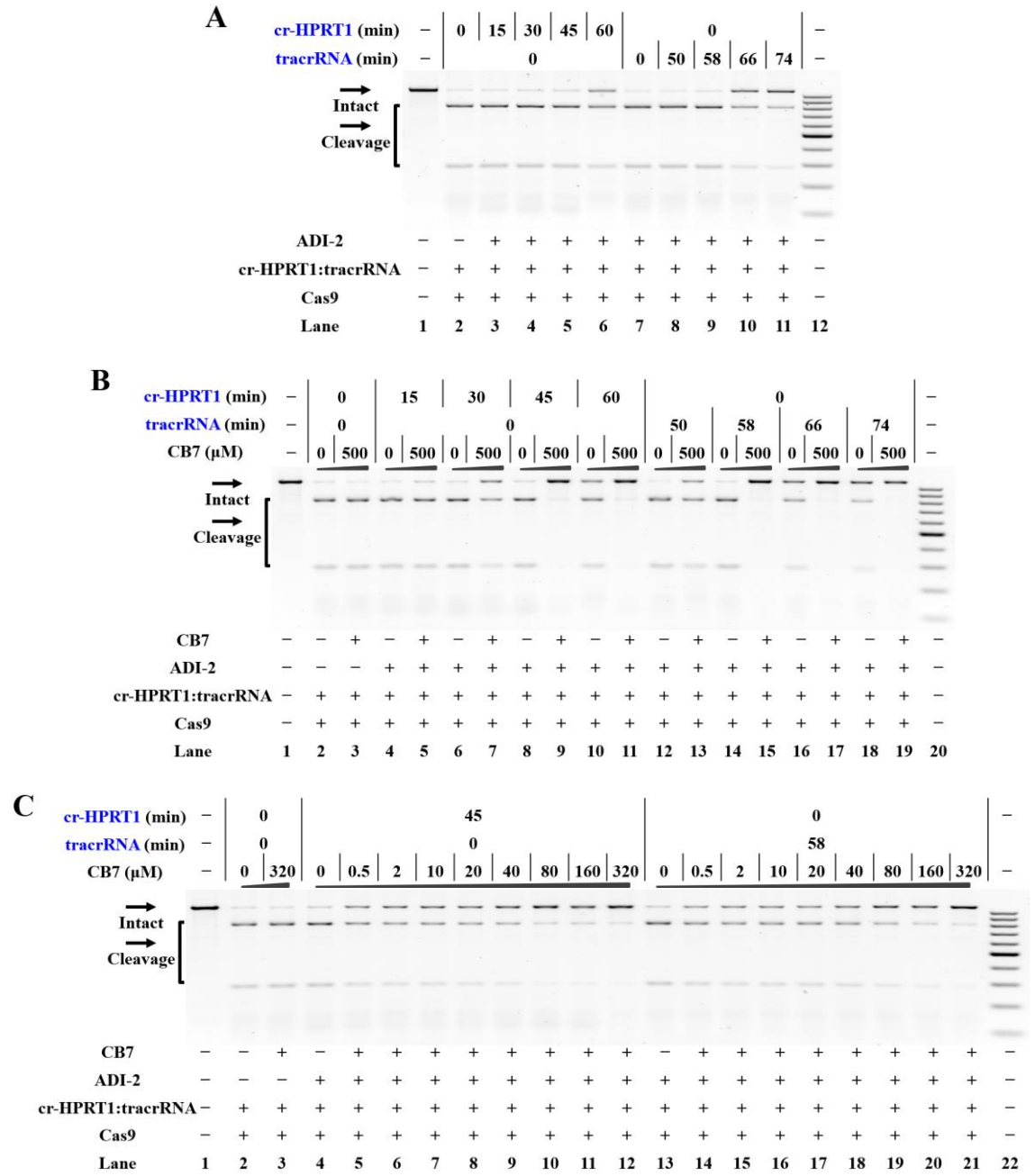

Figure S34. Supramolecular control of Cas9-medated DNA cleavage (either cr-HPRT1 or tracrRNA is modified with ADI-2)

Reactions were performed as described in the Experimental Section. All samples were tested in three biological replicates. Image of representative data was shown here. (**A**) The tolerance of Cas9 to adamantoyl cr-HPRT1 or adamantoyl tracrRNA. Lane 1: no Cas9 control; lanes 2, 7 contain unmodified cr-HPRT1 and unmodified tracrRNA; lanes 3-6 contain unmodified tracrRNA and adamantoyl cr-HPRT1 with increasing modification levels; lanes 8-11 contain unmodified cr-HPRT1 and adamantoyl tracrRNA with increasing modification levels; lane 12: DNA marker (GeneRuler 100-bp DNA Ladder). (**B**) Modification-dependent inhibition of CRISPR/Cas9 with adamantoyl cr-HPRT1 or adamantoyl tracrRNA. Lane 1: no Cas9 control; lanes 2-3 contain unmodified cr-HPRT1 and unmodified tracrRNA; lanes 4-11 contain unmodified tracrRNA and adamantoyl cr-HPRT1 with increasing modification levels; lanes 12-19 contain unmodified cr-HPRT1 and adamantoyl tracrRNA with increasing modification levels; lane 20: DNA marker. (**C**) Dose-dependent effect of CB7 complexation on inhibition of

CRISPR/Cas9 with a separate crRNA and tracrRNA. In this study, either cr-HPRT1 or tracrRNA was adamantoylated with ADI-2. Lane 1: no Cas9 control; lanes 2-3 contain unmodified cr-HPRT1 and tracrRNA; lanes 4-12 contain unmodified tracrRNA and adamantoyl cr-HPRT1 (a 45-min modification with 100 mM ADI-2); lanes 13-21 contain unmodified cr-HPRT1 and adamantoyl tracrRNA (a 66-min modification with 100 mM ADI-2); lane 22: DNA marker.

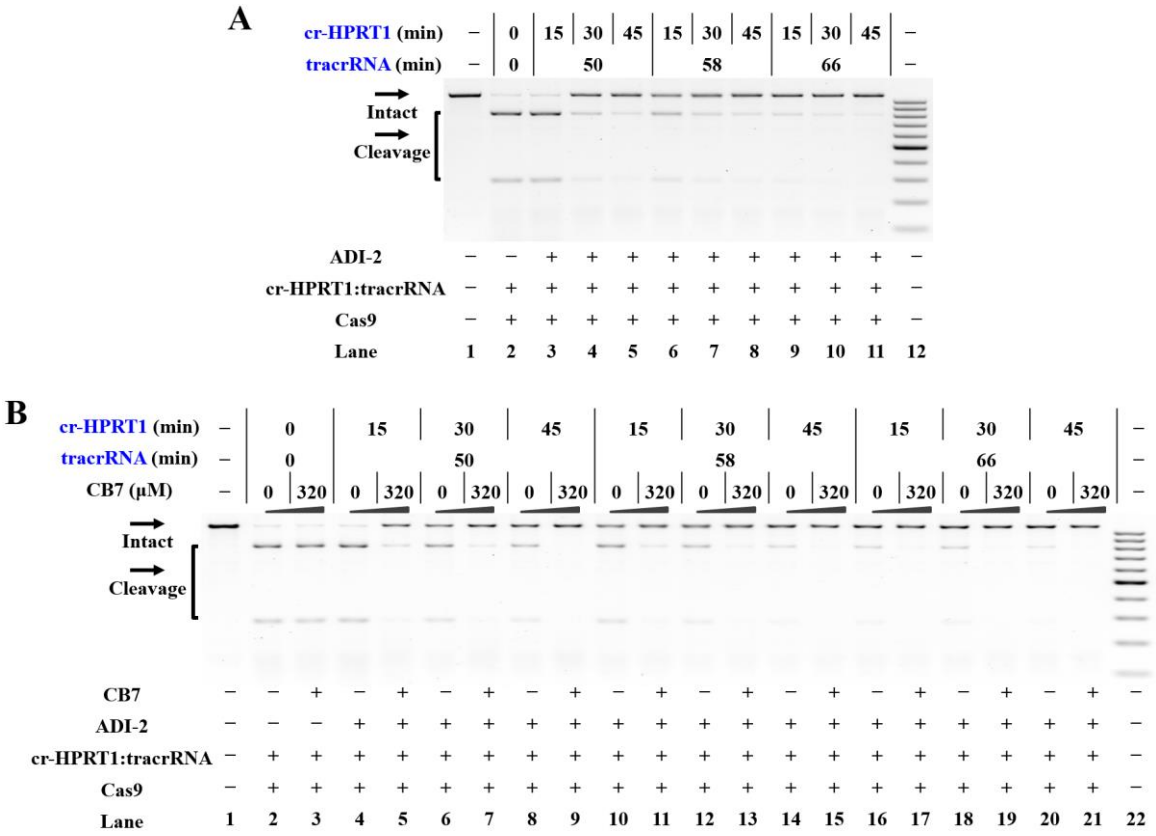

Figure S35. Supramolecular control of Cas9-medated DNA cleavage (both cr-HPRT1 and tracrRNA are modified with ADI-2)

Reactions were performed as described in the Experimental Section. In this study, adamantoyl cr-HPRT1 and adamantoyl tracrRNA were used. The treatment for each sample is indicated by the signs at the bottom of each lane. All samples were tested in three biological replicates. Image of representative data is shown here. (**A**) The tolerance of Cas9 to adamantoyl cr-HPRT1 and adamantoyl tracrRNA. Lane 1: no Cas9 control; lane 2 contains unmodified cr-HPRT1 and unmodified tracrRNA; lanes 3-11 contain adamantoyl cr-HPRT1 and adamantoyl tracrRNA with increasing modification levels; lane 12: DNA marker (GeneRuler 100-bp DNA Ladder). (**B**) Modification-dependent inhibition of CRISPR/Cas9 with adamantoyl cr-HPRT1 and adamantoyl tracrRNA. Lane 1: no Cas9 control; lanes 2-3 contain unmodified cr-HPRT1 and unmodified tracrRNA; lanes 4-9, 10-15, 16-21 contain adamantoyl cr-HPRT1 and adamantoyl tracrRNA with increasing modification levels; lane 22: DNA marker.

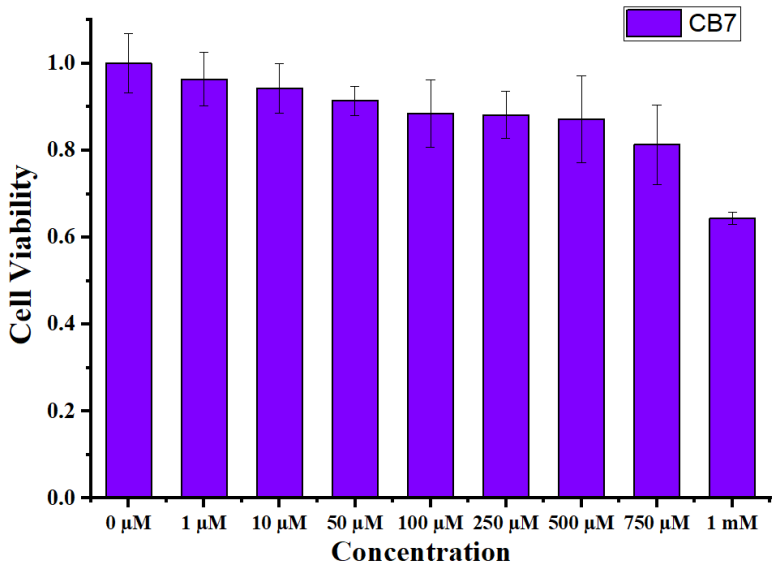

Figure S36. The tolerance of HeLa-OC cells to CB7

HeLa-OC cells were treated with CB7 at different concentrations and toxicity was measured using the the 3-(4,5-dimethylthiazol-2-yl)-2,5-diphenyltetrazolium bromide (MTT) cytotoxicity assay. Values were plotted relative to the mean of DMEM control set to 100% (= relative growth). All data were presented as the means ± SEM from three independent experiments. Error bars: ±SEM. The cytotoxicity threshold for CB7 was higher than 500 μM.

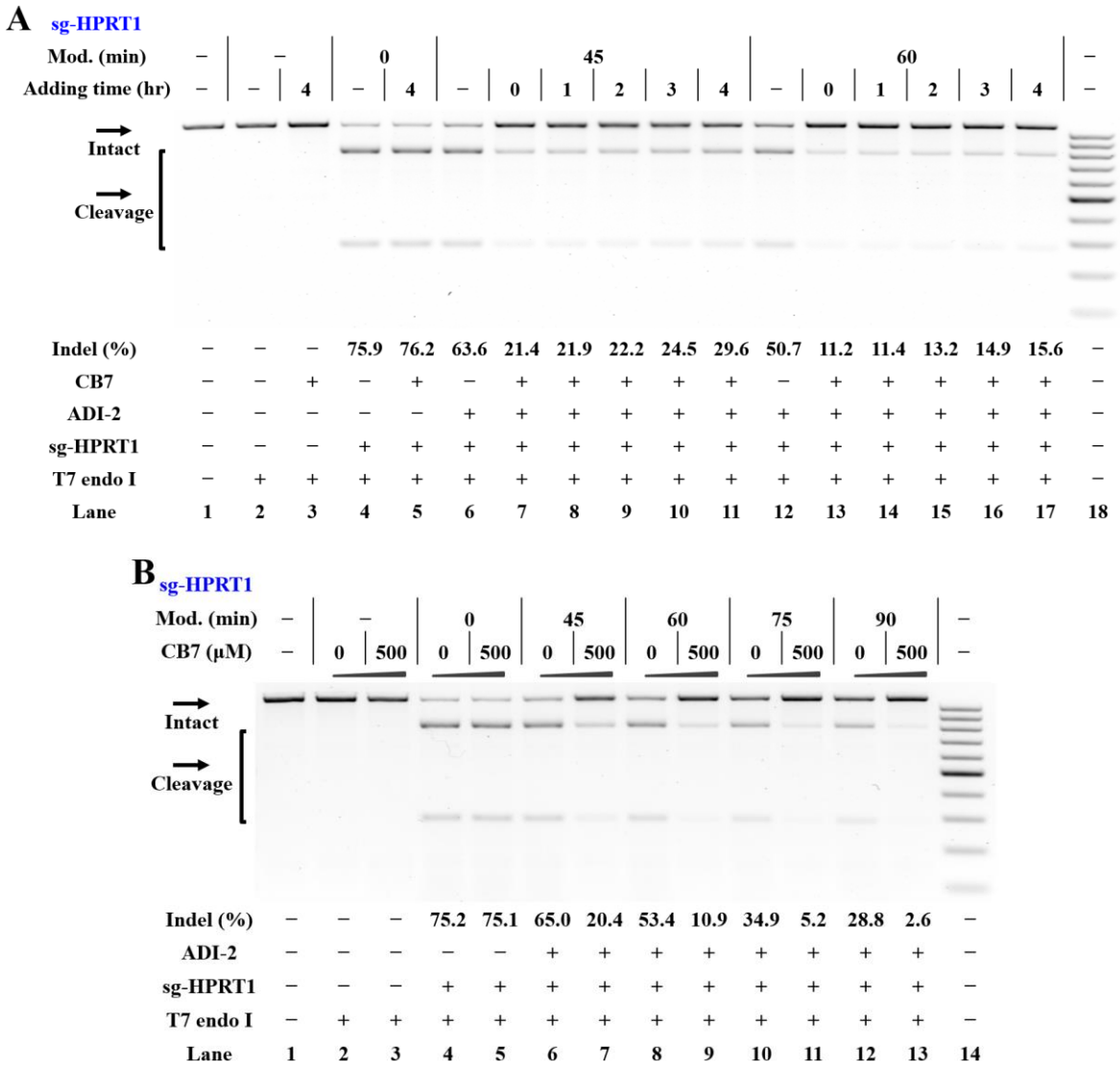

Figure S37. The time course of CB7 addition on inhibition of sg-HPRT1-supported genome editing in cells

The T7E1 nuclease assay was performed 24 hr post-transfection. The treatment for each sample is indicated by the signs at the bottom of each lane. All samples were tested in three biological replicates. Image of representative data is shown here. The percentage of indels of each sample was quantified. (**A**) The CB7 (500 μM) was added to each well at different times after the addition of sg-HPRT1:Lipofectamine complexes. At the end of the 4-hour incubation period, the transfection medium was then replaced with fresh, complete medium supplemented with CB7 (500 μM). Lane 1: target control; lane 2-3: no sgRNA control; lanes 4-5 contain unmodified sg-HPRT1; lanes 6-11, 12-17 contain adamantoyl sg-HPRT1 with increasing modification levels; lane 18: DNA marker. (**B**) Test with transfection in the presence of CB7. For this test, the sg-HPRT1:Lipofectamine complexes were incubated with CB7 at a final concentration of 500 μM. These complexes were left for 20 min at room temperature before transferring them to the well containing cells and growth medium. After a 4-hr incubation, the medium was replaced with fresh, complete medium that contained 500 μM CB7. Lane 1: target control; lane 2-3: no sgRNA control; lanes 4-5 contain unmodified sg-HPRT1; lanes 6-13 contain adamantoyl sg-HPRT1 with increasing modification levels; lane 14: DNA marker (GeneRuler 100-bp DNA Ladder).

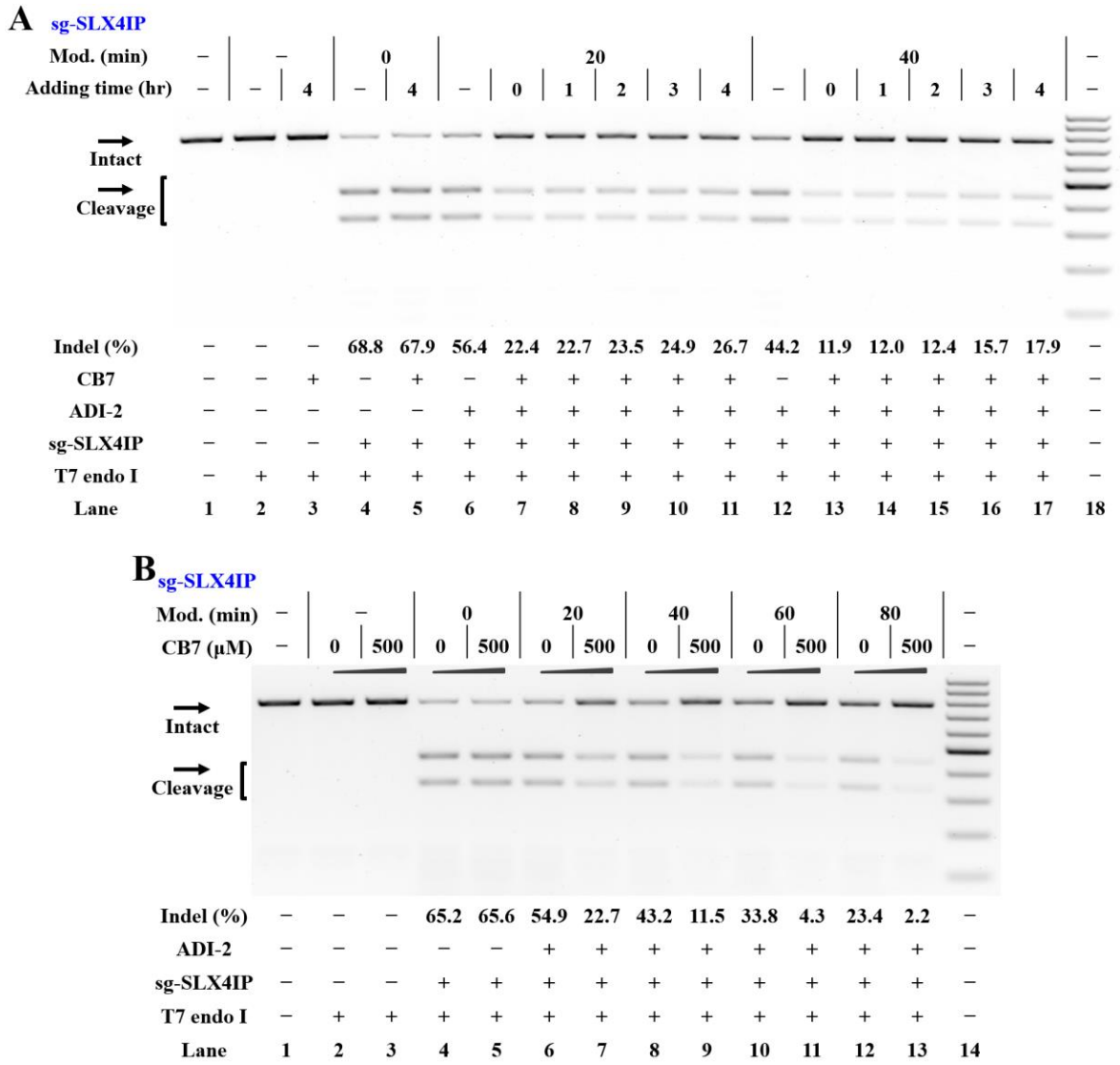

Figure S38. The time course of CB7 addition on inhibition of sg-SLX4IP-supported genome editing in cells

The T7E1 nuclease assay was performed 24 hr post-transfection. The treatment for each sample is indicated by the signs at the bottom of each lane. All samples were tested in three biological replicates. Image of representative data is shown here. The percentage of indels of each sample was quantified. (**A**) The CB7 (500 μM) was added to each well at different times after the addition of sg-SLX4IP:Lipofectamine complexes. At the end of the 4-hour incubation period, the transfection medium was then replaced with fresh, complete medium supplemented with CB7 (500 μM). Lane 1: target control; lane 2-3: no sgRNA control; lanes 4-5 contain unmodified sg-SLX4IP; lanes 6-11, 12-17 contain adamantoyl sg-SLX4IP with increasing modification level; lane 18: DNA marker (GeneRuler 100-bp DNA Ladder). (**B**) Test with transfection in the presence of CB7. For this test, the sg-SLX4IP:Lipofectamine complexes were incubated with CB7 at a final concentration of 500 μM. These complexes were left for 20 min at room temperature before transferring them to the well containing cells and growth medium. After a 4-hr incubation, the medium was replaced with fresh, complete medium that contained 500 μM CB7. Lane 1: target control; lane 2-3: no sgRNA control; lanes 4-5 contain unmodified sg-SLX4IP; lanes 6-13 contain adamantoyl sg-SLX4IP with increasing modification level; lane 14: DNA marker.

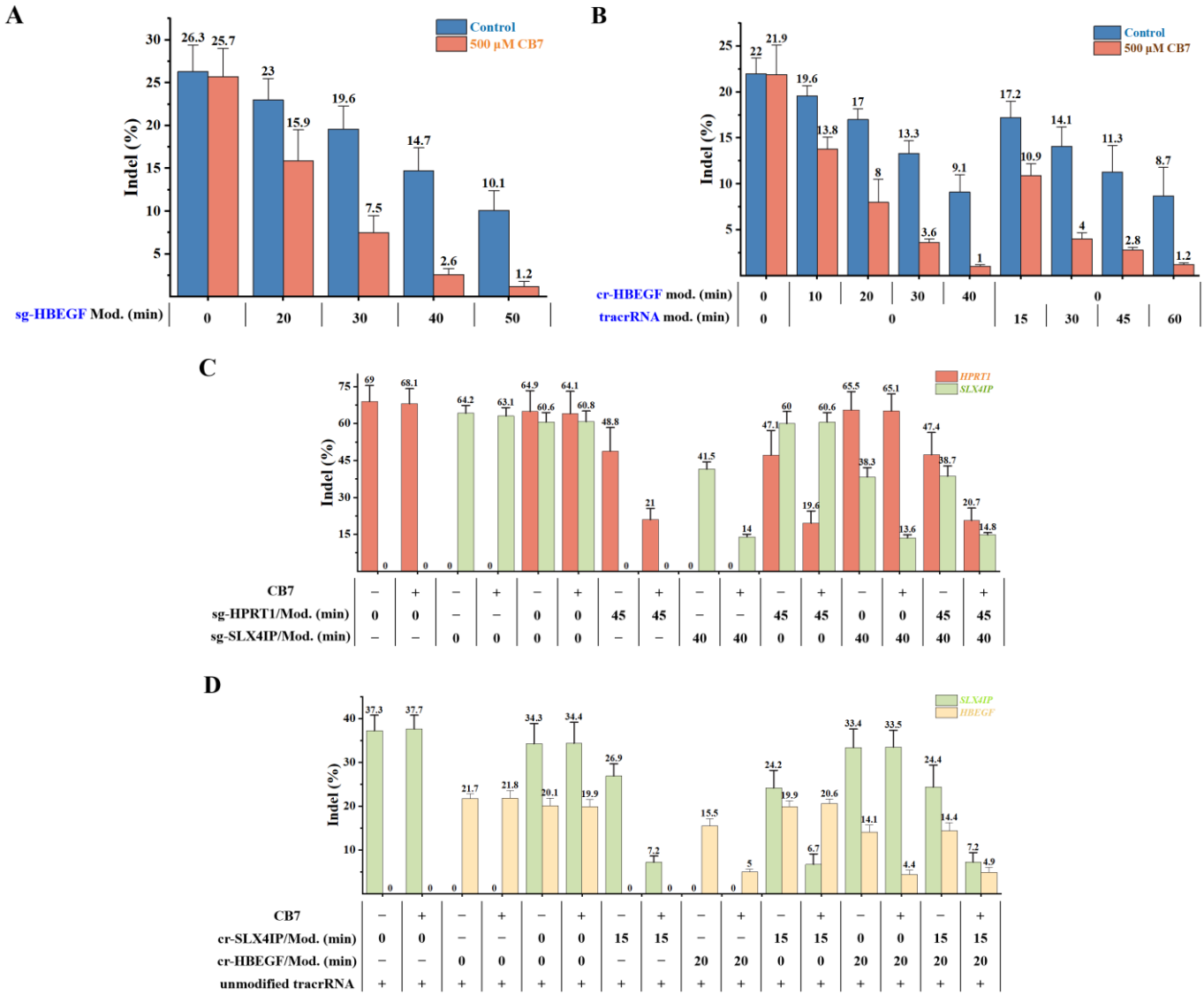

Figure S39. Supramolecular control of CRISPR/Cas9 in human cells

Cellular studies were performed as described in the Experimental Section. The gRNAs were delivered into HeLa-OC cells before CB7 was added. All samples were tested in three biological replicates. The data are presented as the means ± SEM from three independent experiments. (**A**) Supramolecular control of editing of *HBEGF* gene using sgRNAs. Bar graph shows the effect of CB7 complexation on the function of sgRNAs in HeLa-OC cells. (**B**) Supramolecular control of editing of *HBEGF* gene using the 2-part gRNAs. Bar graph shows the effect of CB7 complexation on the function of 2-part gRNAs in HeLa-OC cells. (**C**) Supramolecular control of sgRNA combination. Bar graph shows the ability of CB7 complexation to selectively control target sgRNAs in HeLa-OC cells. (**D**) Supramolecular control of the 2-part gRNA combination. In this study, cells were transfected with crRNA:tracrRNA complexes with different treatments. Bar graph shows the ability of CB7 complexation to selectively control target crRNAs in HeLa-OC cells.

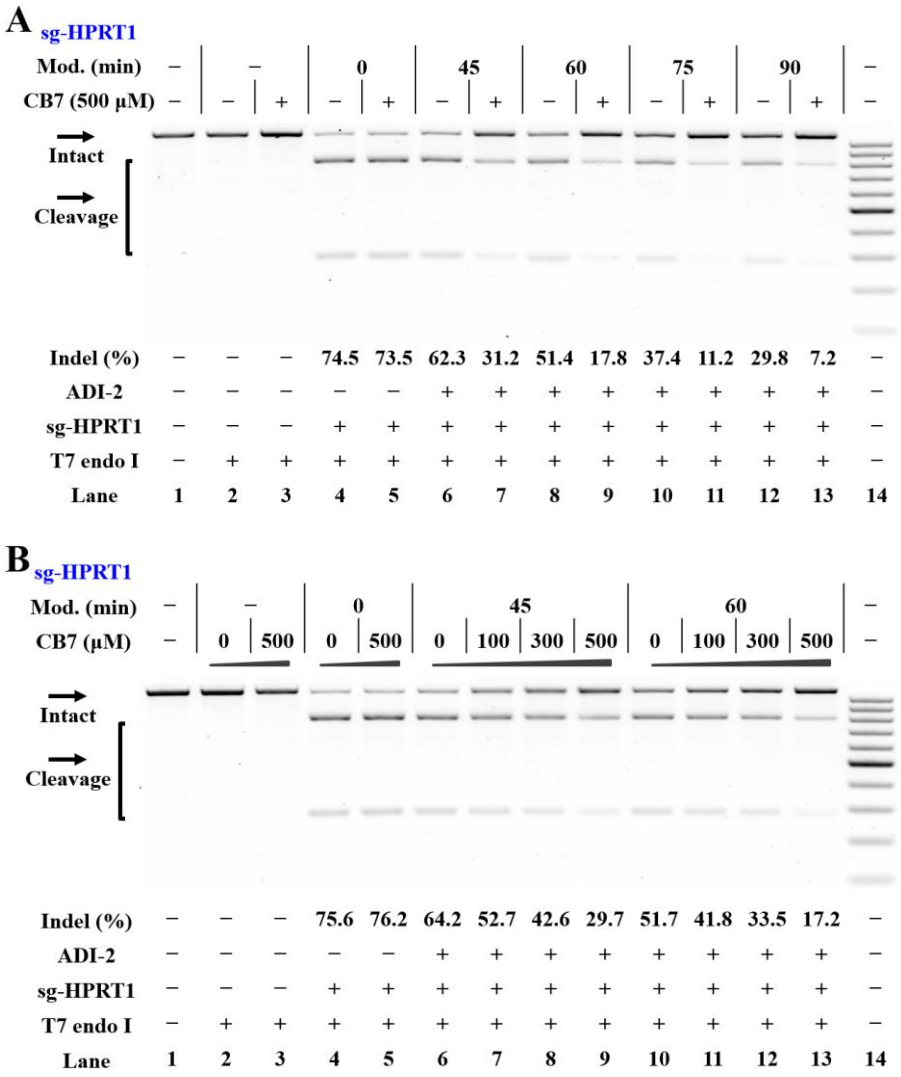

Figure S40. Supramolecular control of CRISPR/Cas9-mediated genome editing in human cells (adamantoyl sg-HPRT1)

Cellular studies were performed as described in the Experimental Section. The gRNAs were delivered into HeLa-OC cells before CB7 was added. The T7E1 nuclease assay was performed 24 hr post-transfection. The treatment for each sample is indicated by the signs at the bottom of each lane. All samples were tested in three biological replicates. Image of representative data is shown here. (**A**) Supramolecular control of editing of a single gene using sgRNAs. Lane 1: target control; lanes 2-3: no sgRNA control; lanes 4-5 contain unmodified sg-HBEGF; lanes 6-7, 8-9, 10-11, 12-13 contain adamantoyl sg-HBEGF with increasing modification level; lane 14: DNA marker (GeneRuler 100-bp DNA Ladder). (**B**) Concentration-dependent inhibitory effect of CB7 on adamantoyl sg-SLX4IP-mediated genome editing. Lane 1: target control; lanes 2-3: no sgRNA control; lanes 4-5 contain unmodified sg-HPRT1; lanes 6-9 contain adamantoyl sg-HPRT1 (a 45-min modification with 100 mM ADI-2); lanes 10-13 contain adamantoyl sg-HPRT1 (a 60-min modification with 100 mM ADI-2); lane 14: DNA marker.

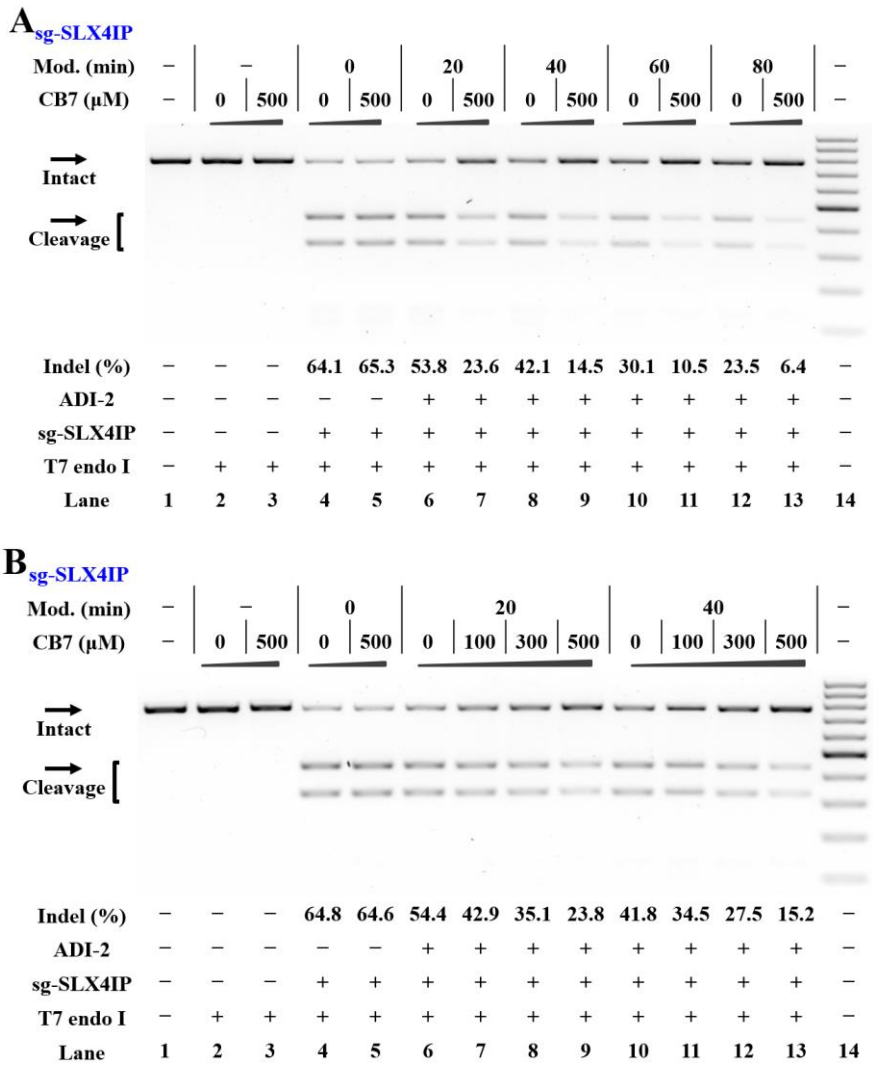

Figure S41. Supramolecular control of CRISPR/Cas9-mediated gene editing in human cells (adamantoyl sg-SLX4IP)

Cellular studies were performed as described in the Experimental Section. The gRNAs were delivered into HeLa-OC cells before CB7 was added. The T7E1 nuclease assay was performed 24 hr post-transfection. The treatment for each sample is indicated by the signs at the bottom of each lane. All samples were tested in three biological replicates. Image of representative data is shown here. (**A**) Supramolecular control of editing of a single gene using sgRNAs. Lane 1: target control; lanes 2-3: no sgRNA control; lanes 4-5 contain unmodified sg-SLX4IP; lanes 6-7, 8-9, 10-11, 12-13 contain adamantoyl sg-SLX4IP with increasing modification levels; lane 14: DNA marker (GeneRuler 100-bp DNA Ladder). (**B**) Concentration-dependent inhibitory effect of CB7 on adamantoyl sg-SLX4IP-mediated genome editing. Lane 1: target control; lanes 2-3: no sgRNA control; lanes 4-5 contain unmodified sg-SLX4IP; lanes 6-9 contain adamantoyl sg-SLX4IP (a 20-min modification with 100 mM ADI-2); lanes 10-13 contain adamantoyl sg-SLX4IP (a 40-min modification with 100 mM ADI-2); lane 14: DNA marker.

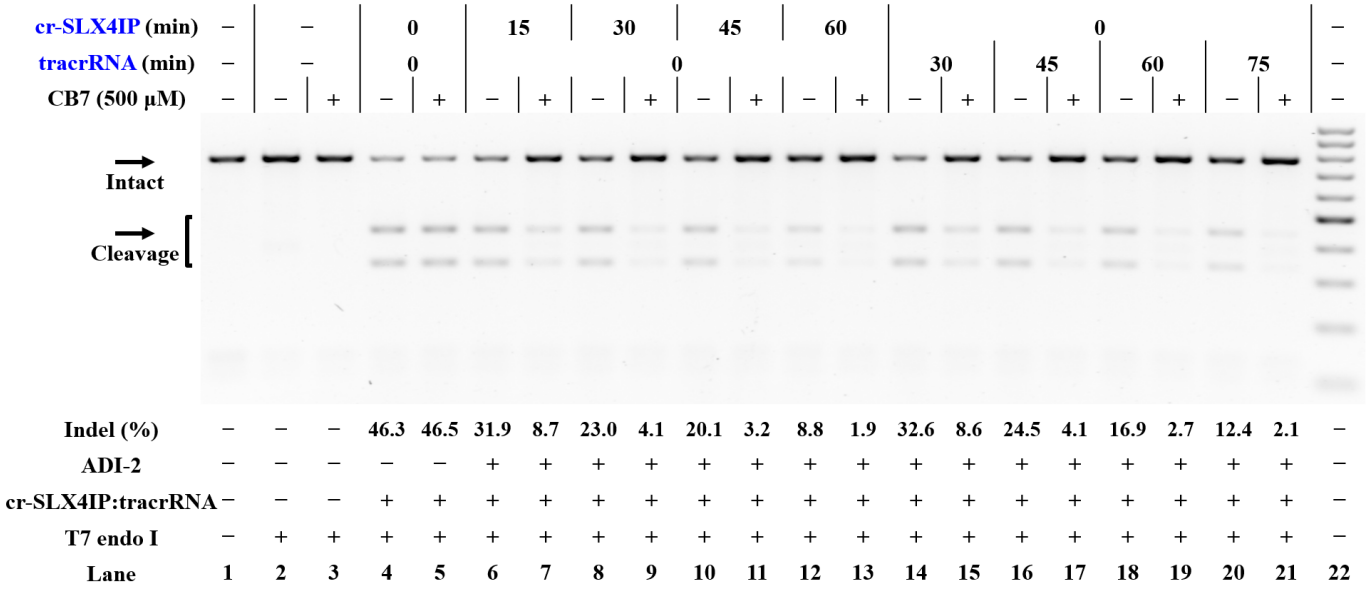

Figure S42. Supramolecular control of the editing of *SLX4IP* gene with the two-part gRNAs

The treatment for each sample is indicated by the signs at the bottom of each lane. All samples were tested in three biological replicates. Image of representative data is shown here. The percentage of indels of each sample was quantified. Adamantoyl gRNAs (cr-SLX4IP or tracrRNAs) were prepared according to the general protocol. For cellular studies with the 2-part gRNAs, 0.6 μg of cr-SLX4IP and 2.0 μg of tracrRNA were annealed by heating to 90 °C for 2 min and slow-cooled to room temperature to form the gRNA complexes. The transfection of 2-part gRNAs was performed according to the transfection steps as described in the Experimental Section. After a 4-hr incubation, the medium was replaced with fresh medium that contained CB7 at a final concentration of 500 μM. The T7E1 nuclease assay was performed 24 hr post-transfection. Supramolecular complexation significantly inhibited the Cas9-mediated genome editing and this effect became more evident with increasing modification level of gRNAs. Lane 1: target control; lane 2-3: no gRNA control; lanes 4-5 contain unmodified cr-SLX4IP and unmodified tracrRNA; lanes 6-13 contain unmodified tracrRNA and adamantoyl cr-SLX4IP with increasing modification level; lanes 14-21 contain unmodified cr-SLX4IP and adamantoyl tracrRNAs with increasing modification level; lane 22: DNA marker (GeneRuler 100-bp DNA Ladder).

SI References:

1. Spitale, R. C.; Flynn, R. A.; Zhang, Q. C.; Crisalli, P.; Lee, B.; Jung, J. W.; Kuchelmeister, H. Y.; Batista, P. J.; Torre, E. A.; Kool, E. T.; Chang, H. Y., Structural imprints in vivo decode RNA regulatory mechanisms. *Nature* **2015,** *519* (7544), 486-90.

2. Cloutier, M.; Roudias, M.; Paquin, J. F., Regioselective Gold-Catalyzed Hydration of CF3- and SF5-alkynes. *Org Lett* **2019,** *21* (10), 3866-3870.

3. Grimme, S.; Ehrlich, S.; Goerigk, L., Effect of the damping function in dispersion corrected density functional theory. *J Comput Chem* **2011,** *32* (7), 1456-65.

4. M. J. Frisch, G. W. Trucks, H. B. Schlegel, G. E. Scuseria, M. A. Robb, J. R. Cheeseman, G. Scalmani, V. Barone, B. Mennucci, G. A. Petersson, H. Nakatsuji, M. Caricato, X. Li, H. P. Hratchian, A. F. Izmaylov, J. Bloino, G. Zheng, J. L. Sonnenberg, M. Hada, M. Ehara, K. Toyota, R. Fukuda, J. Hasegawa, M. Ishida, T. Nakajima, Y. Honda, O. Kitao, H. Nakai, T. Vreven, J. A. Montgomery, Jr., J. E. Peralta, F. Ogliaro, M. Bearpark, J. J. Heyd, E. Brothers, K. N. Kudin, V. N. Staroverov, R. Kobayashi, J. Normand, K. Raghavachari, A. Rendell, J. C. Burant, S. S. Iyengar, J. Tomasi, M. Cossi, N. Rega, J. M. Millam, M. Klene, J. E. Knox, J. B. Cross, V. Bakken, C. Adamo, J. Jaramillo, R. Gomperts, R. E. Stratmann, O. Yazyev, A. J. Austin, R. Cammi, C. Pomelli, J. W. Ochterski, R. L. Martin, K. Morokuma, V. G. Zakrzewski, G. A. Voth, P. Salvador, J. J. Dannenberg, S. Dapprich, A. D. Daniels, Ö. Farkas, J. B. Foresman, J. V. Ortiz, J. Cioslowski, and D. J. Fox. Gaussian 09, Revision **E.01**, Gaussian, Inc., Wallingford CT, **2009**.

5. Deng, W.; Shi, X.; Tjian, R.; Lionnet, T.; Singer, R. H., CASFISH: CRISPR/Cas9-mediated in situ labeling of genomic loci in fixed cells. *Proc Natl Acad Sci U S A* **2015,** *112* (38), 11870-5.

Appendix A: NMR spectra copies of the selected synthesized compounds

This section contains the NMR spectra of the selected synthesized compounds. For each compound, the spectra are shown in the following order: ^{1}H NMR and ^{13}C NMR. The chemical structure of the compound is drawn on each spectrum.

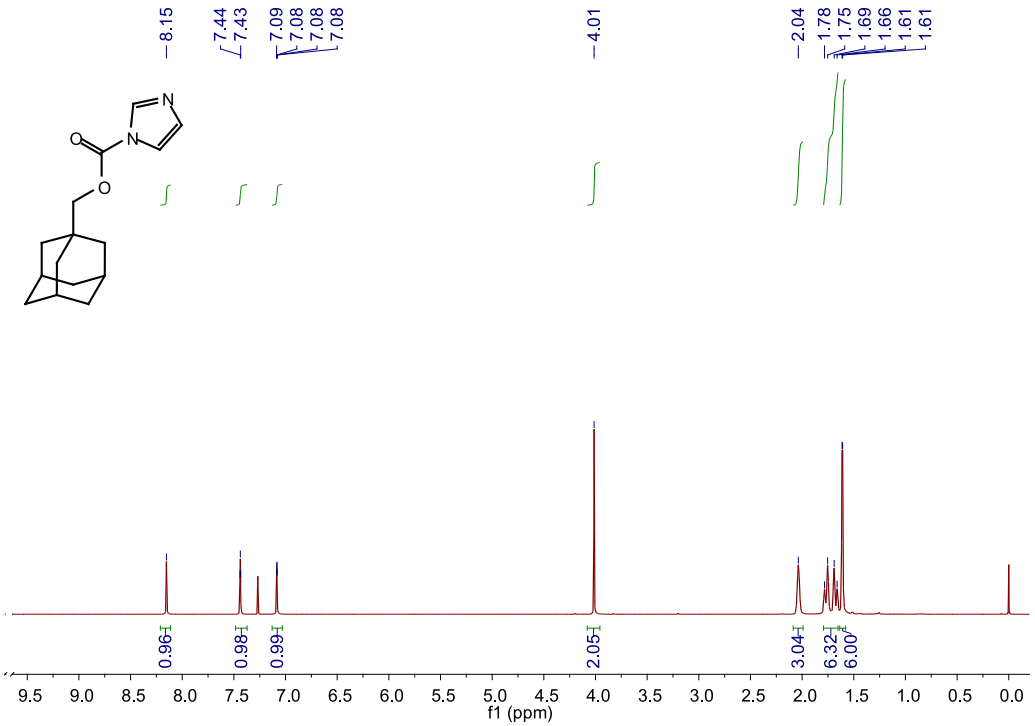

^{1}H NMR spectrum of **ADI-1** in $CDCl_3$

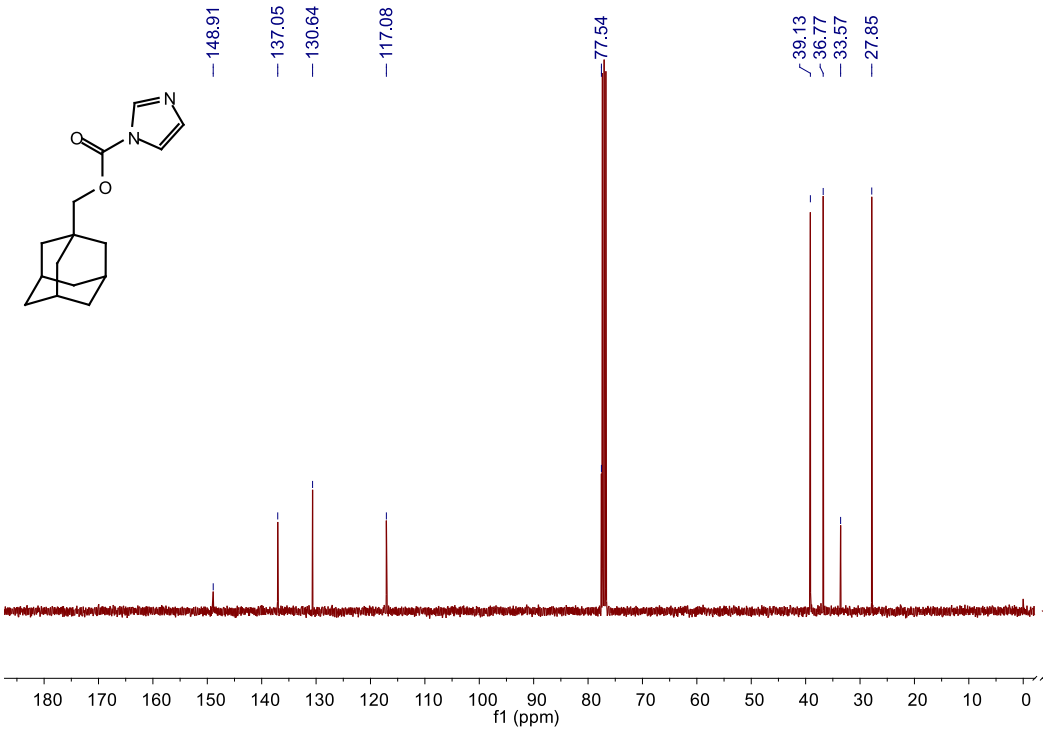

^{13}C NMR spectrum of **ADI-2** in $CDCl_3$

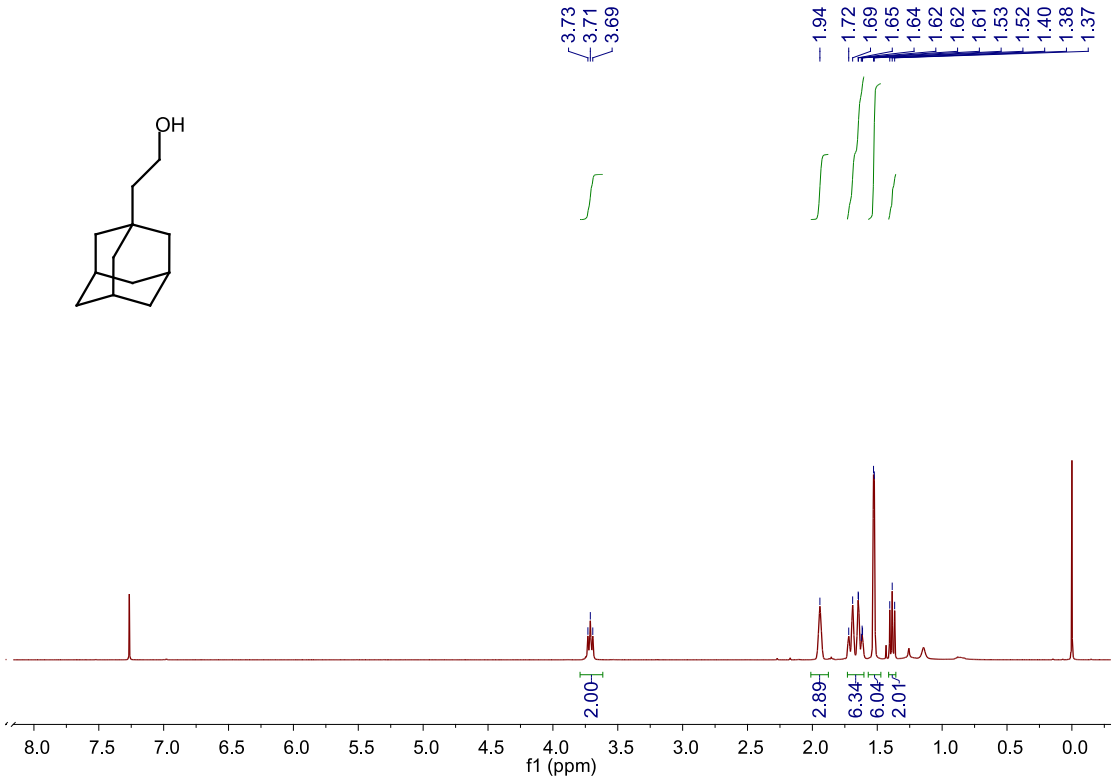

^{1}H NMR spectrum of **2-(Adamant-1yl)ethan-1-ol** in $CDCl_3$

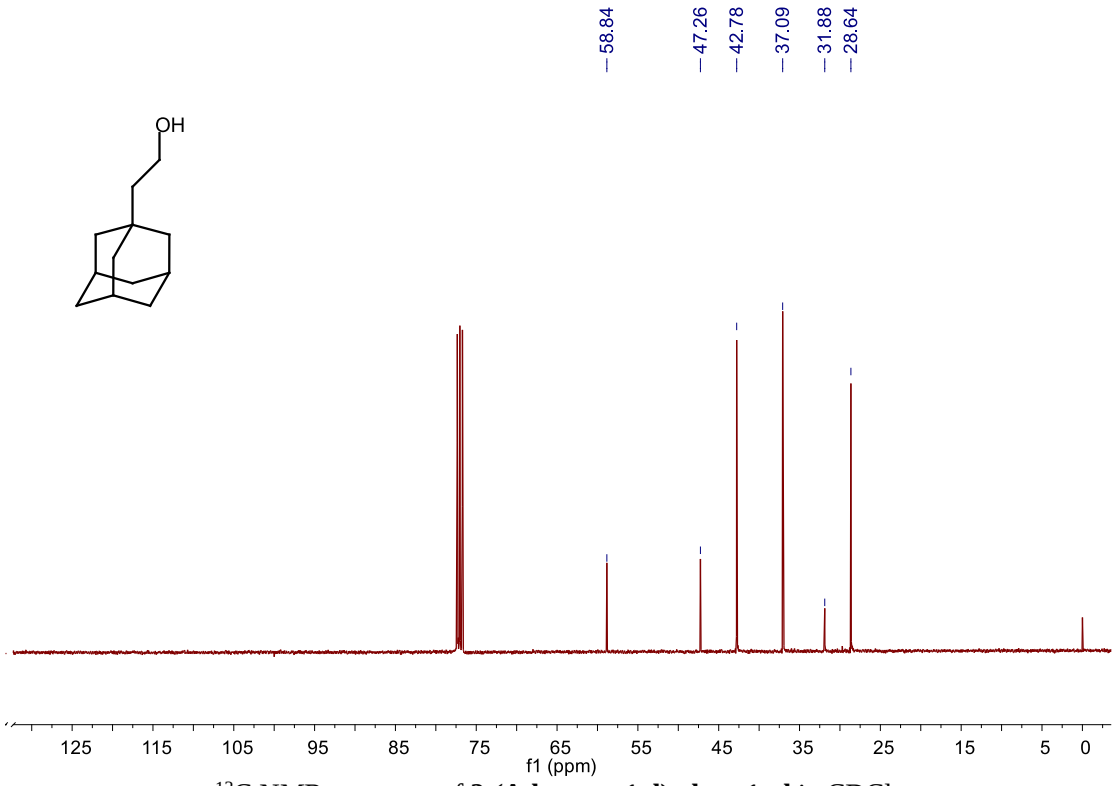

^{13}C NMR spectrum of **2-(Adamant-1yl)ethan-1-ol** in $CDCl_3$

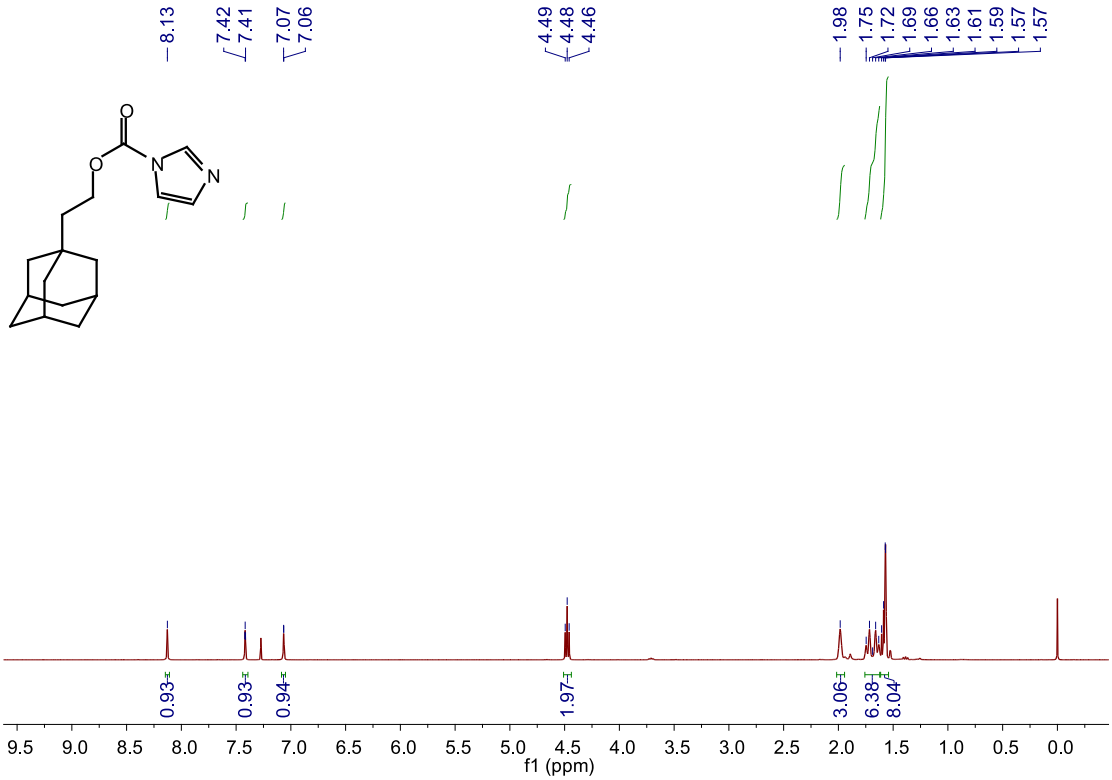

^{1}H NMR spectrum of **ADI-2** in $CDCl_3$

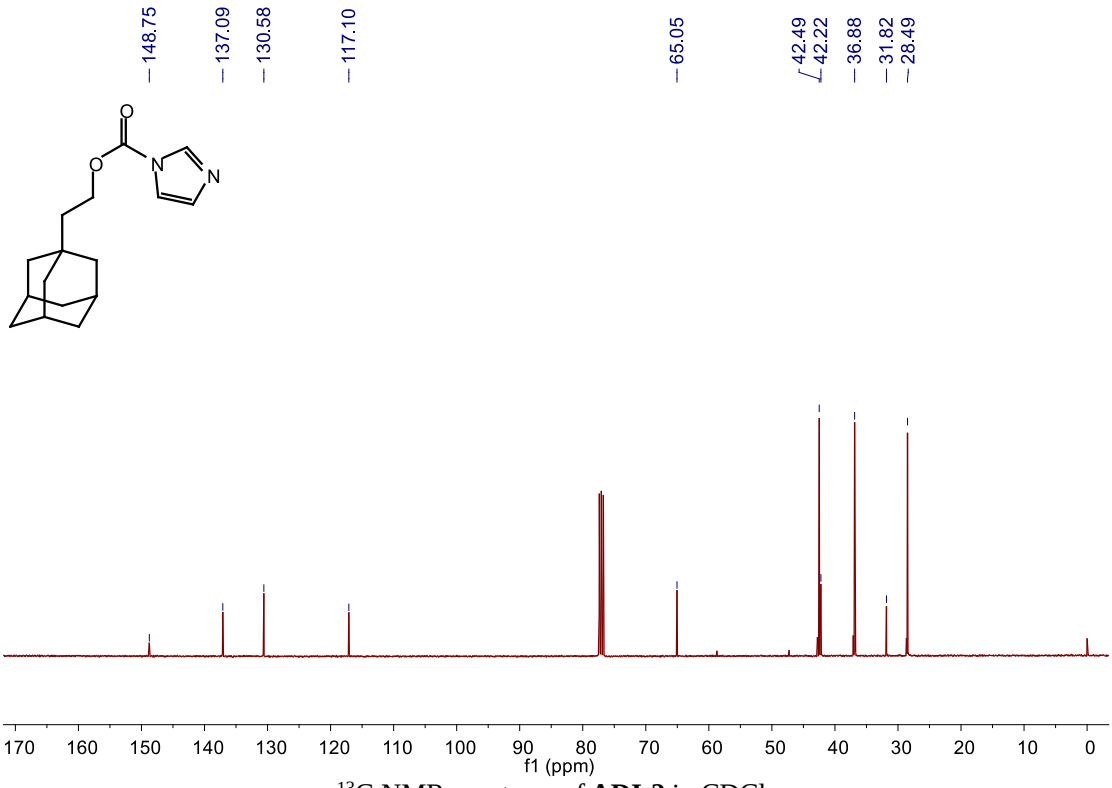

^{13}C NMR spectrum of **ADI-2** in $CDCl_3$

Appendix B: HRMS spectral copies of new compounds

This section contains the HRMS spectra of new compounds. The chemical structure of the compound is drawn on each spectrum.

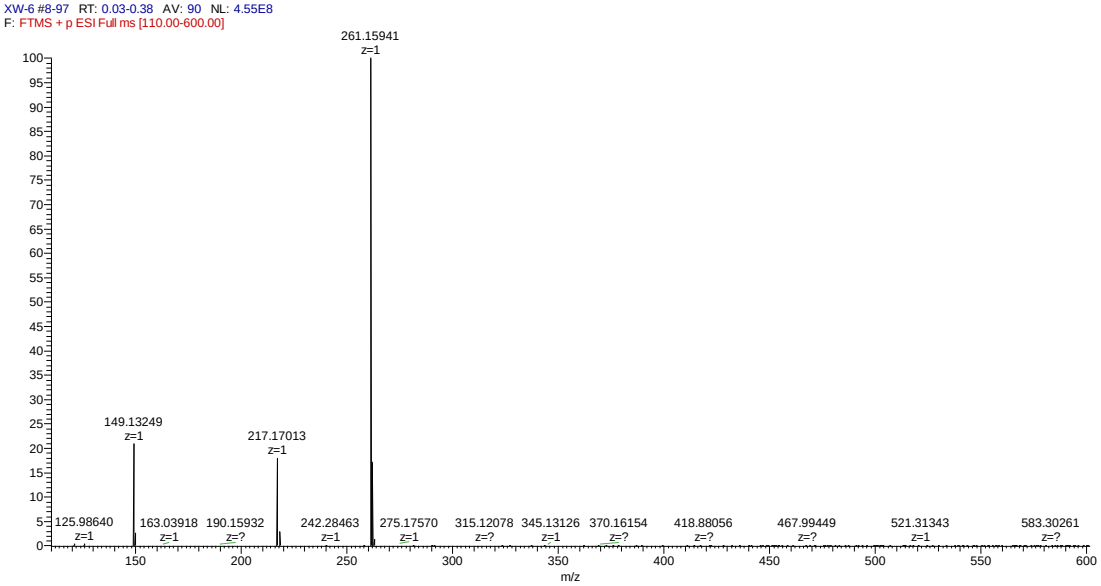

HRMS spectrum of **ADI-1**

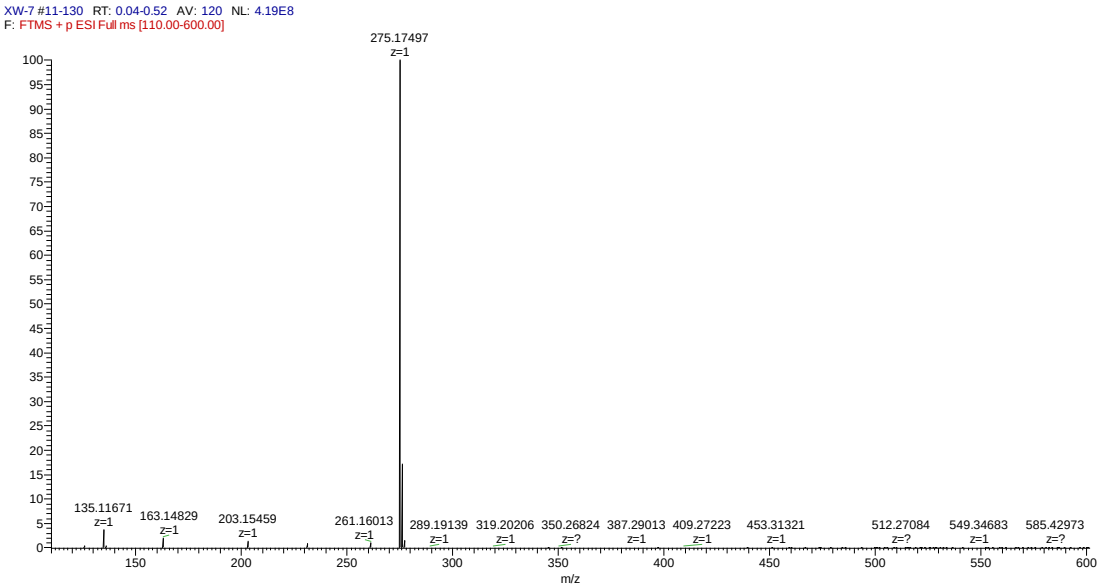

HRMS spectrum of **ADI-2**